Local surface analysis with the Wavejets function basis : definition of new integral invariants and application to geometric details amplification

Yohann Béarzi

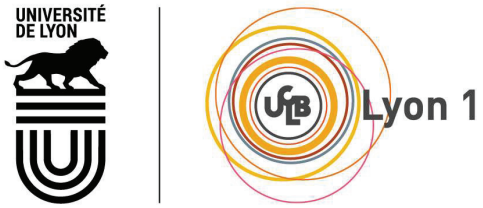

N° d'ordre NNT : xxx

THÈSE DE DOCTORAT

opérée au sein de
l'Université Claude Bernard Lyon 1

École Doctorale ED512
Informatique et Mathématique de Lyon

Spécialité Informatique

Soutenue publiquement le 08/11/2019, par :
Yohann Bearzi

Analyse locale de surface avec la base des *Wavejets* : Définition de nouveaux invariants intégraux et application à l'amplification de détails géométriques

---

Local surface analysis with the *Wavejets* function basis: Definition of new integral invariants and application to geometric details amplification

---

Devant le jury composé de :

Marie Chabert, ENSEEIHT	Rapporteur
Georges-Pierre Bonneau, Université Grenoble-Alpes	Rapporteur
Victor Ostromoukhov, Université Claude Bernard	Examinateur
Enric Meinhardt Llopis, ENS Cachan	Examinateur
Julie Digne, CNRS	Directrice de thèse
Raphaëlle Chaine, Université Claude Bernard	Co-directrice de thèse

Abstract

Surface analysis is a challenging research topic, which has gathered a lot of interest over the last few decades. When surface data is given as a set of points, which are the typical output of 3D laser scanners, the lack of structure makes it even more challenging. In this thesis, we tackle surface analysis by introducing a new function basis: the *Wavejets*. This basis allows to decompose locally the surface into a radial polynomial component and an angular frequency component. Stability properties with regards to a bad normal direction are demonstrated. By linking *Wavejets* coefficients to a high order differential tensor, we also define high order principal directions on the surface. Furthermore, locally splitting surfaces with respect to frequencies leads us to define new integral invariants, permitting to locally describe the surface. Such descriptors are quite robust since they result from an integration process. Finally, we develop an application of these new integral invariants for geometric detail amplification, either based on point position or on normal direction modification, creating in this case the illusion of a surface change.

Résumé

L'analyse de surface est un domaine de recherche difficile, qui a été un sujet de recherche très actif ces dernières décennies. Quand une surface est représentée par un ensemble de points, typiquement issus de scanners laser 3D, le manque de structure entre ces points rend leur traitement compliqué. Dans cette thèse, on propose une méthode d'analyse de surface en introduisant une nouvelle base de fonctions: les *Wavejets*. Cette base permet de décomposer localement une surface radialement en polynômes et angulairement en fréquences. Des propriétés de stabilité en fonction d'une mauvaise direction de normal sont démontrées. En liant les coefficients des *Wavejets* a des tenseurs différentiels à hauts ordres, on définit aussi des directions principales à haut ordre sur la surface. De plus, séparer localement les surfaces fréquentiellement nous amène à la définition de nouveaux invariants intégraux, permettant de décrire localement la surface. De tels descripteurs sont assez robutes car ils sont calculés par intégration. Enfin, Nous proposons une application à ces invariants intégraux pour l'amplification de détails géométriques, soit en changeant la position des points de la surface, soit en changeant la direction des normales, créant dans ce dernier cas l'illusion d'un changement de géometrie sur la surface.

Acknowledgements

I would like to thank my wife Corey and family for their support, as well as my cat Skyler for her amazing ideas regarding my thesis.

I would also like to Julie Digne and Raphaëlle Chaine for their great help and support during this thesis, as well as my co-PhD students: Maxime, Simon, Alexis, Thomas, Samuel, Arthur, Antoine and Antoine, Mathieu, Julia.

Contents

Introduction

En Français

La présente thèse se propose d'étudier une nouvelle approche pour la description locale de surfaces 3D. Plus précisément, nous nous intéressons à caractériser les dynamiques locales autour de chaque point d'une surface. Cette caractérisation est en général faite à travers un vecteur de coefficients associé à chaque point, appelé descripteur, permettant de transformer une géométrie locale d'une surface en des quantités descriptives. Une des difficultés de cette description vient de l'échantillonnage. En effet, il n'existe pas de théorie de l'échantillonnage efficace sur les surfaces. Ainsi, la même surface peut être échantillonnée de manières très différentes, sans que l'on puisse forcément déterminer quel échantillonnage est le meilleur. Il est alors difficile, voir impossible, de comparer points par points des voisinages locaux en ne prenant en compte que les positions. Au contraire, un descripteur permet de condenser un voisinage de points en un nombre fini, constant, de scalaires. Dès lors, une fois le descripteur calculé en chaque point, il est possible de considérer les points indépendamment de leur voisinage, puisque ce voisinage est encodé dans le descripteur. Un descripteur peut caractériser des propriétés très diverses. Il peut servir à recaler des surfaces entre elles en comparant directement les descripteurs entre eux. Mais si la description consiste en des coefficients d'une décomposition sur une base de fonctions, alors elle permet de calculer des quantités.

Nous introduisons une base locale de polynômes complexes, que nous nommons les *Wavejets*, pouvant servir à décomposer localement des surfaces vues sous forme de champs de hauteurs par rapport à un plan de paramétrisation. Cette base de fonctions décompose les surfaces localement en séparant l'évolution radiale de l'évolution angulaire. La partie radiale contient des quantités relatives à des dérivées à ordres élevés, alors que la partie angulaire offre une interprétation fréquentielle de la surface. Après l'étude de certaines propriétés de cette base, elle est utilisée pour calculer des quantités différentielles angulairement orthogonales. Ces quantités peuvent servir pour l'amplification ou la modification de détails sur la position géométrique ou les normales des points.

Ce qui suit résume le contenu de chaque chapitre:

Chapitre 1

Ce chapitre développe un état de l'art sur l'analyse locale de surface se divisant en deux grandes familles: l'analyse différentielle et l'analyse spectrale. Certaines comparaisons sont faites avec le domaine du traitement d'images, de sorte à montrer la transposabilité relative de ces méthodes.

Chapitre 2

Ce chapitre introduit la base des Wavejets. Cette base de fonctions est très proche de celle des Jets introduits par Cazals et al. [CP05], ainsi que de celle des polynômes

de Zernike [Zer34]. Les similitudes ainsi que les différences sont explicitées. Les propriétés de cette base sont explorées. Nous établissons que des sous-ensembles de cette base génèrent des espaces vectoriels de fonctions notamment ℓ-harmoniques. De même, nous explicitons la relation très nette entre les Wavejets et les dérivées de Wirtinger [Wir27]. Enfin, la généralisation des vecteurs et valeurs propres aux supermatrices symétriques proposée par Qi et al. [Qi05; Qi06; Qi07] est mise en relation avec l'écriture angulaire des Wavejets pour les supermatrices de dimension 2.

Ce chapitre détaille les contributions suivantes:

- Une nouvelle base de fonctions pour l'analyse locale de surfaces: les *Wavejets*
- Equivalence entre les Wavejets et les Jets ou les polynômes de Zernike
- Interprétation des dérivées d'ordre k sous forme de combinaisons linéaires de coefficients Wavejets
- Démonstration d'un lien de proportionalité entre les coefficients Wavejets et les dérivées de Wirtinger
- Etude des supermatrices symétriques de dimension 2 et relation des directions principales avec le contenu fréquentiel des Wavejets

Chapitre 3

Dans ce chapitre, nous introduisons de nouveaux invariants intégraux. Les invariants intégraux sont des quantités intégrales servant à la caractérisation locale de fonctions ou de surfaces. Les invariants intégraux que nous introduisons généralisent le *Volume descriptor* introduit dans [Pot+09], permettant ainsi de quantifier les propriétés différentielles de plus hauts ordres. Chaque invariant intégral est lié à un ordre n. Par exemple, le *Volume descriptor* est le cas particulier pour $n = 0$. Le cas $n = \pm 2$ permet d'extraire l'orientation des directions principales. Une généralisation de la notion de courbure moyenne et de courbure Gaussienne est aussi développée dans ce chapitre. Cette généralisation se base sur une écriture des Première et Seconde Formes Fondamentales utilisant les dérivées de Wirtinger.

Ce chapitre introduit les contributions suivantes:

- Définitions de nouveaux invariants intégraux angulairement orthogonaux
- Généralisation du *Volume descriptor* de [Pot+09]
- Lien entre ces invariants intégraux et les dérivées de Wirtinger

Chapitre 4

Dans ce chapitre nous proposons une application directe des invariants intégraux introduits dans le chapitre 3: l'amplification de détails géométriques. Deux méthodes sont proposées. La première amplifie les détails en bougeant chaque point dans la direction normale d'un déplacement lié au *Volume descriptor* d'ordre 0. Cet invariant intégral étant lié à la courbure moyenne, on peut ainsi modifier la dynamique locale de la position des points. La seconde amplifie les détails sans toucher aux positions, mais en amplifiant la dynamique de l'orientation des normales le long de la surface. Pour ce faire, on se base sur les *Volume descriptor* d'ordres ± 1. Comme on le verra, la dynamique locale des normales y est encodée.

Ce chapitre introduit les contributions suivantes:

- Méthode d'amplification de détails géométriques à partir des invariants intégraux introduits
- Amplification de la dynamique des positions ainsi que de la dynamique des normales
- Possibilité de tordre les détails géométriques de façon cohérente en amplifiant les normales.

Chapter 1

An overview on local surface analysis

In this thesis, we adopt a signal processing point of view on surface analysis. This chapter introduces surface processing tools and recalls some basics of signal processing and how both are related. Signal processing is most used on one dimensional temporal signals. These signals can be continuous or discrete and regularly sampled. Signal processing tools can be generalized to spatial signals. Image processing is a well-studied example of regularly sampled spatial data on which signal processing routines can almost directly be applied. Surface analysis, on the other hand, because of the lack of structure in the input data, does not directly inherit all of the nice properties that are used in image processing. Thus, new tools need to be created to perform similar filters. In this chapter, we discuss how we define a surface, and review the most common signal processing tools already existing. Existing implementations of these tools are discussed in image processing and geometry processing.

1.1 Surface definition

We consider surfaces defined as 2-manifolds embedded in $\mathbb{R}^3$. In the general case, an N-manifold is a topological space such that there exists a neighborhood around each point of the N-manifold which is homeomorphic to $\mathbb{R}^N$. In our case of study, surfaces are 2-manifolds such that there exists a neighborhood around each point homeomorphic to $\mathbb{R}^2$. For each point P of the surface, the Euclidean space attached to P is called the tangent plane, and the unit vector orthogonal to this plane is called a vector normal to the surface at P. By convention, we assume that normals are oriented in a coherent manner over the surface, i.e. the field of normals on the surface is continuous. Hence, each point P of the surface can feature a local coordinate systems $(\boldsymbol{x}, \boldsymbol{y}, \boldsymbol{n})$, where $\boldsymbol{n}$ is the normal at P and $(\boldsymbol{x}, \boldsymbol{y})$ is an arbitrary direct orthonormal basis spanning the tangent plane such that $(\boldsymbol{x}, \boldsymbol{y}, \boldsymbol{n})$ is direct. This local coordinate system is said to locally parameterize the surface, i.e. one can assign for any $(x, y) \in \mathbb{R}^2$ in the tangent plane, a unique point Q on the surface around P. If the neighborhood is small enough and if the map is the orthogonal projection of the neighborhood on the tangent plane, the normal displacement of such a map from the tangent plane to the surface is a function $f(x, y) = h$, which we call a heightfield.

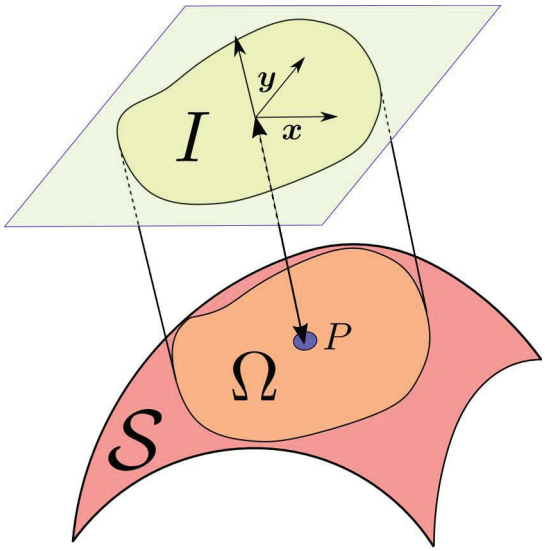

FIGURE 1.1: Example of a local parameterization of a surface $\mathcal{S}$ at point P

1.2 Differential analysis

1.2.1 Definition

Differential quantities give much information about the dynamics of a geometric signal. Contour extraction or mean curvature flow are a few quantities which can be informative.

Derivatives need a coordinate system to be expressed. In this section, we consider a function $f : I \subset \mathbb{R}^2 \to \mathbb{R}$ parameterizing $\Omega \subset \mathcal{S}$, $\Omega \in \mathcal{C}^\infty$. Let $P \in \mathcal{S}$ be the point of coordinates $(0,0)$ in I. A visual example is shown in Figure 1.1.

Let $\boldsymbol{u}$ be $\boldsymbol{x}$ or $\boldsymbol{y}$. The derivative operator $\frac{\partial}{\partial \boldsymbol{u}}$ applied to f near 0 is defined as follows:

$$\frac{\partial f}{\partial \boldsymbol{u}}(0,0) = \lim_{h \to 0} \frac{f(h\boldsymbol{u}) - f(0,0)}{h} \tag{1.1}$$

One can obtain k^{th} order derivatives by recursively differentiating f in wanted directions in any order.

$$\frac{\partial^k}{\partial \boldsymbol{x}^{k-j} \boldsymbol{y}^j} f = \frac{\partial^{k-j}}{\partial \boldsymbol{x}^{k-j}} \frac{\partial^j}{\partial \boldsymbol{y}^j} f = \frac{\partial^j}{\partial \boldsymbol{y}^j} \frac{\partial^{k-j}}{\partial \boldsymbol{x}^{k-j}} f \tag{1.2}$$

For the sake of simplicity, let us note $f_{\boldsymbol{x}^{k-j}\boldsymbol{y}^j} = \frac{\partial^k f}{\partial \boldsymbol{x}^{k-j} \partial \boldsymbol{y}^j}$.

Let us assume the local coordinate system is orthonormal. The values of the derivatives of a surface heavily rely on the choice of the orientation of the coordinate system $(\boldsymbol{x}, \boldsymbol{y})$. Such values are not coordinate system invariant quantities on $\mathcal{S}$. Luckily, some non-linear combinations of coefficients of the derivatives of a function can induce coordinate system invariant quantities. For example, the Gaussian curvature $\mathcal{K}$ or the mean curvature $\mathcal{H}$ are invariant quantities that can be inferred from first and second order derivatives of f:

$$\mathcal{K}_f = \frac{f_{xx} f_{yy} - f_{xy}^2}{\left(1 + f_x^2 + f_y^2\right)^2} \tag{1.3}$$

$$\mathcal{H}_f = \frac{\left(1+f_y^2\right) f_{xx} + \left(1+f_x^2\right) f_{yy} - 2 f_x f_y f_{xy}}{2\left(1+f_x^2+f_y^2\right)^{3/2}} \tag{1.4}$$

Furthermore, all the derivatives of f appear explicitly in its decomposition as a polynomial series called Taylor series:

$$f(x,y) = \sum_{k=0}^{\infty} \sum_{j=0}^{k} \frac{1}{(k-j)!j!} f_{x^{k-j}y^j}(0,0) x^{k-j} y^j \tag{1.5}$$

This means that expressing f as a sum of mononomials can be a way to estimate high order derivatives of f. Taking advantage of this fact, [CP05] used truncated Taylor expansion (see section 2.1.1), which are named osculating Jets, to do differential analysis on surfaces.

Let $(\boldsymbol{x}, \boldsymbol{y})$ be the coordinate system in the plane locally parameterizing $\mathcal{S}$ at a certain point $P \in \mathcal{S}$. We call a parameterizing plane at P a plane spanned by $(\boldsymbol{x}, \boldsymbol{y})$ passing by P endowed with a coordinate systeme such that P has coordinates $(0,0)$. Let $\boldsymbol{z} = \boldsymbol{x} \wedge \boldsymbol{y}$ where $\wedge$ is the vector product. The tangent plane $\mathcal{T}(P)$ at point P is spanned by the two unit vectors $(\boldsymbol{x}_\mathcal{T}, \boldsymbol{y}_\mathcal{T})$ expressed as follows in basis $(\boldsymbol{x}, \boldsymbol{y}, \boldsymbol{z})$:

$$\begin{aligned} \boldsymbol{x}_\mathcal{T} \sqrt{1 + f_x(0,0)^2} &= (1, 0, -f_x(0,0)) \\ \boldsymbol{y}_\mathcal{T} \sqrt{1 + f_y(0,0)^2} &= (0, 1, -f_y(0,0)) \end{aligned} \tag{1.6}$$

The vector $\boldsymbol{n} = \boldsymbol{x}_\mathcal{T} \wedge \boldsymbol{y}_\mathcal{T}$ is the normal of $\mathcal{S}$ at point P. Note that if the parameterization plane is the tangent plane at point P, $\boldsymbol{n} = (0,0,1)$ in local coordinates. As a consequence, the first derivatives of f are equal to zero.

1.2.2 Convolution-based differentiation

In the definition of differentiation given in last section, there is no notion of scaling. One might want to introduce scaling in the variation computation. Convolution appears as a flexible tool to address scale issues. Blurring $\mathcal{S}$ will annihilate small, fast varying details, and give the possibility to characterize the surface at scale s. In the case of a discrete noisy surface or function, blurring helps to get more stable quantities. Let us first recall the convolution product $*$ given a kernel K and a function f, both Lebesgue-integrable:

$$(K * f)(x,y) = \int_{-\infty}^{\infty} \int_{-\infty}^{\infty} K(x-u, y-v) f(u,v) du dv \tag{1.7}$$

Kernel K can have many properties depending on what kind of filtering one wants to do. Let us restrict for now to isotropic 2D Gaussian kernel G of standard deviation σ:

$$G^\sigma(x,y) = \frac{1}{2\pi\sigma^2} \exp\left(-\frac{x^2+y^2}{2\sigma^2}\right) \tag{1.8}$$

Since G^σ is a distribution, $\lim_{\sigma \to 0} G^\sigma = \delta$, the Dirac distribution. The property $(K * f)_{\boldsymbol{x}^{k-j}\boldsymbol{y}^j} = K_{\boldsymbol{x}^{k-j}\boldsymbol{y}^j} * f = K * f_{\boldsymbol{x}^{k-j}\boldsymbol{y}^j}$ yields:

$$f_{\boldsymbol{x}^{k-j}\boldsymbol{y}^j} = \lim_{\sigma \to 0} G^\sigma_{\boldsymbol{x}^{k-j}\boldsymbol{y}^j} * f \tag{1.9}$$

A direct consequence is that convolving a function f with the derivatives of a Gaussian function gives a way to approximate the derivatives of f at a scale σ. This allows to control at which scale the local dynamics of f are quantified. More evolved kernels K can be imagined. For example, an anisotropic Gaussian function can be used to have a finer approximation of the variations in a chosen direction.

Convolution is a straightforward operation in the case of a grid sampled function. This is the case of 2D images. Given a square regular grid sampling pattern III, the discretization $f|_{\text{III}}$ of f can be convolved with a sampled kernel $K|_{\text{III}}$ through matrix convolution. If III is finite, boundary conditions need to be added to compute the discrete convolution:

$$\forall (x,y) \in \text{III}, \left(K|_{\text{III}} * f|_{\text{III}}\right)(x,y) = \sum_{(u,v)\in \text{III}} K(x-u, y-v) f(u,v) \tag{1.10}$$

Irregular sampling patterns Ξ are much harder to deal with. A common way to deal with it is to use an interpolator function $\mathcal{I}$ to estimate a continuous function function $\tilde{f} = \mathcal{I}(f|_{\Xi})$. Then, $\tilde{f}$ is resampled on a regular pattern III. The choice of $\mathcal{I}$ is important and errors are mainly induced from it. Another solution to deal with irregular samplings is to weight each term of the sum in equation (1.10) by the area of the Voronoi cell in the sampling space of the corresponding point in sampling pattern Ξ. Let $\mathcal{A}_{\Xi}(x,y)$ be the Voronoi cell area of point $(x,y) \in \Xi$. Given proper boundary conditions avoiding infinite Voronoi cells, an estimate of the convolution product is given by:

$$\forall (x,y) \in \Xi, \left(K|_{\Xi} * f|_{\Xi}\right)(x,y) = \sum_{(u,v)\in \Xi} \mathcal{A}_{\Xi}(u,v) K(x-u, y-v) f(u,v) \tag{1.11}$$

1.2.3 Integral invariants

Performing a convolution on a surface is not straightforward because of the data structure. It is not possible to take a point set or a mesh as is and perform a convolution with a matrix. Furthermore resampling regularly the function to take derivatives is error-prone. [Man+04] introduced integral invariants. An integral invariant is an integral quantity computed locally around a point on a surface. They produce more stable results because of the integration process, which is also present in convolution-based differentiation. Integrating a signal corrupted by a centered noise gives a noise-free quantity.

The main difference between integral invariants proposed in the literature and convolution is the use of a binary mask in the case of integral invariants. Indeed, an integral invariant can be seen as the convolution of the signal with a window function of amplitude 1. One of the integral invariants proposed by [Pot+09] is obtained by computing at each point of the surface the volume of the intersection with a ball and the interior of the surface (see figure 1.2). Links to mean curvature is shown in this particular case. For example, the integral invariant $\mathcal{V}(P)$ illustrated in figure 1.2 has the following form given a ball of radius r:

$$\mathcal{V}(P) = \frac{2\pi}{3} r^3 - \frac{\pi H}{4} r^4 + O(r^5) \tag{1.12}$$

Where H is the mean curvature.

Using a ball here permits to be robust. Using the volume between the surface and a parameterization plane induces a bias due to the multiplicity of possible

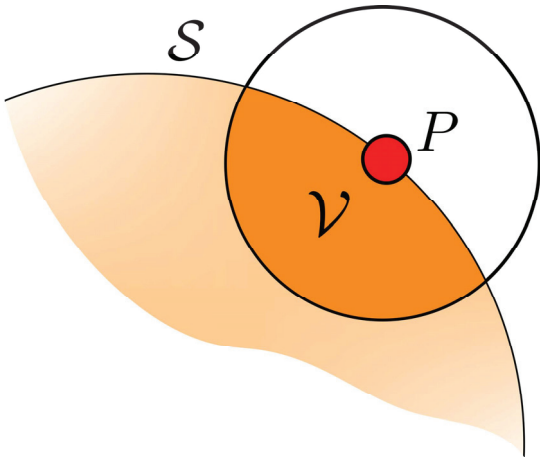

FIGURE 1.2: Illustration of an integral invariant being the volume $\mathcal{V}$ of the intersection of a ball with the interior of a surface $\mathcal{S}$ centered at point $P \in \mathcal{S}$.

parameterization planes at a point. Such integral invariants would require stability properties w.r.t. the parameterization plane orientation.

1.3 Spectral analysis

Spectral analysis is a powerful tool of signal processing. The idea is to project the temporal or spatial function into a frequency space. The most widely used spectral analysis tool is the Fourier Transform, which splits any signal in a sum of cosines of different frequencies. Fourier space has an interesting property: multiplication is equivalent to convolution in the origin space.

1.3.1 Continuous periodic signals

Continuous spectral processing has applications in many fields, such as hologram creation, MRI, electronics, radio waves, etc. Given a continuous (X, Y)-periodic function f defined on $\mathbb{R}^2$, its Fourier series is:

$$f(x,y) = \sum_{n=-\infty}^{\infty} \sum_{m=-\infty}^{\infty} \hat{f}_{n,m} e^{2\pi i \left(\frac{nx}{X} + \frac{my}{Y}\right)} \tag{1.13}$$

Each coefficient $\hat{f}_{n,m}$ has the following expression:

$$\hat{f}_{n,m} = \frac{1}{XY} \int_{-\frac{Y}{2}}^{\frac{Y}{2}} \int_{-\frac{X}{2}}^{\frac{X}{2}} f(x,y) e^{-2\pi i \left(\frac{nx}{X} + \frac{my}{Y}\right)} dxdy \tag{1.14}$$

This enables to filter f by operating on the coefficients of $\hat{f}$, i.e. on the frequency components of f. Reducing low frequencies tends to blur the signal, while amplifying high frequencies tends to amplify fast varying components of the signal. Fourier series function basis is orthogonal and thus allows one to independently compute any Fourier coefficient by projection with the following inner product on function space $\mathscr{L}^2(\mathbb{C}, \mathbb{C})$:

$$\langle f, g \rangle = \int_{-\infty}^{\infty} \int_{-\infty}^{\infty} f(x,y) g^*(x,y) dxdy \tag{1.15}$$

As shown in equation (1.15), the spectral decomposition of the signal is performed on the whole function f for each frequency. This makes it a global procedure on the signal which fails at extracting spatially localized properties in the signal. An exception to that restriction is *phase congruency*, which evaluates how much all the frequency components of the signal are in phase at each position. Near edges in the signal, a lot of components are in phase, which makes phase congruency $PC(t)$ a very robust quantity for extracting edges in a signal. The counter part is that its computation is tedious:

$$PC(x,y) = \sup_{(\bar{x},\bar{y})} \frac{\sum_{n=-\infty}^{\infty}\sum_{m=-\infty}^{\infty} \hat{f}_{n,m} e^{2\pi i\left(n\frac{x-\bar{x}}{X}+m\frac{y-\bar{y}}{Y}\right)}}{\sum_{n=-\infty}^{\infty}\sum_{m=-\infty}^{\infty} \hat{f}_{n,m}} \tag{1.16}$$

1.3.2 Discrete uniformly sampled signals

The Fourier series coefficients can be computed on uniformly sampled signals by directly projecting the signal on each Fourier basis element with the discrete inner product defined on $\mathscr{L}^2(\mathbb{C},\mathbb{C})$:

$$\langle f,g\rangle_{\text{Ш}} = \sum_{\ell\in\text{Ш}} f_\ell g_\ell^* \tag{1.17}$$

Given $\text{Ш} = \{(x,y) \in \mathbb{N}^2 | x < X, y < Y\}$, the Discrete Fourier Transform of $f|_{\text{Ш}} = \{f_{x,y} | (x,y) \in \text{Ш}\}$ is:

$$\hat{f}_{n,m} = \sum_{(x,y)\in\text{Ш}} f_{x,y} e^{-2\pi i\left(\frac{nx}{X}+\frac{my}{Y}\right)} \tag{1.18}$$

This transform is invertible:

$$f_{x,y} = \frac{1}{\text{card}(\text{Ш})} \sum_{(n,m)\in\text{Ш}} \hat{f}_{n,m} e^{2\pi i\left(\frac{nx}{X}+\frac{my}{Y}\right)} \tag{1.19}$$

Basis $\left(e^{2\pi i\left(\frac{nx}{X}+\frac{my}{Y}\right)}\right)_{(n,m)\in\text{Ш}}$ is orthogonal w.r.t $\langle .,. \rangle_{\text{Ш}}$. The complexity for computing all coefficients of the Fourier series of a signal $f_{\text{Ш}}$ of N samples in a naive way is $O(N^2)$. The Fast Fourier Transform (FFT) algorithm reduces the complexity to $O(N \log N)$. The FFT is widely used in image processing.

1.3.3 Discrete non-uniformly sampled signals

When f is non-uniformly sampled with a sampler Ξ, spectral analysis on f_Ξ is not so straightforward. Direct projection on the Fourier series basis element is not guaranteed to work anymore. It is difficult to have small error bounds on the estimation of the coefficients. A commonly used tool to determine whether Discrete Fourier Transform can be applied or not on a set of samples is the Fourier Frame which:

Let $(e_\ell)_{\ell\in\mathbb{N}} = \left(e^{2\pi i\left(\frac{\ell x}{X}+\frac{\ell y}{Y}\right)}\right)_{\ell\in\mathbb{N}}$ s.t. $\left(\frac{\ell x}{X}, \frac{\ell y}{Y}\right) \in \mathbb{Z}^2$ be a sequence of complex functions. Given $\mathcal{H}$ a Hilbert space, such a sequence is called a Fourier Frame if and only if:

$$\exists (A,B) > 0, \ \ \forall f \in \mathcal{H}, \ \ A\|f\|^2 \leq \sum_{\ell\in\mathbb{N}} \langle f, e_\ell\rangle \leq B\|f\|^2 \tag{1.20}$$

In the case of uniformly sampled signal, $A = B = 1$ and the Fourier Frame is called a *tight frame* and equation (1.20) becomes the Parseval equality. A and B can be bounded if each e_ℓ is weighted by the squared root of the area of its corresponding cell in the Voronoi diagram of the set $(e_\ell)_{\ell\in\mathbb{N}}$ seen as points of $\mathbb{R}^2$, and if the local sequence density near each e_ℓ is larger than $\frac{\ln 2}{2\pi}$. Sadly, even if A and B are bounded, the induced error can be too big to be negligible. For further development, the reader can refer to the work of [Mil15].

Non-Uniform Fast Fourier Transform (NUFFT) is another existing method to estimate the spectrum of non uniformly sampled signals. They rely on a fast interpolation method of sampled points to regular grid. [DR95] propose to interpolate points using Gaussian weights. [Bey95] use a multi-resolution analysis. The results with best bounds are obtained by **[Liu1998]** with Regular Fourier Matrices, a class of matrices they introduced. The accuracy of such methods highly depends on the interpolator resampling the signal.

1.3.4 Spectral analysis on manifolds

Spectral analysis can also be done on functions defined on a manifold. The key to defining an extension of Fourier series basis to manifolds was studied by [Tau95] who noticed that Fourier basis are the eigenfunctions of the Laplacian operator Δ. Given the one dimensional T-periodic Fourier basis function $(e^{2\pi i\frac{nt}{T}})_{n\in\mathbb{Z}}$, the proof is straightforward:

$$\Delta e^{2\pi i\frac{nt}{T}} = -\left(2\pi\frac{n}{T}\right)^2 e^{2\pi i\frac{nt}{T}} \tag{1.21}$$

Fourier basis functions being the eigenfunctions of the Laplacian operator Δ means that if one has a definition of this operator on a manifold $\mathcal{S}$, extracting its eigenvectors gives a Fourier-like basis on $\mathcal{S}$. Those eigenfunctions are called *manifold harmonics*. The signal defined on the manifold can be any scalar or vector valued signal but using 3D coordinate will permit to filter the shape itself.

The Laplacian operator on a Manifold $\mathcal{S}$ is called the *Laplace-Beltrami* operator $\Delta_\mathcal{S}$. In order to define it, the differential operator ∇ on manifold is needed. Given ∇ the gradient operator and div the divergence operator, the definition of $\Delta_\mathcal{S}$ is as follows:

$$\Delta_\mathcal{S} f = \operatorname{div}(\nabla f) \tag{1.22}$$

Given $(H_n)_{n\in\mathbb{N}}$ the set of eigenvectors of $\Delta_\mathcal{S}$, computing the Manifold Harmonic transform $\hat{f}$ of a function $f : \mathcal{S} \to \mathbb{C}$ is done by projecting f on each basis element H_n:

$$\hat{f}_n = \langle f, H_n\rangle \tag{1.23}$$

Discretization of the Laplacian operator for manifolds surface meshes of n points is not an easy task. [War+07] showed that it is impossible to construct a discrete Laplace-Beltrami $\Delta = (w_{i,j})_{(i,j)\leq n}$ operator satisfying simultaneously the four properties concerning the weights $w_{i,j}$ in the matrix representing the discretized operator:

- Symmetry: $w_{i,j} = w_{j,i}$
- Locality: $w_{i,j} = 0$ if i and j do not share an edge on a mesh
- Linear precision: $\sum_j w_{i,j}(x_i) = 0$
- Positive weights: $w_{i,j} \geq 0$

This implies that there is a variety of different definition of the discrete Laplace-Beltrami operator. Let us give some examples. A combinatorial Laplacian on a mesh is an adjacency matrix. [Zha04] studied some of them, but it has been shown by [Mey+02] that this definition is only correct on uniform sampling. Various weighting schemes were proposed to estimate a Laplace-Beltrami, leading to weights making spectral processing be mesh-independent [VL08]. Actually, this whole trend is related to spectral analysis of general graph [Big74], but the way the Laplacian is discretized takes into account the geometry. If the surface is given by point sets, a way to define the Laplace-Beltrami operator on point sets is to create an adjacency matrix, each edge being weighted by a Gaussian kernel of the distance between the points and the area of triangles computed out of a local Delaunay Triangulation.

1.4 Local spectral analysis

Spectral analysis, as it is defined with Fourier series, defines quantities depending on the whole function f. The projection of f on the space of Fourier series expresses f depending only on frequencies (ξ, ν). Having a space where both spatial and spectral quantities can exist together was a missing piece in signal processing. Solutions for treating both temporal and spectral quantities exist in nature. Indeed, when someone listens to music, both temporal (the rythm) and spectral (the notes) aspects are processed at the same time by our ears. There has been many attempts linking them, leading to ill-formed solutions, until the revolution of the Wavelet basis [GGM84]. A review on spectral processing using Wavelets can be found in [Mal99]

A temporal signal ψ, is a called Wavelet, if and only if:

$$\begin{cases} \int_{-\infty}^{\infty} \psi(t)dt = 0 \\ \int_{-\infty}^{\infty} |\psi(t)|^2 dt < \infty : \end{cases} \tag{1.24}$$

Bases of Wavelets are built from a mother Wavelet Ψ. Given Ψ, a wavelet family $\psi_{s,\tau}$ is defined as follows:

$$\psi_{s,\tau}(t) = \frac{1}{\sqrt{s}} \Psi \left(\frac{t-\tau}{s} \right) \tag{1.25}$$

s is called the *scale* of the wavelet and τ is its position. This writing offers a multiresolution expression of a signal. Such wavelets family are orthogonal. Thus, given a wavelet basis $\psi_{s,\tau}$, a function f can be projected in the space generated by this wavelet basis:

$$\hat{f}_{s,\tau} = \langle f, \psi_{s,\tau} \rangle \tag{1.26}$$

Wavelets can be easily computed on a regularly sampled discrete signal and are much used in image processing to extract textures or to do compression. There is not much successful implementation on manifolds, with the exception of lifted Wavelets [SS95] and the bandelets generalization [PM05].

Chapter 2

The Wavejets basis: definition and properties

2.1 Overview

This chapter introduces a complex polynomial basis for local surface analysis which we call *Wavejets* [BDC18]. The surface is locally expressed as a heightfield over its tangent plane, which is decomposed on our function Basis. The Wavejets basis gives an angular frequency interpretation to high order derivatives of a surface. In particular, we show that a subset of this basis spans a vectorial space of ℓ-harmonic functions with the Wirtinger derivatives [Wir27]. We also link the Wavejets coefficients to the eigen decomposition of symmetric supermatrices, which was studied by [Qi05; Qi06; Qi07]. This basis will then be used in chapter 3, splitting it by frequency in order to construct new integral invariants [Man+04; Pot+09]. Let us first introduce a few notations and hypothesis concerning the type of surfaces studied in this work.

Let $\mathbb{K} = \mathbb{R}$ or $\mathbb{K} = \mathbb{C}$. Let $\mathcal{S}$ be a surface and $\mathcal{P}$ be a plane passing by some point $P \in \mathcal{S}$ such that the angle difference between $\mathcal{P}$ and the tangent plane at P is small enough. Let $(\boldsymbol{x}, \boldsymbol{y})$ be an arbitrary direct orthonormal basis spanning $\mathcal{P}$, such that the coordinates of P in this plane are $(0,0)$. Given a radius $R \in \mathbb{R}^{*+}$, let $\mathcal{D}_R \subset \mathbb{R}^2$ be a disk of radius R centered at $(0,0)$. Let $\mathscr{F}(\mathcal{D}_R, \mathbb{K})$ be the set of continuous functions $f : \mathcal{D}_R \to \mathbb{K}$. Given $\mathscr{C}^K(\mathcal{D}_R, \mathbb{K})$ the vector space of K times continuously differentiable functions $f \in \mathscr{F}(\mathcal{D}_R, \mathbb{K})$, let $\mathcal{B}$ be a set of linearly independent elements in $\mathscr{F}(\mathcal{D}_R, \mathbb{K})$ and $\mathscr{F}_\mathcal{B}(\mathcal{D}_R, \mathbb{K}) \subset \mathscr{F}(\mathcal{D}_R, \mathbb{K})$ be a vector space spanned given a basis $\mathcal{B}$. If $\mathcal{B}$ is a family of K times derivable functions, then $\mathscr{F}_\mathcal{B}(\mathcal{D}_R, \mathbb{K}) \subset \mathscr{C}^K(\mathcal{D}_R, \mathbb{K})$.

Let $\mathcal{S} \in \mathscr{S}$ be a surface as defined in chapter 1. Let $\Omega \subset \mathcal{S}$ be a compact subset of $\mathcal{S}$ such that for a radius R, there exists a function $f \in \mathscr{F}(\mathcal{D}_R, \mathbb{R})$, mapping $\mathcal{D}_R$ to Ω such that $\forall Q \in \Omega$, the coordinates of Q can be locally written as $(x, y, f(x,y))$. Let $P \in \Omega$ such that P is mapped to the center of $\mathcal{D}_R$. Let $\mathscr{S}^K$ be the set of surfaces $\mathcal{S}$ such that all functions $f \in \mathscr{F}(\mathcal{D}_R \to \mathbb{R})$ representing the heightfield between the tangent plane at each point $P \in \mathcal{S}$ and the surface $\mathcal{S}$ are K times differentiable, i.e. $f \in \mathscr{C}^K$. IF, in addition, $f \in \mathscr{F}_\mathcal{B}(\mathcal{D}_R, \mathbb{R})$, the decomposition of $f \in \mathscr{F}_\mathcal{B}(\mathcal{D}_R, \mathbb{R})$ in basis $\mathcal{B}$ yields a set of coefficients. Each coefficient of such a decomposition holds information on f, and consequently on $\mathcal{S}$ at point P. f is a parameterization of Ω with respect to $\mathcal{D}_R$. Since f is bounded on a compact, f is in the space of square-integrable function $\mathscr{L}^2(\mathcal{D}_R, \mathbb{C})$ from $\mathcal{D}_R \subset \mathbb{R}^2 \to \mathbb{C}$. In this chapter, we will also use the standard inner product on $\mathscr{L}(\mathcal{D}_R, \Omega)$.

$$\langle f, g \rangle = \int_{(x,y)\in\mathcal{D}_R} f(x,y) g^*(x,y) dy dx \tag{2.1}$$

If $\mathcal{B}$ is orthonormal, the decomposition on $\mathcal{B}$ can be used to define a distance

between functions of $\mathscr{F}_{\mathcal{B}}(\mathcal{D}_R, \mathbb{R})$ by considering the Euclidian distance between the coefficients of the decomposition. For example, [Max+11] used Zernike polynomial basis, an orthogonal polar polynomial basis, to do local shape matching by computing distances between the local decompositions of surfaces at distinct points. In some other cases, non-orthogonal basis can be used if its elements express properties. Cazals et al. [CP05] used a basis giving direct access to high order derivatives of f at $(0,0)$. Given an positive integer K, this basis is the bivariate canonical polynomial basis of order lower than K, which they called osculating Jets. A method is proposed to estimate the Jets decomposition of a surface $\mathcal{S}$ on a point $P \in \mathcal{S}$. One can show that Jets coefficients are proportional to derivatives of f at $(0,0)$. They can be used to approximate with a high precision the normal and curvatures of $\mathcal{S}$ at P.

2.1.1 Jets fitting

[CP05] introduced the Jets, which are truncated bivariate Taylor expansion. They can be used for normal as well as curvature estimation. The Jets basis of order K is the family formed out of the bivariate monomials of total order lower than K. Given $R \in \mathbb{R}^{+*}$ and $(j,k) \in \mathbb{N}^2, 0 \leq j \leq k \leq K$, we note:

$$e^{\mathcal{J}}_{k-j,j} : \begin{array}{ccc} \mathcal{D}_R & \to & \mathbb{R} \\ (x,y) & \mapsto & x^{k-j}y^j \end{array} \tag{2.2}$$

The function basis of the Jets of order $K \in \mathbb{N}$ is the following:

$$\mathcal{B}^K_{\mathcal{J}} = \left\{ e^{\mathcal{J}}_{k-j,j} \middle| (j,k) \in \mathbb{N}^2 \text{ and } 0 \leq j \leq k \leq K \right\} \tag{2.3}$$

$\mathcal{B}^K_{\mathcal{J}}$ spans the function space:

$$\mathscr{F}^K(\mathcal{D}_R, \mathbb{R}) = \left\{ f \in \mathscr{C}^\infty(\mathcal{D}_R, \mathbb{R}) \middle| \, \forall k \in]K, \infty[, \forall j \in [\![0,k]\!], f_{x^{k-j}y^j} = 0 \right\} \tag{2.4}$$

A function $f \in \mathscr{F}^K(\mathcal{D}_R, \mathbb{R})$ approximating a local heighfield around a point P in a surface $\mathcal{S}$ can be decomposed in the Jets basis as:

$$f(x,y) = \sum_{k=0}^{K} \sum_{j=0}^{k} J_{k-j,j} x^{k-j} y^j \tag{2.5}$$

With $J_{k-j,j}$ the coefficient corresponding to $e^{\mathcal{J}}_{k-j,j}$. The cardinal of $\mathcal{B}^K_{\mathcal{J}}$ is $\frac{(K+1)(K+2)}{2}$. Let $\boldsymbol{J}$ be the vector of coefficients $J_{k-j,j}$ sorted in the same manner as function basis $e^{\mathcal{J}}_{k,n}$. Let us give the following definition for $\boldsymbol{J}$ given $f \in \mathscr{L}^2(\mathcal{D}_R, \mathbb{R})$:

$$\boldsymbol{J} = \underset{J}{\operatorname{argmin}} \left\| f - \sum_{k=0}^{K} \sum_{j=0}^{k} J_{k-j,j} e^{\mathcal{J}}_{k-j,j} \right\|^2 \tag{2.6}$$

Where $\|f\|^2 = \langle f, f \rangle$ is the squared norm of f following the canonical inner product of $\mathscr{L}^2(\mathcal{D}_R, \mathbb{R})$. If $f \in \mathscr{F}^K(\mathcal{D}_R, \mathbb{R})$, each coefficient $J_{j,k-j}$ is proportional to the corresponding derivative $f_{x^{k-j}y^j}(0,0)$. If f is K times continously differentiable, which we write $f \in \mathscr{C}^K(\mathcal{D}_R, \mathbb{R})$, [CP05] showed that each coefficient retrieved with equation (2.6) is such that:

$$J_{k-j,j} = \frac{1}{(k-j)!j!} f_{x^{k-j}y^j}(0,0) + o\left(R^{K-k}\right) \tag{2.7}$$

Equation (2.7) highlights a major interest of computing Jets out of a neighborhood on a surface: it permits to compute highly accurate differential quantities given a high order K. Given a surface $\mathcal{S} \in \mathscr{S}^K$, given a parameterization plane $\mathcal{P}$ passing by $P \in \mathcal{S}$, [CP05] proposed a method to retrieve an accurate tangent plane $\mathcal{T}$ at a point P out of estimated Jets. The tangent plane can be estimated from Jets computed w.r.t. $\mathcal{P}$ with a precision depending on the order K of the Jets.

This description is however limited to the continuous domain. In practice, when given a point set surface, if N points P_ℓ sample $\Omega \subset \mathcal{S}$, noting (x_ℓ, y_ℓ) the coordinates of P_ℓ in a local orthogonal basis of $\mathcal{P}$, and h_ℓ the heightfield orthogonal to $\mathcal{P}$ between $\mathcal{P}$ and the surface $\mathcal{S}$, Jets can be computed by linear regression. Given the vector of heights $H = (h_\ell)_{\ell \in [\![1,N]\!]}$, let M_J^K be the matrix whose coefficients are the values of each function basis at position (x_ℓ, y_ℓ). $\boldsymbol{J}$ is computed by solving:

$$\boldsymbol{J} = \underset{J}{\operatorname{argmin}} \left\| M_J^K J - H \right\|^2 \tag{2.8}$$

Jets are particularly useful to compute high accurate differential quantities. On the contrary, they are not well suited to build local surface descriptors because $\mathcal{B}_J^K$ is not orthogonal. The choise of the basis vectors $(\boldsymbol{x}, \boldsymbol{y})$ in $\mathcal{P}$ is also an issue since J varies a lot depending on the parameterization orientation.

Remark 1. *Given a neighborhood of cardinal N, if the chosen Jet order K is such that $\frac{(K+1)(K+2)}{2} > N$, then the system is underconstrained. Thus, the precision of differential quantities of order k that can be computed using osculating jets is bounded by the local point density.*

2.1.2 Zernike polynomials

Zernike polynomials are complex polar polynomials defined on the unit disk $\mathcal{D}_1$ introduced by [Zer34]. The family of Zernike polynomials of order lower than K is orthogonal w.r.t. the inner product $\langle f, g \rangle = \int_0^{2\pi} \int_0^1 f(r,\theta) g^*(r,\theta) r dr d\theta$. They were introduced to model efficiently lense optical aberrations. Each function in this basis has a specific name related to a class of optical aberration. They were later used to characterize 2D shapes in image processing [KH90; Lia93] as well as for 3D shapes [NK03; Max+11].

Let us define for $(n, m) \in \mathbb{Z} \times \mathbb{N}$ a radial polynomial $R_{n,m}$ defined on $[0, 1]$:

$$R_{n,m}(r) = \sum_{j=0}^{\frac{m-n}{2}} \frac{(-1)^j (m-j)!}{j! \left(\frac{n+m}{2} - j\right)! \left(\frac{m-n}{2} - j\right)!} r^{m-2j} \tag{2.9}$$

With $R_{n,m} = 0$ if n and m do not share the same parity. Given the function:

$$e_{n,m}^{\mathcal{Z}} : \begin{array}{ccc} [0,1] \times [0, 2\pi] & \to & \mathbb{C} \\ (r, \theta) & \mapsto & R_{n,m}(r) e^{in\theta} \end{array} \tag{2.10}$$

We note $\mathcal{B}_{\mathcal{Z}}^K$ the basis of Zernike polynomials of order lower than K:

$$\mathcal{B}_{\mathcal{Z}}^K = \left\{ e_{n,m}^{\mathcal{Z}} \middle| (n,m) \in \mathbb{Z} \times \mathbb{N} \text{ and } |n| \leq m \leq K \text{ and } |m-n| \equiv 0 \pmod 2 \right\} \tag{2.11}$$

There exists a linear map between $\mathcal{B}_{\mathcal{Z}}^K$ and $\mathcal{B}_{\mathcal{J}}^K$ restricted to functions defined on the unit disk, as we will show in section 2.2.2. Given f a function in the vector space

spanned by the Zernike polynomials of order lower than K, f can be expressed in polar coordinates as follows:

$$f(r,\theta) = \sum_{m=0}^{K} \sum_{n=-m}^{m} Z_{n,m} R_{n,m}(r) e^{in\theta} \tag{2.12}$$

Given a parameterization plane $\mathcal{P}$ parameterized by an arbitrary direct orthogonal basis $(\boldsymbol{x}, \boldsymbol{y})$, the magnitude of coefficients $Z_{n,m} \in \mathbb{C}$ is invariant w.r.t. the choice of the basis. This is a nice property which allows to build a local descriptor being invariant to the choice of local parameterizations. However, such a basis does not give a straightforward access to any differential quantities. This can be problematic because even if the magnitude of the coefficients are rotation invariant w.r.t. the choice of basis $(\boldsymbol{x}, \boldsymbol{y})$ within $\mathcal{P}$, they are not invariant w.r.t. the orientation of $\mathcal{P}$ in the ambient space $\mathbb{R}^3$, i.e. the choise of the normal to $\mathcal{P}$.

Zernike polynomials can be computed by regression in the same way Jets are, or by interpolating sampled points $P \in \mathcal{S}$ on a regular grid and then directly projecting on $\mathcal{B}^K_{\mathcal{Z}}$ with a Discrete Fourier Transform-like algorithm [Max+11]. The interpolation step could be alleviated by extending the work of [Mil15], who developped a method for applying Fast Fourier Transform algorithm to irregularly sampled data with a bounded error. To do so, a Voronoi diagram is computed on the samples positions, and each sample is weighted with the squared root of the area of the corresponding voronoi cell when computing the Discrete Fourier Transform. Even if this work does not directly apply to Zernike polynomials, a similar approach might give similar bounds on the estimation.

2.1.3 Angular Fourier series and differential analysis

While Jets are arranged by derivative order k and cross-order j, Zernike polynomials are arranged by an angular frequency n and orthogonal radial polynomials. This gives the intuition that derivatives of order k can be mapped to certain angular frequencies of order n. Decomposing local functions using Fourier series seems natural since the angular signal is periodic by construction.

Some approaches have tried to link differential quantities with local angular frequencies. [MT98] first introduced a frequency interpretation of the local variations on a surface. Given known principal curvatures, they construct a local descriptor which is named *second order smoothness operator*. It is defined as the integral over a circle of the square of Euler's curvature formula. In order to derive a closed form for the second order smoothness operator, the second order polynomial is written in polar coordinates and linearized to angular cosines using Euler's formula. A similar process is proposed to define a third order smoothness operator. Following this work, [JS10] proposed to interpret third order derivatives of a surface as Fourier series coefficients. Given a surface locally of order 3 estimated along a circle in the tangent plane, the Fourier coefficients of frequency 1 and 3 of this signal can be directly mapped to third order cross-derivatives of the surface. Hence, a one dimensional signal around a point is sufficient to extract high order derivatives. Unfortunately, if the surface has locally a non negligible 5^{th} order, this property does not hold. As we will show in chapter 3, the errors in the estimation of 3^{rd} order derivatives out of the Fourier decomposition of the surface along a circle in the tangent plane is in $O(R^2)$, where R is the radius of the circle, as shown in our work in [BD16]. Another limitation of this method is that one needs to be able to estimate the surface accurately along a circle in the tangent plane, in order to compute a Fourier Transform.

Interpreting high order derivatives as Fourier coefficients is interesting since it makes the orientation of the local tangential parameterization irrelevant. Indeed, a rotation in the parameterization plane around its normal is equivalent to a shift in the phase of Fourier series coefficients. [BD16] extend the work of [JS10] by directly expressing all derivatives of smooth surfaces $\mathcal{S} \in \mathscr{S}$ as Fourier series coefficients coupled with a Vandermonde matrix inversion. The surface is locally sampled on concentric circles. Fourier series coefficients are computed on each circle.

In the next section, we introduce the Wavejets: a local function basis giving a frequency interpretation of high order derivatives,interpreting surface derivatives as angular frequencies. Even if the Wavejets denomitation was first used in [BDC18], we first discovered them in [BD16]. Links with the Jets [CP05] and Zernike polynomials [Zer34] were discovered afterwards. The strong relationship between Wavejets and Jets should make the reason for their naming obvious. The last part of next section focuses on importants links between the Wavejets and differentiation operators called the Wirtinger derivatives [Wir27], which will be found quite useful when writing equations involving the Wavejets.

2.2 The Wavejets basis

The idea behind the introduction of the basis is to mix properties of both Jets and Zernike polynomial basis. Wavejets are polar polynomials whose radial parts contain differential information while being angularly orthogonal. Wavejets thus inherit from accuracy properties of differential quantities from osculating Jets. We will show that Wavejets are useful in surface analysis. Moreover, we show how a local Wavejet decomposition on a surface can be used to compute high order principal directions, using the framework of [Qi05; Qi06; Qi07] on tensors and supermatrices.

2.2.1 Definition

Given the following functions for $R \in \mathbb{R}^{+*}$:

$$e^{\Phi}_{k,n} : \begin{array}{ccc} [0,R] \times [0,2\pi[& \rightarrow & \mathbb{C} \\ (r,\theta) & \mapsto & r^k e^{in\theta} \end{array} \tag{2.13}$$

We define the Wavejets family as follow:

$$\mathcal{B}^K_\Phi = \left\{ e^{\Phi}_{k,n} \middle| (k,n) \in \mathbb{N} \times \mathbb{Z} \text{ and } |n| \leq k \leq K \text{ and } |k-n| \equiv 0 \pmod 2 \right\} \tag{2.14}$$

Figure 2.1 illustrates the first elements of the Wavejets basis. Since it would be difficult to visualize a surface decomposed in complex parts, positive and negative frequencies are bound together. The phase of the coefficient for those function basis for frequency n yields which angular direction the surface outlined by positive and negative frequencies of same order points to, while the module tells about the magnitude of the wave.

Property 1. *The Wavejets family forms a basis of the space of functions* $f : [0,R] \times [0,2\pi[\rightarrow \mathbb{R}$.

Proof. Given a polar coordinate system (r,θ) in the plane, the family of radial monomials $(r^k)_{k \in [\![0,K]\!]}$ for $r \in [0,R]$ is a basis of radial polynomials for any $K \in [\![0,\infty]\!]$. The family of exponential monomials, also known as the Fourier series basis $(e^{in\theta})_{|n| \leq K}$ for $\theta \in [0,2\pi[$ is also a basis of complex functions for $K \in [\![0,\infty]\!]$. One can span a

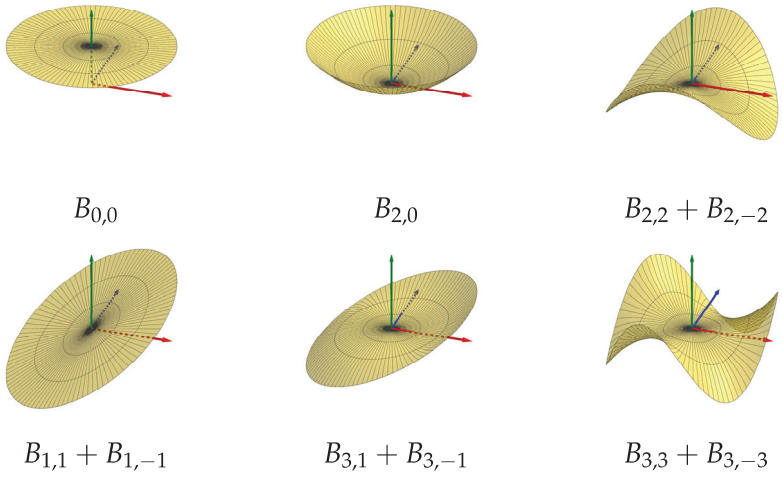

FIGURE 2.1: First elements of the Wavejets basis. Positive and negative frequencies of elements of same order are bound in order to be able to be visualized.

subspace of the real functions vector space $\mathscr{L}([0, 2\pi[, \mathbb{R})$ with this basis if all the coefficients bound with n equal the conjugate of the coefficients of $-n$ for $|n| \leq K$. Noticing that the Wavejets family is a subset of the cartesian product of those two first basis, the Wavejets family is a basis of real polar functions on a disc of radius R centered at the origin of the polar coordinate system. □

Decomposing a function f in $\mathcal{B}_\Phi^K$ on this basis yields:

$$f(r,\theta) = \sum_{k=0}^{K} \sum_{n=-k}^{k} \phi_{k,n} r^k e^{in\theta} \tag{2.15}$$

Each coefficient $\phi_{k,n}$ is said to be of polynomial order k and of angular frequency n. Wavejets inherit differential stability properties from Jets and angular orthogonality from Zernike Polynomials as we will see in the next section.

The cardinal of $\mathcal{B}_\Phi^K$ is $\frac{(K+1)(K+2)}{2}$. This can be deduced from the formula of the sum of an arithmetic sequence given in equation (2.15).

Similarly to the definition given Jets in section 2.1.1, given a function $f \in F^K$ and a disk U of radius R, the vector of coefficients $\boldsymbol{\phi}$ has the following definition:

$$\boldsymbol{\phi} = \underset{\boldsymbol{\phi}}{\operatorname{argmin}} \left\| f - \sum_{k=0}^{K} \sum_{n=-k}^{k} \phi_{k,n} e_{k,n}^{\phi} \right\|^2 \tag{2.16}$$

Where $\boldsymbol{\phi}$ is a vector of coefficients $\phi_{k,n}$ sorted in the same manner as the corresponding basis functions $e_{k,n}^{\Phi}$. If $f \notin \mathscr{F}^K$, then the decomposition yields an approximation of f on $\mathcal{B}_\Phi^K$.

2.2.2 Links with Jets and Zernike polynomials

Property 2. *There exists a linear mapping from Wavejets coefficients to Jets coefficients*

Proof. Let us begin from the Jets decomposition of a function $f \in \mathscr{F}^K(\mathcal{D}_R, \mathbb{R})$ and then write it in polar coordinate s.t. $(r\cos\theta, r\sin\theta) = (x, y)$:

$$
\begin{aligned}
f(x,y) &= \sum_{k=0}^{K}\sum_{j=0}^{k} J_{k-j,j}x^{k-j}y^j \\
&= \sum_{k=0}^{K}\sum_{j=0}^{k} \frac{f_{x^{k-j}y^j}(0,0)}{(k-j)j!}x^{k-j}y^j \\
&= \sum_{k=0}^{K}\sum_{j=0}^{k} \frac{f_{x^{k-j}y^j}(0,0)}{(k-j)!j!}r^{k-j}\cos^{k-j}\theta r^j \sin^j\theta \\
&= \sum_{k=0}^{K} r^k \sum_{j=0}^{k} \frac{f_{x^{k-j}y^j}(0,0)}{(k-j)!j!}\cos^{k-j}\theta \sin^j\theta \\
&= \sum_{k_0=0}^{\lfloor \frac{K}{2} \rfloor} \left(r^{2k_0} \sum_{j=0}^{2k_0} \frac{f_{x^{2k_0-j}y^j}(0,0)}{(2k_0-j)!j!}\cos^{2k_0-j}\theta\sin^j\theta \right. \\
&\qquad \left. + r^{2k_0+1}\sum_{j=0}^{2k_0+1}\frac{f_{x^{2k_0+1-j}y^j}(0,0)}{(2k_0+1-j)!j!}\cos^{2k_0+1-j}\theta\sin^j\theta \right) \\
&= \sum_{k_p=0}^{1}\sum_{k_0=0}^{\lfloor \frac{K}{2} \rfloor} r^{2k_0+k_p} \sum_{j=0}^{2k_0+k_p} \frac{f_{x^{2k_0+k_p-j}y^j}(0,0)}{(2k_0+k_p-j)!j!}\cos^{2k_0+k_p-j}\theta\sin^j\theta \\
&= \sum_{k_p=0}^{1}\sum_{k_0=0}^{\lfloor \frac{K}{2} \rfloor} r^{2k_0+k_p} \sum_{j=0}^{2k_0+k_p} \frac{f_{x^{2k_0+k_p-j}y^j}(0,0)}{(2k_0+k_p-j)!j!} \\
&\qquad \times \sum_{n_0=0}^{k_0} \left(a_{j,2k_0+k_p,2n_0+k_p}\cos(2n_0+k_p)\theta \right. \\
&\qquad\qquad \left. + b_{j,2k_0+k_p,2n_0+k_p}\sin(2n_0+k_p)\theta \right) \\
&= \sum_{k=0}^{K} r^k \sum_{j=0}^{k} \frac{f_{x^{k-j}y^j}(0,0)}{(k-j)!j!} \sum_{\substack{n=0 \\ (n+k)\%2=0}}^{k} \left(a_{j,k,n}\cos n\theta + b_{j,k,n}\sin n\theta\right) \\
&= \sum_{k=0}^{K} \sum_{\substack{n=0 \\ (n+k)\%2=0}}^{k} r^k \sum_{j=0}^{k} \frac{f_{x^{k-j}y^j}(0,0)}{(k-j)!j!} \left(a_{j,k,n}\cos n\theta + b_{j,k,n}\sin n\theta\right) \\
&= \sum_{k=0}^{K} \sum_{\substack{n=-k \\ (n+k)\%2=0}}^{k} r^k \left(\mathrm{Re}(\phi_{k,n})\cos n\theta + \mathrm{Im}(\phi_{k,n})\sin n\theta\right) \\
&= \sum_{k=0}^{K} \sum_{\substack{n=-k \\ (n+k)\%2=0}}^{k} \phi_{k,n} r^k e^{in\theta}
\end{aligned}
$$

Where $\phi_{k,n} \in \mathbb{C}$ s.t. $\phi_{k,n} = \phi^*_{k,-n}$. n and k share the same parity everywhere since if k is odd (resp. even), the decomposition of $\cos^{k-j}\theta\sin^j\theta$ will only make odd (resp. even) frequencies appear, as we will show in the following. To simplify the final expression of last equation, recall that $\phi_{k,n} = 0$ if k and n do not share parity, which allows us to remove the constraint $(n+k)\%2 = 0$, which is unnecessary.

$a_{j,k,n}$ and $b_{j,k,n}$ are the coefficients of the linearization of power of cosines using Euler's formula and Newton's binomial, which we derive in the following part of the proof. Let us give an explicit expression for a and b by linearizing power of cosines:

$$\cos^{2k_0+k_p-j}\theta\sin^j\theta = \sum_{n_0=0}^{k_0}\left(a_{j,2k_0+k_p,2n_0+k_p}\cos(2n_0+k_p)\theta + b_{j,2k_0+k_p,2n_0+k_p}\sin(2n_0+k_p)\theta\right)$$

$$\begin{aligned}
\cos^{2k_0+k_p-j}\theta\sin^j\theta &= \left(\frac{e^{i\theta}+e^{-i\theta}}{2}\right)^{2k_0+k_p-j}\left(\frac{e^{i\theta}-e^{-i\theta}}{2i}\right)^j \\
&= \left(\frac{1}{2^{2k_0+k_p-j}}\sum_{l_1=0}^{2k_0+k_p-j}\binom{2k_0+k_p-j}{l_1}e^{-i(2k_0+k_p-j-l_1)\theta}e^{-il_1\theta}\right) \\
&\quad\times\left(\frac{1}{(2i)^j}\sum_{l_2=0}^{j}(-1)^{l_2}\binom{j}{l_2}e^{i(j-l_2)\theta}e^{-il_2\theta}\right) \\
&= \left(\frac{1}{2^{2k_0+k_p-j}}\sum_{l_1=0}^{2k_0+k_p-j}\binom{2k_0+k_p-j}{l_1}e^{-i(2k_0+k_p-j-2l_1)\theta}\right) \\
&\quad\times\left(\frac{1}{(2i)^j}\sum_{l_2=0}^{j}(-1)^{l_2}\binom{j}{l_2}e^{i(j-2l_2)\theta}\right) \\
&= \frac{1}{2^{2k_0+k_p}i^j}\sum_{l_1=0}^{2k_0+k_p-j}\sum_{l_2=0}^{j}(-1)^{l_2}\binom{2k_0+k_p-j}{l_1}\binom{j}{l_2}e^{2i(k_0+k_p-l_1-l_2)\theta} \\
&= \frac{1}{2^{2k_0+k_p}i^j}\sum_{l=0}^{2k_0+k_p}\left(\sum_{l_1+l_2=l}(-1)^{l_2}\binom{2k_0+k_p-j}{l_1}\binom{j}{l_2}\right)e^{i(2k_0+k_p-2l)\theta} \\
&= \frac{1}{2^{2k_0+k_p}i^j}\sum_{l=0}^{2k_0+k_p}c_{l,2k_0+k_p,j}e^{i(2k_0+k_p-2l)\theta} \\
&= \frac{1}{2^{2k_0+k_p}i^{2j_0+j_p}}\sum_{l=0}^{2k_0+k_p}c_{l,2k_0+k_p,j}e^{i(2k_0+k_p-2l)\theta} \\
&= \frac{1}{2^{2k_0+k_p}(-1)^{j_0}i^{j_p}}\sum_{l=0}^{2k_0+k_p}c_{l,2k_0+k_p,j}e^{i(2k_0+k_p-2l)\theta} \\
&= \frac{1}{2^{2k_0+k_p}(-1)^{j_0}i^{j_p}}\sum_{l=0}^{2k_0+k_p}c_{l,2k_0+k_p,j}\Big(\cos(2k_0+k_p-2l)\theta \\
&\qquad\qquad + i\sin(2k_0+k_p-2l)\theta\Big)
\end{aligned}$$

Where $j = 2j_0 + j_p$ and $c(l,k,j) = \sum_{l_1+l_2=l}(-1)^{l_2}\binom{k-j}{l_1}\binom{j}{l_2}$.

Last equation states that if j is odd, since $\cos^{k-j}\theta\sin^j\theta \in \mathbb{R}$, this expression is necessarily a sum of sines. If j is even, then it is a sum of cosines. $a(j,k,n)$ and $b(j,k,n)$ are the coefficients in front of every coefficient of frequency n, so they depend on

$c(l,k,j)$ and values of a and b can be deduced depending on the parity of j:

$$\begin{aligned}
a_{2j_0,2k_0+k_p,2n_0+k_p} &= \frac{1}{2^{2k_0+k_p}(-1)^{j_0}} \sum_{2k_0+k_p-2l=|2n_0+k_p|} c_{l,2k_0+k_p,2j_0} \\
&= \frac{1}{2^{2k_0+k_p}(-1)^{j_0}} \left(c_{k_0-n_0,2k_0+k_p,2j_0} + c_{k_0+n_0+k_p,2k_0+k_p,2j_0} \right) \\
a_{2j_0+1,2k_0+k_p,2n_0+k_p} &= 0 \\
a_{2j_0,2k_0,0} &= \frac{1}{2^{2k_0}(-1)^{j_0}} c_{k_0,2k_0,2j_0} \\
b_{2j_0,2k_0+k_p,2n_0+k_p} &= 0 \\
b_{2j_0+1,2k_0+k_p,2n_0+k_p} &= \frac{1}{2^{2k_0+k_p}(-1)^{j_0}} \left(c_{k_0-n_0,2k_0+k_p,2j_0+1} - c_{k_0+n_0+k_p,2k_0+k_p,2j_0+1} \right) \\
b_{2j_0+1,2k_0,0} &= 0
\end{aligned} \tag{2.17}$$

We showed the closed form expression for $a_{j,k,l}$ and $b_{j,k,l}$ and that:

$$\begin{aligned}
\phi_{k,n} &= \sum_{j=0}^{k} \frac{f_{\boldsymbol{x}^{k-j}\boldsymbol{y}^j}(0,0)}{(k-j)!j!}(a_{j,k,n} + \boldsymbol{i} b_{j,k,n}) \\
&= \sum_{j=0}^{k} J_{k-j,j}(a_{j,k,n} + \boldsymbol{i} b_{j,k,n})
\end{aligned} \tag{2.18}$$

We thus expressed the linear application mapping Jets coefficients to Wavejets coefficients. □

A direct consequence of Property 2 is that $\mathcal{B}_\Phi^K$ spans $\mathscr{F}^K(\mathcal{D}_R, \mathbb{R})$. Let us now link Zernike polynomials and Wavejets.

Corollary 1. *Zernike polynomials and Wavejets on the unit disk are linearly mapped.*

Proof. Each element from the Zernike polynomial basis is a linear combination of monomials of order m times complex exponentials of frequency n with n and m always sharing parity. In other words, Zernike polynomials are directly written as linear combinations of Wavejets. □

An important osculating Jet property can now directly be applied to Wavejets coefficients: Given a Wavejet decomposition of a local heightfield estimated for an order K, the error of coefficient $\phi_{k,n}$ is in $o(R^{K-k})$.

Corollary 2. *Given $f \in \mathscr{C}^\infty$ in a neighborhood of radius R centered at $(0,0)$, given ϕ^∞ the Wavejet decomposition of infinite order and ϕ the projection of f on $\mathscr{F}^K(\mathcal{D}_R, \mathbb{R})$ in the Wavejet basis:*

- $f \in \mathscr{F}^K(\mathcal{D}_R, \mathbb{R}) \Leftrightarrow \sum_{k=0}^{K} \sum_{n=-k}^{k} \phi_{k,n} \boldsymbol{e}_{k,n}^{\phi} = f$
- $f \in \mathscr{C}^K(\mathcal{D}_R, \mathbb{R}) \Rightarrow \phi_{k,n} = \phi_{k,n}^\infty + o(R^{K-k})$

Proof.

- Since $\mathcal{B}_\phi^K$ spans $\mathscr{F}^K(\mathcal{D}_R, \mathbb{R})$, if $f \in \mathscr{F}^K(\mathcal{D}_R, \mathbb{R})$, the Wavejets decomposition $\phi_{k,n}$ of f is exact.
- Since coefficients $\phi_{k,n}$ of a Wavejet of order K are linear combinations of coefficients $J_{k-j,j}$ of a K-jet, equation (2.7) is applied to Wavejets. Note that the derivative $f_{\boldsymbol{x}^{k-j}\boldsymbol{y}^k}(0,0)$ can be exactly derived from coefficient $J_{k-j,j}$ of an ∞-Jet.

□

The distribution of cross-derivatives $\frac{\partial^k f}{\partial x^{k-j}\partial y^j}$ in Wavejets coefficients $\phi_{k,n}$ can be directly deduced from the proof of Property 2.

Corollary 3. *If k and n share same parity:*

$$\begin{aligned} Re(\phi_{k,n}) &= \sum_{j=0}^{k} \frac{f_{\boldsymbol{x}^{k-j}\boldsymbol{y}}}{(k-j)!j!} a_{j,k,n} \\ Im(\phi_{k,n}) &= \sum_{j=0}^{k} \frac{f_{\boldsymbol{x}^{k-j}\boldsymbol{y}}}{(k-j)!(j)!} b_{j,k,n} \end{aligned} \tag{2.19}$$

Moreover, $Re(\phi_{k,n})$ (resp. $Im(\phi_{k,n})$) is a linear combination of $f_{\boldsymbol{x}^{k-j}\boldsymbol{y}^j}$ restricted to j even, (resp. odd).

Proof. If j is odd (resp. even), $a(j,k,n) = 0$ (resp. $b(j,k,n) = 0$) (refer to equation (2.17) from proof of Property 2). □

2.2.3 Wavejets for surfaces

Given a surface $\mathcal{S} \in \mathscr{S}^K$, the Wavejets decomposition ϕ of functions $f \in \mathscr{F}^K(\mathcal{D}_R, \mathbb{R})$ encoding the local heightfield between a parameterizing plane $\mathcal{P}$ passing by $P \in \mathcal{S}$ have a few interesting properties. For example, $\phi_{0,0} = f(0,\theta) = 0$ by construction. Coefficients $\phi_{1,\pm1}$ yield a direct link between the tangent plane $\mathcal{T}(P)$ and $\mathcal{P}$. More precisely, if $\mathcal{P} = \mathcal{T}(P)$, then $\phi_{1,\pm1} = 0$.

Property 3. *Let $\mathcal{S} \in \mathscr{S}^K$. Let $f \in \mathscr{F}^K(\mathcal{D}_R, \mathbb{R})$ be the local height field between $\mathcal{S}$ and a plane $\mathcal{P}$ passing by a point $P \in \mathcal{S}$ in an arbitrary direct orthonormal basis, expressed in polar coordinates in the tangent plane. Let $\mathcal{T}(P)$ be the tangent plane at P. Let $\boldsymbol{\phi}$ be the Wavejets decomposition of f of order K defined by equation (2.16). If $\mathcal{P}(P) = \mathcal{T}(P)$, then:*

$$\phi_{1,\pm1} = o\left(R^{K-1}\right) \tag{2.20}$$

Proof. Using equation (2.19), it is straightforward to show that $\phi_{1,1} + \phi_{1,-1} = J_{1,0}$ and that $\phi_{1,1} - \phi_{1,-1} = \boldsymbol{i} J_{0,1}$ where $J_{k-j,j}$ are Jets coefficients. Since $\mathcal{P}(P) = \mathcal{T}(P) \Rightarrow J_{1,0} = J_{0,1} = o\left(R^{K-1}\right)$ (see [CP05]), the property is true. □

A parameterization plane correction procedure similar to the one using osculating Jets can thus be applied to Wavejets to infer the tangent plane, which leads to the following corollary:

Corollary 4. *Let $\mathcal{S} \in \mathscr{S}^K$. Let $f \in \mathscr{F}^K(\mathcal{D}_R, \mathbb{R})$ be the local height field between $\mathcal{S}$ and a plane $\mathcal{P}$ passing by a point $P \in \mathcal{S}$ in an arbitrary direct orthonormal basis, expressed in polar coordinates in the tangent plane $\mathcal{T}(P)$ at P. Let $\boldsymbol{\phi}$ be the Wavejets decomposition of f defined by equation (2.16). If $\mathcal{P}(P) \neq \mathcal{T}(P)$, given $R_{\boldsymbol{u},\gamma}$ the rotation matrix of axis $\boldsymbol{u}$ and angle γ defined as follows:*

$$\begin{aligned} \boldsymbol{u} &= \boldsymbol{x}\sin\left(\arg(\phi_{1,1})\right) - \boldsymbol{y}\cos\left(\arg(\phi_{1,1})\right) \\ \gamma &= \tan^{-1}\left(\frac{1}{2}\sqrt{\phi_{1,1}\phi_{1,-1}}\right) \end{aligned} \tag{2.21}$$

$R_{\boldsymbol{u},\gamma}$ corrects $\mathcal{P}(P)$ to $\mathcal{T}(P)$ with an error in $o(R^{K-1})$.

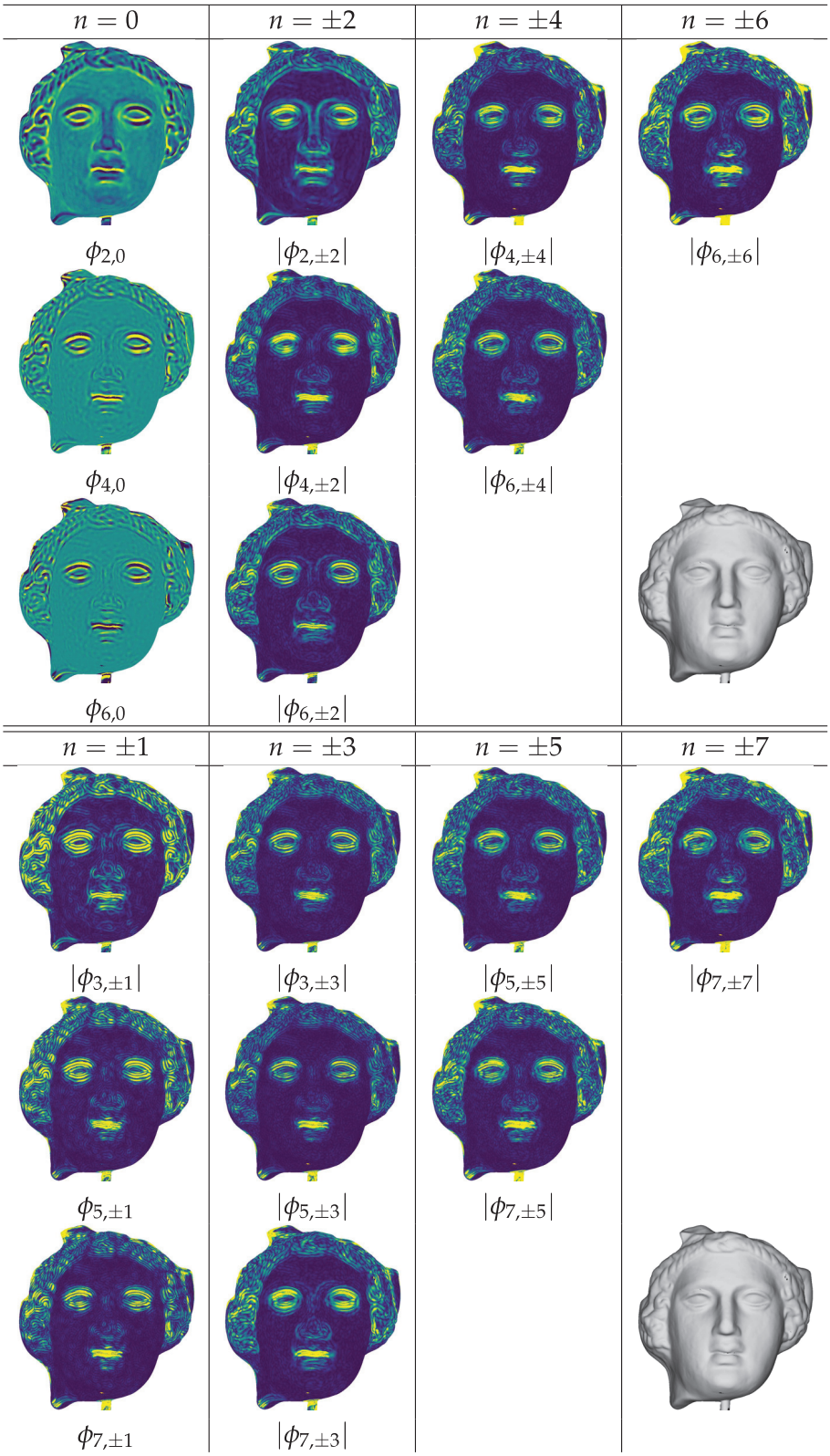

FIGURE 2.2: Example of coefficients $\phi_{k,n}$ computed over a surface $\mathcal{S}$ in the tangent plane. Note that $\phi_{k,0} \in \mathbb{R}$ while if $n \neq 0$, $\phi_{k,n} \in \mathbb{C}$. $\phi_{0,0}$ and $|\phi_{1,\pm 1}|$ are not show because they are equal to zero by construction.

Proof. The axis $\boldsymbol{u}$ of rotation transforming the vector $\boldsymbol{x} \wedge \boldsymbol{y}$ to the normal of the tangent plane $\boldsymbol{n}$ has the same direction as:

$$\boldsymbol{u} = \begin{pmatrix} 0 \\ 0 \\ 1 \end{pmatrix} \wedge \begin{pmatrix} -f_x \\ -f_y \\ 1 \end{pmatrix} = \begin{pmatrix} f_y \\ -f_x \\ 0 \end{pmatrix} = f_y \boldsymbol{x} - f_x \boldsymbol{y} \tag{2.22}$$

Identifying $\mathcal{P}$ with the complex plane, $\boldsymbol{u}$ is the direction of $-i\phi_{1,1}$, i.e. it is $\boldsymbol{x} \sin\left(\arg(\phi_{1,1})\right) - \boldsymbol{y} \cos\left(\arg(\phi_{1,1})\right)$.

Let us now discuss angle γ, the angle between the current normal and the *true* normal:

$$\begin{aligned} \cos\gamma &= \langle \boldsymbol{x} \wedge \boldsymbol{y}, \boldsymbol{n} \rangle = \frac{1}{\sqrt{1 + f_x^2 f_y^2}} \\ \sin\gamma &= \|(\boldsymbol{x} \wedge \boldsymbol{y}) \wedge \boldsymbol{n}\| = \sqrt{\frac{f_x^2 + f_y^2}{1 + f_x^2 f_y^2}} \end{aligned} \tag{2.23}$$

Thus, $\tan\gamma = \sqrt{f_x^2 + f_y^2} = \frac{1}{2}\sqrt{\phi_{1,1}\phi_{1,-1}}$, which concludes the proof.

□

A visualization of Wavejets coefficients as scalar fields over a surface is shown in Figure 2.2. While derivatives are usually sorted by their order, Wavejets coefficients $\phi_{k,n}$ of different order k but of same frequency n exhibit a similar aspect over the surface. It is thus interesting to sort them by frequency and to rearrange the orders in a good manner. This will be done in chapter 3 in which we introduce new integral invariants.

Let $(\boldsymbol{x}, \boldsymbol{y})$ be an orthonormal basis of in a plane $\mathcal{P}(P)$ passing by $P \in \mathcal{S}$. Let us express the local heightfield $f \in \mathscr{F}^2(\mathcal{D}_R, \mathbb{R})$ in this parameterization. Concerning second order coefficients, $\phi_{2,n}$ can be expressed out of the second derivatives of f:

$$\phi_{2,0} = \frac{1}{2}(f_{xx} + f_{yy}) \; ; \phi_{2,2} = \phi_{2,-2}^* = \frac{1}{4}(f_{xx} - f_{yy} + i f_{xy}) \tag{2.24}$$

The mean curvature $\mathcal{H}(P)$ and Gaussian curvature $\mathcal{K}(P)$ can be computed using Wavejets coefficients at point P given any parameterization plane $\mathcal{P}(P)$. Since the Gaussian curvature $\mathcal{K}(P)$ can be expressed w.r.t. partial derivatives of f at P as $\mathcal{K}(P) = \frac{f_{xx}f_{yy} - f_{xy}^2}{(1+f_x^2+f_y^2)^2}$, we get:

$$\mathcal{K}(P) = \frac{4\phi_{2,0}^2 - 16\phi_{2,-2}\phi_{2,2}}{\left(1 + 4\phi_{1,-1}\phi_{1,1}\right)^2} \tag{2.25}$$

Similarly, the mean curvature can be expressed as $\mathcal{H}(P) = \frac{(1+f_x^2)f_{xx} + (1+f_y^2)f_{yy} - 2f_x f_y f_{xy}}{2(1+f_x^2+f_y^2)^{\frac{2}{3}}}$:

$$\mathcal{H}(P) = \frac{2\phi_{2,0}\left(1 + 4\phi_{1,-1}\phi_{1,1}\right) + 4\phi_{2,-2}\phi_{1,1}^2 + 4\phi_{2,2}\phi_{1,-1}^2}{\left(1 + 4\phi_{1,-1}\phi_{1,1}\right)^{\frac{3}{2}}} \tag{2.26}$$

If $\mathcal{P}(P) = \mathcal{T}(P)$, the tangent plane to $\mathcal{S}$ at P, then $\phi_{1,1} = \phi_{1,-1} = 0$, and :

$$\mathcal{K}(P) = 4\left(\phi_{2,0}^2 - 4\phi_{2,-2}\phi_{2,2}\right) \; , \; \mathcal{H}(P) = 2\phi_{2,0} \tag{2.27}$$

The principal directions can be found using Wavejets by considering the signal $\sum_{n=-2}^{2} \phi_{2,n} e^{in\theta}$. This signal contains a constant component $\phi_{2,0}$ and a component that oscillates angularly twice and whose maximum is aligned with the first principal curvature direction (corresponding to the phase of $\phi_{2,-2}$). As a consequence, the principal curvatures κ_1 and κ_2 can also be recovered using Wavejets if $\mathcal{P}(P) = \mathcal{T}(P)$:

$$\kappa_1 = 2\left(\phi_{2,0} + \phi_{2,2} + \phi_{2,-2}\right) \text{ and } \kappa_2 = 2\left(\phi_{2,0} - \phi_{2,2} - \phi_{2,-2}\right) \tag{2.28}$$

Let us now focus on invariant properties of Wavejets coefficients. Similarly to Zernike polynomials, Wavejets coefficients magnitude are invariant w.r.t. a rotation with axis $\boldsymbol{x} \wedge \boldsymbol{y}$. Given a tangential parameterization $(\boldsymbol{x}, \boldsymbol{y})$, Wavejets coefficients $\phi_{k,n}$ can be expressed in any other parameterization $(\boldsymbol{x}', \boldsymbol{y}')$ by a phase shift using the delay formula of the Fourier Transform. Wavejets coefficients $\phi_{k,n}$ of the decomposition of a function f expressed in $(\boldsymbol{x}, \boldsymbol{y})$ can be used to get the new coefficients $\phi^{\boldsymbol{u}}_{k,n}$ in another parameterization $(\boldsymbol{u}, \boldsymbol{u}^{\perp})$ in plane $\mathcal{P}(P)$, where $\boldsymbol{u} \perp \boldsymbol{u}^{\perp}$ and $\boldsymbol{u} = \boldsymbol{x}\cos\mu + \boldsymbol{y}\sin\mu$. $\phi^{\boldsymbol{u}}_{k,n}$ is expressed as follows:

$$\forall (k,n) \in \mathbb{N} \times \mathbb{Z}, \phi^{\boldsymbol{u}}_{k,n} = \phi_{k,n} e^{-in\mu} \tag{2.29}$$

2.2.4 l-harmonic functions

We show in this section that a subset of Wavejets basis vectors $\mathcal{B}^K_\phi$ spans the space of l-harmonic functions with derivatives of order greater than K equal to zero. We call $\mathscr{H}^K_l(\mathcal{D}_R, \mathbb{R}) \subset \mathscr{F}^K(\mathcal{D}_R, \mathbb{R})$ the set of such functions. Let us first give the definition of an l-harmonic function and then link them to the Wavejets basis.

$$\mathscr{H}^K_l(\mathcal{D}_R, \mathbb{R}) = \left\{ f \in \mathscr{F}^K(\mathcal{D}_R, \mathbb{R}) \middle| \nabla^{2l} f = \Delta^l f = 0 \right\} \tag{2.30}$$

Theorem 1. *Given $\phi_{k,n}$ the decomposition of a function $f \in \mathscr{F}^K$ or $\mathcal{B}^K_\phi$, the following equivalence holds: $f \in \mathscr{H}^K_l$ if and only if for all $(k,n) \in \mathbb{N} \times \mathbb{Z}$ such that $k - |n| \geq 2l$, then $\phi_{k,n} = 0$*

Proof. Let us write the Laplacian operator in polar coordinates:

$$\Delta = \frac{\partial^2}{\partial r^2} + \frac{1}{r}\frac{\partial}{\partial r} + \frac{1}{r^2}\frac{\partial^2}{\partial \theta^2} \tag{2.31}$$

Given $K \geq 2$,

$$\begin{aligned}
\frac{\partial^2 f}{\partial r^2} &= \sum_{k=2}^{K} \sum_{n=-k}^{k} \phi_{k,n}(k-1) k r^{k-2} e^{in\theta} \\
\frac{1}{r}\frac{\partial f}{\partial r} &= \frac{1}{r}\left(\phi_{1,1} e^{i\theta} + \phi_{1,-1} e^{-i\theta}\right) + \sum_{k=2}^{K} \sum_{n=-k}^{k} \phi_{k,n} k r^{k-2} e^{in\theta} \\
\frac{1}{r^2}\frac{\partial^2 f}{\partial \theta^2} &= -\frac{1}{r}\left(\phi_{1,1} e^{i\theta} + \phi_{1,-1} e^{-i\theta}\right) - \sum_{k=2}^{K} \sum_{n=-k}^{k} \phi_{k,n} n^2 r^{k-2} e^{in\theta}
\end{aligned} \tag{2.32}$$

This leads to:

$$\Delta f = \sum_{k=2}^{K} \sum_{n=-k}^{k} (k^2 - n^2) \phi_{k,n} r^{k-2} e^{in\theta} \tag{2.33}$$

Let us now consider function $\Delta^l f$ whose Wavejets coefficients of order $(K-2l)$ are $\phi^{(l)}_{k,n}$. Noticing that $\Delta^{l+1} f = \Delta(\Delta^l f)$, equation (2.33) leads to the following relationship for $l \geq 0$:

$$\phi^{(l+1)}_{k,n} = \left((k+2)^2 - n^2\right) \phi^{(l)}_{k+2,n} \tag{2.34}$$

With $\phi^{(0)}_{k,n} = \phi_{k,n}$. Equation (2.34) can be rewritten as follows for $l > 0$:

$$\phi^{(l)}_{k-2l,n} = \phi_{k,n} \prod_{\substack{m=k-2l+2 \\ (m-k)\%2=0}}^{k} \left(m^2 - n^2\right) \tag{2.35}$$

Recalling that f is l-harmonic if and only if $\Delta^l f = 0$, equation (2.35) states that $f \in \mathscr{H}^K_\ell$ if and only if all coefficients $\phi_{k,n}$ such that n is between $k-2l+2$ and k are equal to zero, which concludes the proof. □

Corollary 5. *The following function basis*

$$\mathcal{B}^K_{\mathscr{H}_l} = \left\{ r^k e^{in\theta} \middle| (k,n) \in \mathbb{N} \times \mathbb{Z} \text{ and } k \leq K \text{ and } |n| \leq k \text{ and } k - |n| < 2l \right\} \tag{2.36}$$

Spans $\mathscr{H}^K_\ell(\mathcal{D}_R, \mathbb{R})$

Proof. This is a direct consequence of Theorem 1. □

2.2.5 Stability

As shown by [CP05], the tangent plane $\mathcal{T}(P)$ at point $P \in \mathcal{S}$ can be retrieved with a high accuracy from the Jets coefficients. This property is interesting, but there is no results on how coefficients $J_{k-j,j}$ vary when the parameterization plane is corrected. Given a corrected parameterization plane to the tangent plane, Jets can be recomputed, which is computationally expensive. In this section, we show a stability theorem for Wavejets, allowing to retrieve all coefficients $\phi_{k,n}$ given a small parameterization plane orientation angle change γ in $\mathbb{R}^3$.

Theorem 2. *The coefficients $\Phi_{k,n}$ w.r.t. $\mathcal{P}(P)$ can be expressed w.r.t the coefficients $\phi_{k,n}$ in the tangent plane $\mathcal{T}(P)$, where $\mathcal{P}(P)$ and $\mathcal{T}(P)$ intersect along a vector $\boldsymbol{u}$ and where $\phi_{k,n}$ and $\Phi_{k,n}$ are both beforehand rephased w.r.t. $\boldsymbol{u}$ thanks to equation 2.29, as follows:*

$$\begin{aligned} \Phi_{0,0} &= 0 \\ \Phi_{1,1} &= \Phi^*_{1,-1} = \frac{\gamma}{2} e^{-\boldsymbol{i}\frac{\pi}{2}} + o(\gamma) \\ \Phi_{k,n} &= \phi_{k,n} + \gamma F_{k,n}(\phi) + o(\gamma) \end{aligned} \tag{2.37}$$

Where $F_{k,n}(\phi)$ is a linear combination of Wavejets coefficients with lower order that k and lower frequency magnitude than $|n|$, and where γ is the angle error between $\mathcal{P}(P)$ and $\mathcal{T}(P)$.

Proof. Let us first recall the setting of this theorem. Let us call $\mathcal{T}(P)$ the true tangent plane and $\mathcal{P}(P)$ the chosen parameterization plane, also passing through P. One can find an axis $(P, \boldsymbol{u})$ and angle γ such that the rotation of axis $(P, \boldsymbol{u})$ and angle γ transforms $\mathcal{P}(P)$ into $\mathcal{T}(P)$. Since P belongs to both planes, $(P, \boldsymbol{u})$ is aligned with line $\mathcal{T}(P) \cap \mathcal{P}(P)$. Let us parameterize $\mathcal{T}(P)$ and $\mathcal{P}(P)$ so that a point of the surface has coordinates $(x = r\cos\theta, y = r\sin\theta, h)$ over $\mathcal{T}(P)$ and $(x = R\cos\Theta, y = R\sin\Theta, H)$ over $\mathcal{P}(P)$. Let us first assume that θ (resp. Θ) corresponds to the angular coordinate

of point Q with respect an origin vector aligned with $\boldsymbol{u}$ in $\mathcal{T}(P)$ (resp. with $\boldsymbol{u}$ in $\mathcal{P}(P)$). We will state our main theorem in this setting and the generalization will follow naturally. In this setting the surface Wavejets decomposition at point Q writes $\sum_{n=0}^{K}\sum_{k=0}^{K}\phi_{k,n}r^k e^{in\theta}$ over the tangent plane $\mathcal{T}(P)$ and as $\sum_{n=0}^{K}\sum_{k=0}^{K}\Phi_{k,n}r^k e^{in\Theta}$ over $\mathcal{P}(P)$. We can express the $\Phi_{k,n}$ coefficients with respect to $\phi_{k,n}$ and the rotation angle γ. To generalize the theorem to arbitrary origin vectors for the angular coordinate in $\mathcal{T}(P)$ and $\mathcal{P}(P)$ for θ and Θ, recall that a change of reference vector in $\mathcal{T}(P)$ amongs to a phase shift μ, one can always change the origin vector, compute the wavejets coefficients $\phi_{k,n}$ and recover the real wavejets coefficients as $\phi_{k,n}e^{in\mu}$ (similar formulas hold for $\Phi_{k,n}$).

The rotation matrix $\mathbf{R}$ of axis $\boldsymbol{u} = (1,0,0)_{\mathcal{P}}$ and angle γ transforms the coordinates (X,Y,H) of a surface point p in the parameterization of $\mathcal{P}(P)$ into coordinates (x,y,h) in the parameterization of $\mathcal{P}(P)$. Let us assume that γ^2 is small enough. Then the rotation has the following expression:

$$\mathbf{R} = \begin{pmatrix} 1 & 0 & 0 \\ 0 & 1 & -\gamma \\ 0 & \gamma & 1 \end{pmatrix} + o(\gamma) \tag{2.38}$$

Thus, relation between $(x,y,f(x,y)=h)$ and $(X,Y,F(X,Y)=H)$ is the following:

$$\begin{cases} x &= X + o(\gamma) \\ y &= Y - \gamma H + o(\gamma) \\ h &= \gamma Y + H + o(\gamma) \end{cases} \tag{2.39}$$

Let us switch to polar coordinates (r,θ) (resp. (R,Θ)) such that $x = r\cos\theta$ and $y = r\sin\theta$ (resp. $X = R\cos\Theta$ and $Y = R\sin\Theta$). Let $z = x + \boldsymbol{i}y$ and $Z = X + \boldsymbol{i}Y$. Equation (2.39) yields:

$$h = H + \gamma RT(\Theta) + o(\gamma) \tag{2.40}$$

With $T(\Theta) = \frac{1}{2}\left(e^{\boldsymbol{i}\left(\Theta-\frac{\pi}{2}\right)} + e^{-\boldsymbol{i}\left(\Theta-\frac{\pi}{2}\right)}\right)$.

The following equation for r follows from $z = x + \boldsymbol{i}y$ and Equation 2.39:

$$r^k = \sqrt{|zz^*|}^k = R^k + \frac{kR^{k-1}H}{2}\gamma\left(e^{\boldsymbol{i}\left(\Theta+\frac{\pi}{2}\right)} + e^{-\boldsymbol{i}\left(\Theta+\frac{\pi}{2}\right)}\right) + o(\gamma) \tag{2.41}$$

Similarly, we have for all $n \in \mathbb{N}$:

$$z^n = R^n e^{\boldsymbol{i}n\Theta} + nR^{n-1}H\gamma e^{\boldsymbol{i}\left((n-1)\Theta+\mu-\frac{\pi}{2}\right)} + o(\gamma) \tag{2.42}$$

which yields, since $e^{\boldsymbol{i}n\theta} = (z/|z|)^n = (z/r)^n$:

$$e^{\boldsymbol{i}n\theta} = e^{\boldsymbol{i}n\Theta} + \frac{nH}{2R}\gamma\left(e^{\boldsymbol{i}\left((n-1)\Theta-\frac{\pi}{2}\right)} - e^{\boldsymbol{i}\left((n+1)\Theta+\frac{\pi}{2}\right)}\right) + o(\gamma) \tag{2.43}$$

Combining Equations 2.41 and 2.43, and setting $A_{k,n} = \frac{(k+n)}{2}e^{-\boldsymbol{i}\frac{\pi}{2}}$ yields:

$$r^k e^{\boldsymbol{i}n\theta} = R^k e^{\boldsymbol{i}n\Theta} + R^{k-1}e^{\boldsymbol{i}n\Theta}\gamma H\left(A_{k,n}e^{-\boldsymbol{i}\Theta} + A^*_{k,-n}e^{\boldsymbol{i}\Theta}\right) + o(\gamma) \tag{2.44}$$

Plugging Equation 2.44 in Equation 2.40, one has:

$$\begin{aligned} H &= \frac{\left(\sum_{k=0}^{K}\sum_{n=-k}^{k}\phi_{k,n}R^k e^{in\Theta}\right) - \gamma RT(\Theta)}{1-\gamma\sum_{k=0}^{K}\sum_{n=-k}^{k}\phi_{k,n}R^{k-1}\left(A_{k,n}e^{i(n-1)\Theta}+A^*_{k,n}e^{i(n+1)\Theta}\right)} + o(\gamma) \\ &= \left(\sum_{k=0}^{K}\sum_{n=-k}^{k}\phi_{k,n}R^k e^{in\Theta}\right) - \gamma(RT(\Theta)+F(\Theta)+G(\Theta)) + o(\gamma) \end{aligned} \tag{2.45}$$

With:

$$\begin{aligned} F(\Theta) &= \left(\sum_{k=0}^{K}\sum_{n=-k}^{k}\phi_{k,n}R^k e^{in\Theta}\right)\left(\sum_{j=1}^{K}\sum_{m=-j}^{j}\phi_{j,m}A_{j,m}R^{j-1}e^{i(m-1)\Theta}\right) \\ G(\Theta) &= \left(\sum_{k=0}^{K}\sum_{n=-k}^{k}\phi_{k,n}R^k e^{in\Theta}\right)\left(\sum_{j=1}^{K}\sum_{m=-j}^{j}\phi_{j,m}A^*_{j,-m}R^{j-1}e^{i(m+1)\Theta}\right) \end{aligned} \tag{2.46}$$

$$\begin{aligned} F(\Theta) &= \left(\sum_{k=0}^{K}\sum_{n=-k}^{k}\phi_{k,n}R^k e^{in\Theta}\right)\left(\sum_{j=0}^{K}\sum_{m=-j-1}^{j+1}\phi_{j+1,m}A_{j+1,m}R^{j}e^{i(m-1)\Theta}\right) \\ &= \left(\sum_{k=0}^{K}\sum_{n=-k}^{k}\phi_{k,n}R^k e^{in\Theta}\right)\left(\sum_{j=0}^{K}\sum_{m=-j-2}^{j}\phi_{j+1,m+1}A_{j+1,m+1}R^{j}e^{im\Theta}\right) \end{aligned} \tag{2.47}$$

Recall that if k and n do not share the same parity, $\phi_{k,n}=0$, then if $m=-j-1$, $\phi_{j+1,m+1}=0$. Furthermore by definition of A, if $m=-j-2$ then $A_{j+1,m+1}=0$. Thus we can write:

$$\begin{aligned} F(\Theta) &= \left(\sum_{k=0}^{K}\sum_{n=-k}^{k}\phi_{k,n}R^k e^{in\Theta}\right)\left(\sum_{j=0}^{K}\sum_{m=-j}^{j}\phi_{j+1,m+1}A_{j+1,m+1}R^{j}e^{im\Theta}\right) \\ &= \sum_{\ell=0}^{2K}\sum_{s=0}^{\ell}R^\ell\left(\sum_{n=-\ell+s}^{\ell-s}\phi_{\ell-s,n}e^{in\Theta}\right)\left(\sum_{m=-s}^{s}\phi_{s+1,m+1}A_{s+1,m+1}e^{im\Theta}\right) \\ &= \sum_{\ell=0}^{2K}\sum_{s=0}^{\ell}R^\ell\left(\sum_{n=-\ell+s}^{\ell-s}\phi_{\ell-s,n}e^{in\Theta}\right)\left(\sum_{m=-s}^{s}\phi_{s+1,m+1}A_{s+1,m+1}e^{im\Theta}\right) \end{aligned} \tag{2.48}$$

Finally:

$$F(\Theta) = \sum_{k=0}^{2K}\sum_{n=-k}^{k}\left(\sum_{j=0}^{k}\sum_{\substack{p+m=n\\ |p|\le k-j\\ |m|\le j}}\phi_{k-j,p}\phi_{j+1,m+1}A_{j+1,m+1}\right)R^k e^{in\Theta} \tag{2.49}$$

A similar computation yields:

$$G(\Theta) = \sum_{k=0}^{2K} \sum_{n=-k}^{k} \left(\sum_{j=0}^{k} \sum_{\substack{p+m=n \\ |p|\leq k-j \\ |m|\leq j}} \phi_{k-j,p} \phi_{j+1,m-1} A^*_{j+1,-m+1} \right) R^k e^{in\Theta} \tag{2.50}$$

Since $H = \sum_{k=0}^{2K} \sum_{n=-k}^{k} \Phi_{k,n} R^k e^{in\Theta} + o(\gamma)$, by coefficient identification one has $\Phi_{0,0} = \phi_{0,0} + o(\gamma)$ and $\Phi_{1,1} = \phi_{1,1} + \frac{\gamma}{2} e^{-i\frac{\pi}{2}} + o(\gamma)$. However since $\phi_{0,0} = \phi_{1,1} = 0$, since $\mathcal{T}(P)$, is the tangent plane, we have: $\Phi_{0,0} = o(\gamma)$ and $\Phi_{1,1} = \frac{\gamma}{2} e^{-i\frac{\pi}{2}} + o(\gamma)$.

For $k > 1$, one has the following relationship:

$$\begin{aligned} \Phi_{k,n} &= \phi_{k,n} + \gamma \sum_{j=0}^{k} \sum_{\substack{p+m=n \\ |p|\leq k-j \\ |m|\leq j}} \phi_{k-j,p} \left(\phi_{j+1,m+1} A_{j+1,m+1} + \phi_{j+1,m-1} A^*_{j+1,-m+1} \right) + o(\gamma) \\ &= \phi_{k,n} + \gamma F_{k,n}(\phi) + o(\gamma) \end{aligned} \tag{2.51}$$

□

2.3 Wirtinger derivatives

2.3.1 Definition and properties

In this section, we will show that the Wavejets coefficients are proportional to the Wirtinger derivatives up to order K for a function $f \in \mathscr{F}^K$. The Wirtinger derivative [Wir27] is an operator on complex functions that behaves similarly to the ordinary derivative operator for real functions:

Definition 1. *First order Wirtinger derivatives have the following form:*

$$\begin{aligned} \frac{\partial}{\partial z} &= \frac{1}{2} \left(\frac{\partial}{\partial x} - i \frac{\partial}{\partial y} \right) \\ \frac{\partial}{\partial z^*} &= \frac{1}{2} \left(\frac{\partial}{\partial x} + i \frac{\partial}{\partial y} \right) \end{aligned} \tag{2.52}$$

They were first implicitly used by Poincaré in 1899 [Poi99]. Pompeiu, in 1913 [Pom13], also introduced a complex derivative operator:

$$\frac{\partial f}{\partial z^*}(z_0) = \lim_{r \to 0} \frac{1}{2\pi i r^2} \oint_{\partial D(z_0, r)} f(z) dz \tag{2.53}$$

Where $\partial D(z_0, r)$ is the boundary of a disk of radius r centered at z_0. This operator, when applied to differentiable functions w.r.t. their real and imaginary parts, computes the same quantity as the conjugate version of the Wirtinger derivative. Even if this operator was introduced earlier than the Wirtinger derivative, it is more general because one can apply it to any integrable functions [Hen86]. This kind of derivative is called a *weak derivative*.

In order to link Wirtinger derivatives with Wavejets, a polar coordinate form is needed:

$$\begin{aligned}\frac{\partial}{\partial z} &= \frac{1}{2}\left(\frac{\partial}{\partial r} - \boldsymbol{i}\frac{1}{r}\frac{\partial}{\partial \theta}\right)e^{-i\theta} \\ \frac{\partial}{\partial z^*} &= \frac{1}{2}\left(\frac{\partial}{\partial r} + \boldsymbol{i}\frac{1}{r}\frac{\partial}{\partial \theta}\right)e^{i\theta}\end{aligned} \tag{2.54}$$

Proof. Let us write the Jacobian:

$$\begin{aligned}\frac{\partial}{\partial x} &= \cos\theta\frac{\partial}{\partial r} - \frac{1}{r}\sin\theta\frac{\partial}{\partial \theta} \\ \frac{\partial}{\partial y} &= \sin\theta\frac{\partial}{\partial r} + \frac{1}{r}\cos\theta\frac{\partial}{\partial \theta}\end{aligned} \tag{2.55}$$

This yields:

$$\frac{\partial}{\partial x} - \boldsymbol{i}\frac{\partial}{\partial y} = \left(\frac{\partial}{\partial r} - \boldsymbol{i}\frac{1}{r}\frac{\partial}{\partial \theta}\right)e^{-i\theta} \tag{2.56}$$

The second part of the proof is obtained by conjugation of the Wirtinger derivative. □

Let us now recall a few essential well known properties of the Wirtinger derivatives:

$$\begin{aligned}\frac{\partial z^*}{\partial z} &= \frac{\partial z}{\partial z^*} = 0 \\ \frac{\partial z}{\partial z} &= \frac{\partial z^*}{\partial z^*} = 1\end{aligned} \tag{2.57}$$

The product rule also applies to Wirtinger derivatives:

$$\begin{aligned}\frac{\partial fg}{\partial z} &= g\frac{\partial f}{\partial z} + f\frac{\partial g}{\partial z} \\ \frac{\partial fg}{\partial z^*} &= g\frac{\partial f}{\partial^* z} + f\frac{\partial g}{\partial z^*}\end{aligned} \tag{2.58}$$

Remark 2. *The Wirtinger derivatives $\frac{\partial}{\partial z}$ and $\frac{\partial}{\partial z^*}$ shall not be confused with the regular complex derivative $\frac{d}{dz}$. All functions for which Wirtinger derivatives exist are not necessarily differentiable w.r.t. the complex derivative.*

Let us study the relation between those operators. Given a compact $U \subset \mathbb{C}$, for a function $f : U \to \mathbb{C}$ to be differentiable at $z_0 \in U$ w.r.t. $\frac{d}{dz}$, it is necessary and sufficient that its real and imaginary parts are differentiable w.r.t. $\frac{\partial}{\partial x}$ and $\frac{\partial}{\partial y}$ operators, and that f verifies the following Cauchy-Riemann equations, which are equivalent:

- $\frac{\partial f}{\partial x}(z_0) = -\boldsymbol{i}\frac{\partial f}{\partial y}(z_0)$
- $\frac{\partial Re(f)}{\partial x}(z_0) = \frac{\partial Im(f)}{\partial y}(z_0)$ *and* $\frac{\partial Re(f)}{\partial y}(z_0) = -\frac{\partial Im(f)}{\partial x}(z_0)$
- $\frac{\partial f}{\partial z^*}(z_0) = 0$

In that case, $\frac{df}{dz}(z_0) = \frac{\partial f}{\partial x}(z_0) = -\boldsymbol{i}\frac{\partial f}{\partial y}(z_0) = \frac{\partial f}{\partial z}(z_0)$, and f is holomorphic.

A consequence of Cauchy-Riemann equations is that $Re(f)$ and $Im(f)$ of such a function f are harmonic functions, i.e. their Laplacian equals zero, or $\Delta Re(f) = \Delta Im(f) = 0$.

The Wirtinger derivative $\frac{\partial}{\partial z}$ is thus a weak complex derivative compared to $\frac{d}{dz}$. It can differentiate non differentiable functions on the complex plane.

2.3.2 Link between Wirtinger derivatives and Wavejets coefficients

In order to link Wirtinger derivatives with Wavejets decompositions, we need the expression of the Wirtinger derivatives of f. For $f \in \mathscr{F}^K$, given $\phi_{k,n}$ the coefficients of the Wavejets decomposition of f; let us first differentiate p times w.r.t. $\frac{\partial}{\partial z}$:

Lemma 1.

$$\frac{\partial^p f}{\partial z^p}(r,\theta) = \sum_{k=0}^{K-p} \sum_{n=-k}^{k} \frac{\left(p + \frac{k+n}{2}\right)!}{\frac{k+n}{2}!} \phi_{k+p,n+p} r^k e^{i n\theta} \tag{2.59}$$

Proof. To prove this property, let us apply the Wirtinger derivative operator written in polar coordinates to $f \in \mathscr{F}^K$:

$$\begin{aligned}
\frac{\partial f}{\partial z}(r,\theta) &= \frac{1}{2}\left(\sum_{k=0}^{K-1}\sum_{n=-k}^{k}\left((k+1)\phi_{k+1,n} r^k e^{i n\theta} - i^2 n \phi_{k+1,n} r^k e^{i n\theta}\right)\right) e^{-i\theta} \\
&= \frac{1}{2}\sum_{k=0}^{K-1}\sum_{n=-k}^{k}(k+1+n+1)\phi_{k+1,n+1} r^k e^{i n\theta} \\
&= \sum_{k=0}^{K-1}\sum_{n=-k}^{k}\left(\frac{k+n}{2}+1\right)\phi_{k+1,n+1} r^k e^{i n\theta}
\end{aligned} \tag{2.60}$$

We can deduce for $p \in \mathbb{N}$:

$$\begin{aligned}
\frac{\partial^p f}{\partial z^p}(r,\theta) &= \sum_{k=0}^{K-p}\sum_{n=-k}^{k}\left(\prod_{m=1}^{p}\left(\frac{k+n}{2}+m\right)\right)\phi_{k+p,n+p} r^k e^{i n\theta} \\
&= \sum_{k=0}^{K-p}\sum_{n=-k}^{k}\frac{\left(p+\frac{k+n}{2}\right)!}{\frac{k+n}{2}!}\phi_{k+p,n+p} r^k e^{i n\theta}
\end{aligned} \tag{2.61}$$

□

There is a similar result regarding the conjugate of Wirtinger derivative:

Lemma 2.

$$\frac{\partial^q f}{\partial z^{*q}}(r,\theta) = \sum_{k=0}^{K-q} \sum_{n=-k}^{k} \frac{\left(q + \frac{k-n}{2}\right)!}{\frac{k-n}{2}!} \phi_{k+q,n-q} r^k e^{i n\theta} \tag{2.62}$$

Proof. Let us apply the conjugate of Wirtinger derivative to $f \in \mathscr{F}^K$:

$$\begin{aligned}
\frac{\partial f}{\partial z^*}(r,\theta) &= \frac{1}{2}\left(\sum_{k=0}^{K-1}\sum_{n=-k}^{k}\left((k+1)\phi_{k+1,n} r^k e^{i n\theta} + i^2 n \phi_{k+1,n} r^k e^{i n\theta}\right)\right) e^{i\theta} \\
&= \frac{1}{2}\sum_{k=0}^{K-1}\sum_{n=-k}^{k}(k+1-n+1)\phi_{k+1,n-1} r^k e^{i n\theta} \\
&= \sum_{k=0}^{K-1}\sum_{n=-k}^{k}\left(\frac{k-n}{2}+1\right)\phi_{k+1,n-1} r^k e^{i n\theta}
\end{aligned} \tag{2.63}$$

This leads for $q \in \mathbb{N}$ to:

$$\begin{aligned}\frac{\partial^q f}{\partial z^{*q}}(r,\theta) &= \sum_{k=0}^{K-q}\sum_{n=-k}^{k}\left(\prod_{m=1}^{q}\left(\frac{k-n}{2}+m\right)\right)\phi_{k+q,n-q}r^k e^{i n\theta} \\ &= \sum_{k=0}^{K-q}\sum_{n=-k}^{k}\frac{\left(q+\frac{k-n}{2}\right)!}{\frac{k-n}{2}!}\phi_{k+q,n-q}r^k e^{i n\theta}\end{aligned} \tag{2.64}$$

□

The main result concerning Wavejets and Wirtinger derivatives is that Wavejets coefficients of a function f are proportional to its Wirtinger derivatives:

Theorem 3. *Let $f \in \mathscr{F}^K$. Let $\phi_{k,n}$ be the coefficients of the Wavejet decomposition of order K of f. Then:*

$$\phi_{k,k-2j} = \frac{1}{(k-j)!j!}\frac{\partial^k f}{\partial z^{k-j}\partial z^{*j}}(0,0) \tag{2.65}$$

Proof. Let us use Lemmas 1 and 2:

$$\begin{aligned}\frac{\partial^{p+q} f}{\partial z^p \partial z^{*q}}(r,\theta) &= \sum_{k=0}^{K-(p+q)}\sum_{n=-k}^{k}\frac{\left(p+\frac{k+n}{2}\right)!\left(q+\frac{k-n}{2}\right)!}{\frac{k+n}{2}!\frac{k-n}{2}!}\phi_{k+p+q,n+p-q}r^k e^{i n\theta} \\ \frac{\partial^{p+q} f}{\partial z^p \partial z^{*q}}(z,z^*) &= \sum_{k=0}^{K-(p+q)}\sum_{n=-k}^{k}\frac{\left(p+\frac{k+n}{2}\right)!\left(q+\frac{k-n}{2}\right)!}{\frac{k+n}{2}!\frac{k-n}{2}!}\phi_{k+p+q,n+p-q}z^{\frac{k+n}{2}}z^{*\frac{k-n}{2}}\end{aligned} \tag{2.66}$$

Now estimating this function at $r = 0$ and $\theta = 0$:

$$\frac{\partial^{p+q} f}{\partial z^p \partial z^{*q}}(0,0) = p!q!\phi_{p+q,p-q} \tag{2.67}$$

By setting $k = p+q$ and $j = q$:

$$\frac{\partial^k f}{\partial z^{k-j}\partial z^{*j}}(0,0) = (k-j)!j!\phi_{k,k-2j} \tag{2.68}$$

Which concludes the proof. □

Now that Wirtinger derivatives are linked to Wavejets coefficients, we can prove that the Taylor expansion can be extended to Wirtinger derivatives:

$$\forall f \in \mathscr{F}^K,\ f(z) = \sum_{k=0}^{K}\sum_{j=0}^{k}\frac{1}{(k-j)!j!}\frac{\partial^k f}{\partial z^{k-j}\partial z^{*j}}(0)z^{k-j}z^{*j} \tag{2.69}$$

Proof. Proposition 2 states that if f can be expressed as a bivariate Taylor expansion, then f has a Wavejet decomposition where each coefficient $\phi_{k,n}$ is a linear combination of derivatives of order k, with k and $|n|$ sharing same parity. Notice that if $(x,y) = (r\cos\theta, r\sin\theta)$ and $z = x + iy$, then for $(k,j) \in \mathbb{N}$ and $j \leq k$, $z^{k-j}z^{*j} = re^{i(k-2j)\theta}$. Moreover:

$$\sum_{n=-k}^{k}\phi_{k,n}r^k e^{i n\theta} = \sum_{j=0}^{k}\phi_{k,k-2j}r^k e^{i(k-2j)\theta} = \sum_{j=0}^{k}\frac{1}{(k-j)!j!}\frac{\partial^k f}{\partial z^{k-j}\partial z^{*j}}(0)z^{k-j}z^{*j} \tag{2.70}$$

Since, $r^k e^{in\theta} = z^{k-j} z^{*j}$, we can conclude that any real function $f \in \mathscr{F}^K$ can be written as in equation (2.69). □

A direct consequence of equation (2.69) is that Wavejets are linked to Wirtinger derivatives in the same way Jets are linked to ordinary derivatives. Let us call $\frac{\partial^k}{\partial z^{k-j} z^{*j}}$ the j^{th} cross-derivative of order k by analogy with ordinary cross-derivatives found in bivariate Taylor expansions. Wirtinger cross-derivatives for different j are angularly orthogonal. Using this important property, we will show in chapter 3 that for a given j, certain linear combinations of j^{th} Wirtinger cross-derivatives of different orders k result in defining new integral invariants, giving access to stable information related to differential quantities of high order about surface $\mathcal{S}$ at point P.

2.4 High order principal directions

In this section, we generalize the principal directions on surfaces to higher orders principal directions, extending the work of [Qi05; Qi06; Qi07] on symmetric supermatrices. A supermatrix is a representation of a tensor in a given coordinate system. Let us illustrate the difference between a tensor and its representation as a supermatrix: a rotation matrix R of axis $\boldsymbol{u}$ and of angle γ is the matrix representation of the rotation tensor $\boldsymbol{R}$ with same parameters. Depending of the coordinate system, vector $\boldsymbol{u}$ has different expressions, yielding a different expression for R. The rotation tensor $\boldsymbol{R}$, on the other hand, depends on $\boldsymbol{u}$ and γ, but not on the choice of a certain basis.

Definition 2. *An m-dimensional symmetric supermatrix T of order k is a k-dimensional array such that given index $I = (i_j)_{j \in [\![0,k]\!]}$, for any permutation p on I, $T_I = T_{p(I)}$*

For now on, we will always consider $m = 2$. By convention, we define any vector to be a symmetric supermatrix of order 1. Given a vector $v = (x, y)$, we note v^j the symmetric supermatrix of order j generated by multiplying v j times using the cartesian product. In particular, we set $v^0 = 1$ by convention. On the other hand, given a symmetric supermatrix $T = (T_x, T_y)$ of order k, where T_x and T_y are symmetric supermatrices of order $k-1$, we note Tv the following symmetric supermatrix of order $k-1$:

$$Tv = xT_x + yT_y \tag{2.71}$$

Tv reduces the order of T by contracting on an arbitrary index. Since T is symmetric, for any index used for the contraction yields the same list of numbers in Tv. Thus, by convention, we set this arbitrary index to be the first of T. Let us define another convention: $Tv^j = T_j$ is the symmetric supermatrix of order $k-j$ obtained through the sequence $T(n+1) = T(n)v$ and $T(0) = T$.

In the case of Wavejets analysis, $m = 2$ because a surface is a 2-dimensional space, and we set the order $k \leq K$. In this case, a symmetric supermatrix of order k can be seen as a k-dimensional array of vectors of length 2. Multiplying a supermatrix with a vector v given our convention produces a supermatrix of order lowered by 1. Figure 2.3 shows an example of such an operation on a supermatrix of order 3.

Eigenvalues and eigenvectors can be generalized for supermatrices [Qi05]. Let us recall this generalization:

Definition 3. *[Qi05] Given T a symmetric supermatrix of order k, if there exists $\lambda \in \mathbb{C}$ and a vector $v \in \mathbb{R}^2$ such that:*

$$\begin{cases} Tv^{k-1} &= \lambda v \\ v^T v &= 1 \end{cases} \tag{2.72}$$

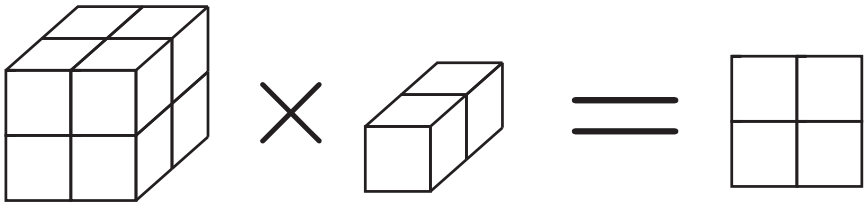

FIGURE 2.3: Visual example of the outcome of a supermatrix of order 3 multiplied by a vector.

Then λ is called an E-eigenvalue of T and $\boldsymbol{v}$ is called an E-eigenvector of T. The set of λ satisfying (2.72) are the roots of a polynomial called the E-characteristic polynomial.

Supermatrices can be used to write Taylor expansions. To give an intuition, let us write the two first terms of a bivariate Taylor expansion. Given $v = (x, y)^T$ an arbitrary vector, $\boldsymbol{n}$ the normal at $(0, 0)$ and H the Hessian of a function $f \in \mathscr{F}^2(\mathcal{D}_R, \mathbb{R})$ at $(0, 0)$:

$$f(v) = f(0,0) + \boldsymbol{n}^T v + v^T H v \tag{2.73}$$

Note that H is symmetric, and so is $\boldsymbol{n}$ since its order is 1. This can be generalized for higher orders using supermatrices.

Property 4. *Given $v = (x, y)^T$, a function $f \in \mathscr{F}^K(\mathcal{D}_R, \mathbb{R})$ can be written as follows:*

$$f(v) = \sum_{k=0}^{K} T_k v^k \tag{2.74}$$

Where T_k is a symmetric supermatrix of order k, where coefficients are as follows: let $x_0 = x, x_1 = y$,

$$(T_k)_{(i_0,\ldots,i_k)} = \frac{\partial^k f}{\partial x_{i_0} \ldots \partial x_{i_k}}(0,0) \tag{2.75}$$

For the following of this section, we need to define the differentiation w.r.t. a vector.

Definition 4. *Let $v = (x, y)^T \in \mathbb{R}^2$. Let $T(v)$ be a symmetric supermatrix of order k such that each element of $T(v)$ is differentiable w.r.t. x and y. Let $\mathcal{I}_k$ be the set of indexes for a supermatrix of order k. Let us note i_x the index of the first element of $\boldsymbol{v}$ and i_y the index of the second element of $\boldsymbol{v}$. Setting i an index on vector $\boldsymbol{v}$, given $I \in \mathcal{I}_k$, let us consider the concatenation of both indexes $(I, i) \in \mathcal{I}_{k+1}$. $T(v)$ is then differentiable w.r.t. $\boldsymbol{v}$, and its derivative $\frac{\partial T}{\partial v}(v)$ is the supermatrix of order $k+1$ whose elements are indexed as follows:*

$$\begin{aligned} \left(\frac{\partial T}{\partial v}(v)\right)_{(I,i_x)} &= \left(\frac{\partial T}{\partial x}(v)\right)_I \\ \left(\frac{\partial T}{\partial v}(v)\right)_{(I,i_y)} &= \left(\frac{\partial T}{\partial y}(v)\right)_I \end{aligned} \tag{2.76}$$

We need one more Lemma prior to linking Wavejets and symmetric supermatrices and the framework of [Qi05; Qi06; Qi07].

Lemma 3. *Let T be a symmetric supermatrix. Let $v = (x, y)^T \in \mathbb{R}^2$ be a vector.*

$$\frac{\partial T v^k}{\partial v} = k T v^{k-1} \tag{2.77}$$

Proof. Let us prove that by recurrence. It is direct for $k = 0$. $v^1 = v$, and one directly has:

$$\frac{\partial T v^1}{\partial v} = T = 1 T v^0 \tag{2.78}$$

Let us prove that if for a certain k, $\frac{\partial T v^k}{\partial v} = k T v^{k-1}$, it is also true for $k+1$.

$$\begin{aligned} \frac{\partial T v^{k+1}}{\partial v} &= \frac{\partial T v^k v}{\partial v} \\ &= T v^k + \frac{\partial T v^k}{\partial v} v \\ &= T v^k + k T v^{k-1} v \\ &= (k+1) T v^k \end{aligned} \tag{2.79}$$

□

Theorem 4. *Given $v = (x, y)$, T_k a real symmetric supermatrix of order $k > 1$ representing the derivatives of order k of a smooth function $f \in \mathscr{F}^K$, the set of vector $v = (x, y)$ such that $\frac{\partial}{\partial \theta} T_k v^k = 0$ and $\|v\| = 1$ are E-eigenvectors of T_k:*

$$\begin{cases} T_k v^{k-1} = v T_k v^k \\ \|v\| = 1 \end{cases} \tag{2.80}$$

Proof. Let us note T_k the supermatrix of order k from the Taylor expansion of $f \in \mathscr{F}^K$ w.r.t. ordinary derivatives. Let us note $v = (r\cos\theta, r\sin\theta)$. Let us first differentiate $T_k v^k$ w.r.t. radius r:

$$\begin{aligned} \frac{\partial}{\partial r} T_k v^k &= \frac{\partial}{\partial r} \sum_{n=-k}^{k} \phi_{k,n} r^k e^{in\theta} \\ &= k \sum_{n=-k}^{k} \phi_{k,n} r^{k-1} e^{in\theta} \\ &= \frac{k}{r} \sum_{n=-k}^{k} \phi_{k,n} r^k e^{in\theta} \\ &= \frac{k}{r} T_k v^k \end{aligned} \tag{2.81}$$

Now, using equation (2.54), we can write:

$$\begin{aligned} \frac{\partial}{\partial \theta} T_k v^k = 0 &\Leftrightarrow \begin{cases} \frac{\partial}{\partial z} T_k v^k &= \frac{1}{2} \frac{\partial}{\partial r} T_k v^k e^{-i\theta} \\ \frac{\partial}{\partial z^*} T_k v^k &= \frac{1}{2} \frac{\partial}{\partial r} T_k v^k e^{i\theta} \end{cases} \\ &\Leftrightarrow \begin{cases} \frac{\partial}{\partial z} T_k v^k &= \frac{k}{2r} T_k v^k e^{-i\theta} \\ \frac{\partial}{\partial z^*} T_k v^k &= \frac{k}{2r} T_k v^k e^{i\theta} \end{cases} \\ &\Leftrightarrow \begin{cases} \frac{\partial}{\partial z} T_k v^k &= \frac{k}{2z} T_k v^k \\ \frac{\partial}{\partial z^*} T_k v^k &= \frac{k}{2z^*} T_k v^k \end{cases} \\ &\Leftrightarrow \begin{cases} \frac{\partial}{\partial z} T_k v^k &= \frac{kz^*}{2|z|^2} T_k v^k \\ \frac{\partial}{\partial z^*} T_k v^k &= \frac{kz}{2|z|^2} T_k v^k \end{cases} \end{aligned} \tag{2.82}$$

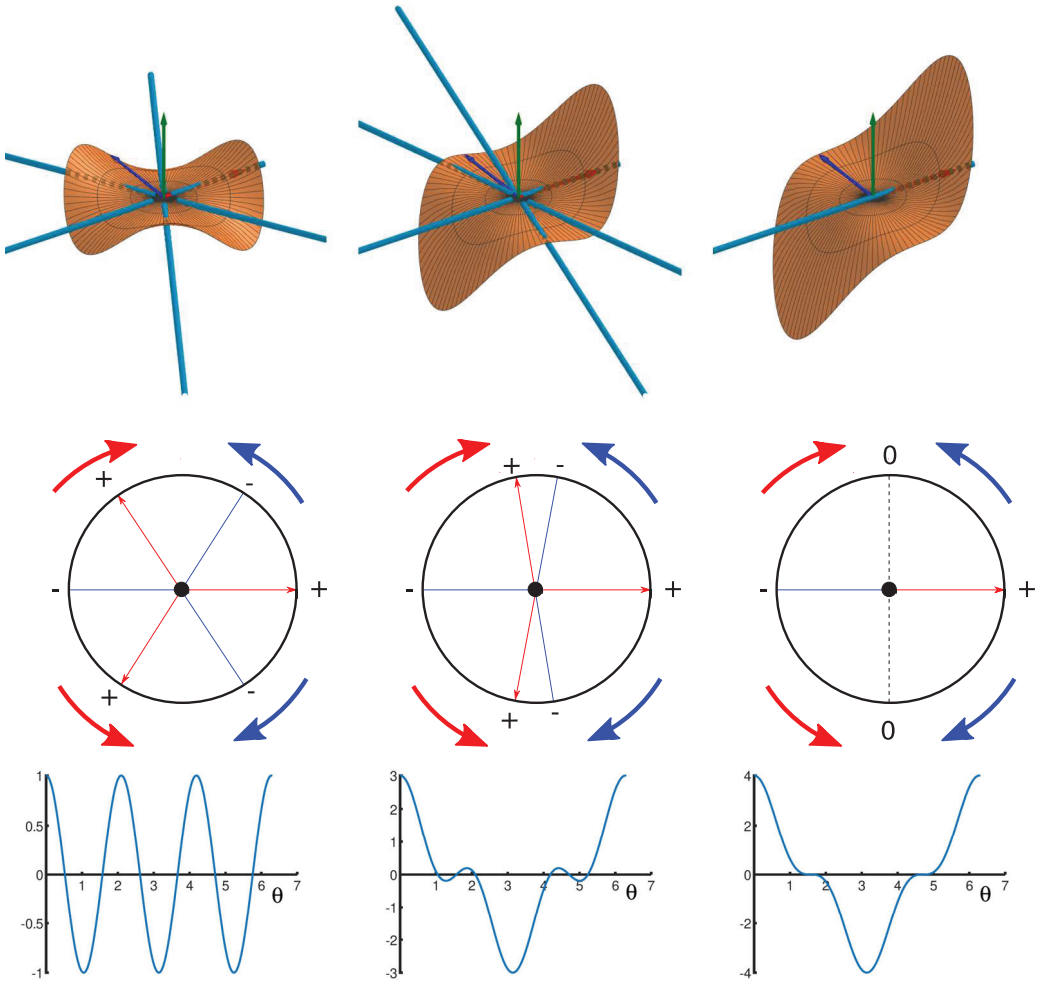

$\phi_{3,\pm3} = 0.5,\ \phi_{3,\pm1} = 0$ $\phi_{3,\pm3} = 0.5,\ \phi_{3,\pm1} = 1$ $\phi_{3,\pm3} = 0.5,\ \phi_{3,\pm1} = 1.5$

FIGURE 2.4: First row: 3D view of third order surfaces with different third order principal directions arrangement. Second row: Top view of the corresponding principal directions. Arrows show the direction of th direction of the motion of the eigenvectors as the ratio $\phi_{3,\pm1}/\phi_{3,\pm3}$ increases. Third row: Angular view of the corresponding signal $T_3 v^3 = r^3 \sum_{n=-3}^{3} \phi_{k,n} e^{in\theta}$ for $r = 1$. As $\phi_{3,\pm1}$ increases from left to one, E-eigenvectors move until a positive and a negative E-eigenvalue collide and become degenerate vectors. E-eigenvalues correspond to local angular maxima. In the left column, the supermatrix has 2 E-eigenvalues, in the middle column, it has 4 E-eigenvalues, while in the last column, it has 2 E-eigenvalues.

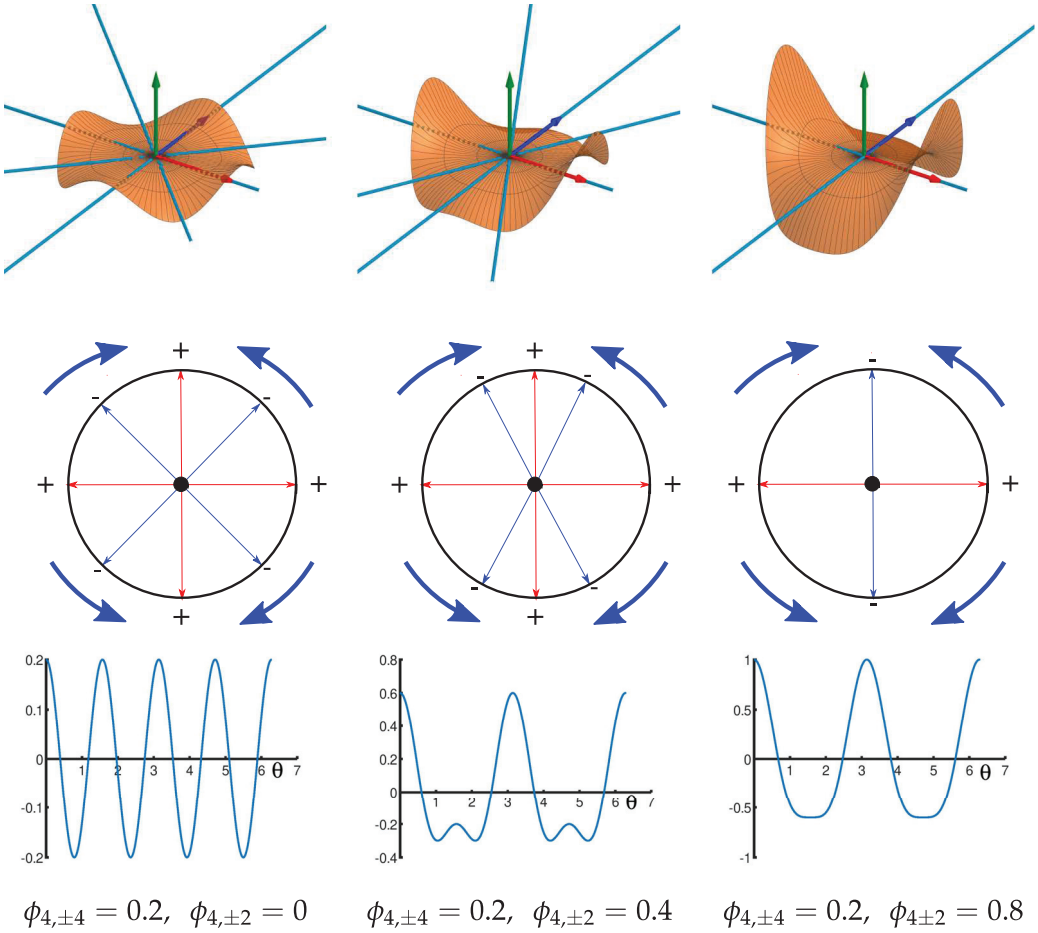

$\phi_{4,\pm4} = 0.2,\ \phi_{4,\pm2} = 0$ $\phi_{4,\pm4} = 0.2,\ \phi_{4,\pm2} = 0.4$ $\phi_{4,\pm4} = 0.2,\ \phi_{4\pm2} = 0.8$

FIGURE 2.5: First row: 3D view of fourth order surfaces with different fourth order principal directions arrangement. Second row: Top view of the corresponding principal directions. Arrows show the direction of the motion of the eigenvectors as the ratio $\phi_{4,\pm2}/\phi_{4,\pm4}$ increases.Third row: Angular view of the corresponding signal $T_4 v^4 = r^4 \sum_{n=-4}^{4} \phi_{k,n} e^{in\theta}$ for $r = 1$. As $\phi_{4,\pm2}$ increases from left to one, E-eigenvectors move until 2 negative E-eigenvectors collide with a positive E-eigenvector. E-eigenvalues correspond to local angular maxima. In the left column, the supermatrix has 3 E-eigenvalues, in the midlle column, it has 4 E-eigenvalues, while in the last column, it has 2 E-eigenvalues.

Noting that:

$$\begin{aligned}\frac{\partial}{\partial x} &= \frac{\partial}{\partial z} + \frac{\partial}{\partial z^*} \\ \frac{\partial}{\partial y} &= \frac{\partial}{\partial z^*} - \frac{\partial}{\partial z}\end{aligned} \tag{2.83}$$

We can deduce that:

$$\begin{aligned}\frac{\partial}{\partial \theta} T_k v^k = 0 \Leftrightarrow \begin{cases} \frac{\partial}{\partial x} T_k v^k &= \frac{kx}{\|v\|^2} T_k v^k \\ \frac{\partial}{\partial y} T_k v^k &= \frac{ky}{\|v\|^2} T_k v^k \end{cases} \\ \Leftrightarrow \frac{\partial}{\partial v} T_k v^k = \frac{k}{\|v\|^2} v T_k v^k\end{aligned} \tag{2.84}$$

Using Lemma 3, this leads to:

$$\frac{\partial}{\partial \theta} T_k v^k = 0 \Leftrightarrow \frac{\partial}{\partial v} T_k v^k = k T_k v^{k-1} = v \frac{k}{\|v\|^2} T_k v^k \tag{2.85}$$

Thus:

$$T_k v^{k-1} = v \frac{T_k v^k}{\|v\|^2} \tag{2.86}$$

Since $\frac{k T_k v^k}{\|v\|^2} = \lambda \in \mathbb{R}$, $T_k v^{k-1} = \lambda v$. Thus, if $\|v\|^2 = 1$ and $\frac{\partial}{\partial \theta} T_k v^k = 0$, v is an E-eigenvector of T_k with E-eigenvalue $T_k v^k$.

□

Remark 3. *Many types of eigenvalues and eigenvectors are developped in [Qi05; Qi06; Qi07]. In particular, if an E-eigenvector v is real and if its corresponding E-eigenvalue λ is also real, then v is a Z-eigenvector and λ is a Z-eigenvalue. In other words, E refers to complex eigenvectors and eigenvalues, while Z refers to real eigenvectors and real eigenvalues. While those 2 families of eigenvectors and eigenvalues are similar, other families have been defined with much greater differences. An interested reader should refer to [Qi05; Qi06; Qi07] for better insight.*

Corollary 6. *Given $v = (x, y)$, the directions of the E-eigenvectors of a supermatrix T_k of order k can be retrieved out of the Wavejet decomposition of $T_k v^k$ by looking at the zeros of:*

$$\frac{\partial}{\partial \theta} \sum_{n=-k}^{k} \phi_{k,n} e^{in\theta} = \sum_{n=-k}^{k} in\phi_{k,n} e^{in\theta} \tag{2.87}$$

Proof. As shown in Theorem 4, the E-eigenvectors direction correspond to the zeros of the angular derivative of $T_k v^k$. Thus, a direct angular differentiation yields the result. □

Corollary 6 shows that one can find the high order principal directions on a surface by localizing the roots of the angular derivative of the heightfield between the surface and the tangent plane. Following the work of Qi et al., they correspond the E-eigenvectors of symmetric supermatrices of dimension 2.

The behavior of the principal directions at order 3 and 4 are illustrated in Figures 2.4 and 2.5. Note that in those Figures, we take $\phi_{k,n} \in \mathbb{R}$. In the general case, $\phi_{k,n} \in \mathbb{C}$,

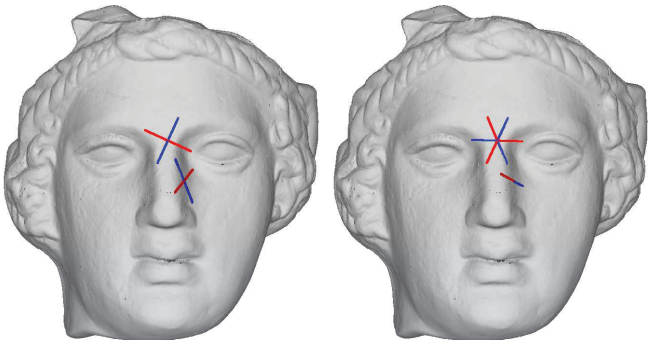

FIGURE 2.6: Second (left) and third (right) order principal directions illustrated at 2 points on a surface. The red vectors are E-eigenvectors associated with a positive E-eigenvalue, while blue vectors are E-eigenvectors associated with a negative E-eigenvalue.

leading to a much wider variety of possible configurations for E-eigenvectors. E-eigenvectors behavior mostly depends on whether the order is odd or even. Cases for $k > 4$ would evolve in a very similar way as shown in Figures 2.4 and 2.5 with an increased degree of freedom. In particular, one can find zero E-eigenvalues bound with E-eigenvectors. [Qi06] defines such vectors as degenerate vectors of degree 1.

Figure 2.6 shows two examples of order 2 and 3 principal directions on a surface. Our experimentations show that order 3 principal directions switch from 6 almost evenly spaced principal directions to 2 principal directions very quickly, making the second column case in Figure 2.4 rarely happening on real dataset.

2.5 Wavejets Fitting for Point Sets

Given a surface $\mathcal{S}$ that is only known through a set of measured points possibly spoiled by noise, we want to compute the Wavejets representation of the underlying surface up to a chosen order K, at an input point P. Let us assume that the surface is locally sufficiently smooth, *i.e.* $\mathcal{C}^K$ in a neighborhood of radius R around P. Our goal is to compute the $\phi_{k,n}$ coefficients that best decompose the underlying surface on the basis functions $e^{\phi}_{k,n}(r,\theta) = r^k e^{in\theta}$ in the neighborhood $\mathcal{N}(p)$ of radius R of P. Let L denote the number of samples in this neighborhood, and let P_ℓ be one of these samples, with cylindrical coordinates $(r_\ell, \theta_\ell, h_\ell)$ w.r.t. an axis that corresponds to a coarse approximation of the normal direction at point P. Then, the decomposition problem is formulated as finding $\phi_{k,n}$ minimizing:

$$E(\phi) = \sum_{\ell=1}^{L} \left\| h_\ell - \sum_{k=0}^{K-1} \sum_{n=-k}^{k} {r_\ell}^k e^{in\theta_\ell} \phi_{k,n} \right\|_2^2 \tag{2.88}$$

For clarity, we state the problem using the ℓ^2 norm even if it is unreliable if there are outliers. When dealing with noisy point sets or outliers we solve this minimization using an iteratively reweighted least squares procedure. This weighting scheme involves the use of a diagonal matrix of weights W that are used to leverage the importance of outliers.

To reformulate this energy minimization, let us reorder the B basis functions $e^{\phi}_{k,n}$ into a vector V_b, and the B unknown $\phi_{k,n}$ into a vector ϕ, such that the b^{th} component of ϕ corresponds to the coefficient of the b^{th} basis function in the decomposition. Let k_b and n_b respectively denote the order of derivation, and the oscillation frequency

of the b^{th} basis function ($0 \leq b \leq B-1$). Using these notations, the energy to be minimized is the following:

$$E(\phi) = \sum_{l=1}^{L} \left(z_l - \sum_{b=1}^{B} {r_l}^{k_b} e^{\boldsymbol{i} n_b \theta_l} \phi_b \right)^2 \tag{2.89}$$

This amounts to the minimization of $\|M\phi - Z\|_2^2$, where Z is a vector of size L containing the heights h_ℓ of neighbors P_ℓ and M is a matrix of size $L \times B$ such that:

$$M_{l,b} = r_l^{k_b} e^{\boldsymbol{i} n_b \theta_l} \tag{2.90}$$

Minimizing $\|M\Phi - Z\|_2^2$, is done by a QR decomposition of M. Thus computing the Wavejets decomposition around a point $\boldsymbol{p}$ amounts to building matrices M and Z and performing the QR decomposition of M. Using a Cholesky decomposition instead of QR fails because MM^* is often ill-conditioned.

In order to compute Wavejets in the tangent plane, one can compute a first estimate of Wavejets in a parameterization plane close enough to the tangent plane. The initial parameterization plane is obtained through a Principal Component Analysis. Importantly enough the orientation is not necessary to compute the Wavejets decomposition, we only need a local parameterization with respect to an approximate tangent plane. Then the parameterization plane is corrected into the tangent plane using equation 2.21 and the Wavejets coefficients themselves are corrected using Theorem 2.

Given a point set of N points and K the Wavejets order, the complexity of the computation, using Equation 2.90 for all points is $O(NK^6)$. As a consequence, when K is large (i.e. 13 for example), the computation cost increases a lot.

Chapter 3

New integral invariants

Integral invariants are an important concept in geometry processing because they allow to robustly compute differential quantities on shapes and to compare shapes [Man+04; Pot+07; Pot+09]. In the literature, integral invariants are volumes or areas computed over the neighborhood of a point P on a surface $\mathcal{S}$. For example, [Pot+09] proposed an integral invariant defined as the volume between the intersection of a ball of radius s and the interior of a surface at point $P \in \mathcal{S}$. These quantities are independent from any coordinate system, and as such, are candidates for shape matching descriptors.

We propose in this chapter the definition of new integral invariants which we deduce from the Wavejets decomposition. Those integral invariants rely on a local parameterization plane. In the general case, this would be a bad idea because of the instability of the decomposition of a surface, which depends on the orientation of the parameterization plane in the ambient space. But we will see that the integral invariant of order 1 we introduce permits to recover the tangent plane in a similar way we can do it with Wavejets or Jets, as explained in chapter 2.

3.1 Definition

In this section, we derive integral invariants from the Wavejets coefficients. As explained in chapter 2, a change in the parameterization orientation in the tangent plane will angularly shift the local Wavejets decomposition of a surface. Thus, considering the magnitude of the Wavejets coefficients makes the local description orientation independent. However, this is not enough to build a robust local description. Indeed, because of the non-orthogonality of the radial part of the Wavejets decomposition, coefficient $|\phi_{k,n}|$ might vary a lot between two similar functions f. On the contrary, integral invariants do not suffer from such an instability. The stability comes from the integration process. Indeed, given a discrete signal spoiled by an additive noise whose distribution is centered at 0, the integration process gives access to quantities with error that can have much lower standard deviation than the initial one.

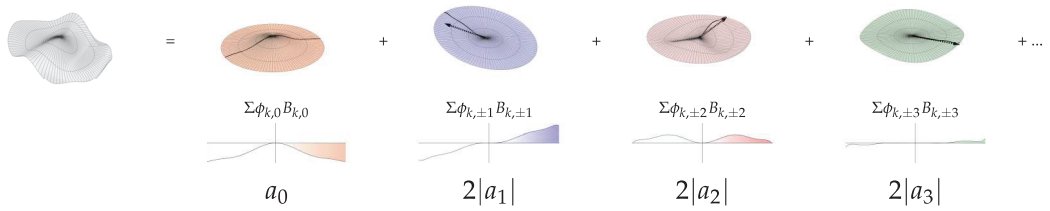

FIGURE 3.1: First row: a local heightfield decomposed by frequencies. Second row: each frequency of the decomposition sliced at its highest magnitude. $a_n(s)$ is the radial cumulated magnitude of the coefficient of frequency n of the Fourier transform of the surface restricted to a circle centered at the origin.

Let us now consider the following angular function given Wavejet coefficients $\phi_{k,n}$ of a function f defined on $[0,s] \times [0,2\pi]$:

$$\begin{aligned}
\mathcal{A}_s(\theta) &= \int_0^s \sum_{k=0}^{\infty} \sum_{n=-k}^{k} \phi_{k,n} r^k e^{in\theta} r dr \\
&= \sum_{k=0}^{\infty} \sum_{n=-k}^{k} \frac{\phi_{k,n}}{k+2} s^{k+2} e^{in\theta} \\
&= \sum_{n=-\infty}^{\infty} \left(\sum_{k=|n|}^{\infty} \frac{\phi_{k,n}}{k+2} s^{k+2} \right) e^{in\theta} \\
&= \sum_{n=-\infty}^{\infty} a_n(s) e^{in\theta}
\end{aligned} \tag{3.1}$$

Where $a_n(s) = \sum_{k=|n|}^{\infty} \frac{\phi_{k,n}}{k+2} s^{k+2}$. $\mathcal{A}_s(\theta)$ is an infinitesimal volume in a given angle direction θ. Each $a_n(s) \in \mathbb{C}$ is a quantity calculated on $f \in \mathscr{C}^\infty$ restricted to frequency n at radius s. Figure 3.1 illustrates such a decomposition.

Definition 5. *Let $\mathcal{V}_s$ be an operator computing the complex volume of a function f on the domain of the disk $\mathcal{D}_s$ of radius s such that $f \in \mathscr{L}^2(\mathcal{D}_s, \mathbb{C})$:*

$$\forall f \in \mathscr{L}^2(\mathcal{D}_s, \mathbb{C}), \mathcal{V}_s(f) = \int_0^{2\pi} \int_0^s f(r,\theta) r dr d\theta \tag{3.2}$$

Given $f \in \mathscr{C}^\infty(\mathcal{D}_s, \mathbb{R})$, $\mathcal{V}_s(f)$ is the signed volume of f, and we can show that $a_0(s)$ is proportional to $\mathcal{V}_s(f)$:

$$\forall f \in \mathscr{C}^\infty,\ \mathcal{V}_s(f) = 2\pi a_0(s) \tag{3.3}$$

Proof.

$$\mathcal{V}_s(f) = \int_0^{2\pi} \mathcal{A}_s(\theta) d\theta = \int_0^{2\pi} \sum_{n=-\infty}^{\infty} a_n(s) e^{in\theta} d\theta = 2\pi a_0(s) \tag{3.4}$$

□

Property 5. *Let $\phi_{k,n}$ be the coefficients of the Wavejets decomposition of a function f representing a surface $\mathcal{S}$ at point P over the tangent plane. Let $\mathcal{A}_s(\theta)$ be the function defined in equation (3.1). Let $|n| < K$, For all $n \in \mathbb{Z}^*$, $|a_n(s)|$ and $a_0(s)$ are integral invariants of $\mathcal{S}$ at point P.*

In the next sections, we show that those new integral invariants are a general case of the *Volume descriptor* defined by [Pot+09] and discuss their properties.

3.2 Generalization of the *Volume descriptor*

Pottmann et al. defined many integral invariants [Pot+09], linking them with the mean curvature. In order to express one of them, from now on, surfaces are assumed to define a separation splitting the ambient space in two, i.e. there is no way to continuously go from one side of the surface to the other without crossing the surface. The normals over the surface define an exterior as well as an interior of the surface. Given a point P on the surface $\mathcal{S}$, given $\varepsilon > 0$ small enough and $\boldsymbol{n}$ the normal at P, the point $Q = P + \varepsilon \boldsymbol{n}$ is said to be in the exterior of $\mathcal{S}$. Any point continuously reachable from Q without crossing the surface is also in the exterior of $\mathcal{S}$. All other points excluding points on $\mathcal{S}$ are said to be in the interior of $\mathcal{S}$. [HT03] expressed the volume of the intersection of a ball centered at a point P and the interior of a hypersurface. Using the special case of this expression for surfaces embedded in 3D, it leads to the volume descriptor definition in [Pot+09], which is an integral invariant. Given a unit ball B following an ℓ^2 norm and $\mathbb{1}_{\mathcal{S}}$ the indicator function s.t. for a point Q, $\mathbb{1}_{\mathcal{S}}(Q) = 1$ if and only if Q is in the interior of $\mathcal{S}$, the *Volume descriptor* is:

$$V_P(s) = \int_{Q \in P + sB} \mathbb{1}_{\mathcal{S}}(Q) dQ \tag{3.5}$$

Hulin [HT03] showed that such a volume has the following Taylor expansion:

$$V_P(s) = \frac{2\pi}{3} s^3 + \frac{\pi \mathcal{H}(P)}{4} s^4 + O(s^5) \tag{3.6}$$

Where $\mathcal{H}(P)$ is the mean curvature of $\mathcal{S}$ at point P. This equation differs a little from the one in [HT03]: we use a different normal orientation convention, yielding a different sign for the mean curvature.

In the remainder of this chapter, let us assume that tangent plane $\mathcal{T}(P)$ is spanned by an arbitrary local orthonormal basis $(\boldsymbol{x}, \boldsymbol{y})$. Let us map the complex plane with $\mathcal{T}(P)$, mapping each point $Q = (x, y) \in \mathcal{T}(P)$ to a complex number $z = x + \boldsymbol{i}y$.

Definition 6. *For any vector $\boldsymbol{v} \in \mathbb{R}^3$, let us note $\theta_{\boldsymbol{v}}$ the argument of the complex number $\langle \boldsymbol{v}, \boldsymbol{x} \rangle + \boldsymbol{i} \langle \boldsymbol{v}, \boldsymbol{y} \rangle$.*

The Volume descriptor *of order n of point $P \in \mathcal{S}$ is:*

$$V_P^n(s) = \int_{Q \in P + sB} \mathbb{1}_{\mathcal{S}}(Q) e^{-\boldsymbol{i} n \theta_{Q-P}} dQ \tag{3.7}$$

The volume of a half ball appears as the first non-zero term in the Taylor expansion of the volume descriptor in equation (3.6). This term vanishes in the volume descriptor expansion of order $n \neq 0$. Indeed, the volume of order $n \neq 0$ of a ball sB or of a half-ball sB^+ composed of points above the local complex plane is:

$$\forall P \in \mathbb{R}^3, \forall s \in \mathbb{R}^+, \begin{cases} \int_{Q \in P + sB} e^{-\boldsymbol{i} n \theta_{Q-P}} dQ = 0 \\ \int_{Q \in P + sB^+} e^{-\boldsymbol{i} n \theta_{Q-P}} dQ = 0 \end{cases} \tag{3.8}$$

Coefficients $a_n(s)$ are defined as integrals on a disk. In particular, $2\pi a_0(s)$ is the volume between the tangent plane and the surface. One may think that linking $a_0(s)$

with the volume descriptor $V_P(s)$ defined in [Pot+09] is not straightforward. In order to do so, one needs to go back to the demonstration expressing the volume of the intersection between a ball of radius s and the interior of a surface, which was done by Hulin [HT03]. The demonstration is done as follows. Instead of using a ball of radius s centered at a point P on the surface $\mathcal{S}$, a cylinder is considered. The cylinder has a base disk of radius s, it is centered at P and its principal axis is colinear with the normal at P. Hulin showed that the difference between computing the volume of the intersection of the interior of a surface with a cylinder or a ball is a quantity in $O(s^7)$.

This yields, for s small enough:

$$V_P(s) = \frac{2\pi}{3}s^3 + 2\pi a_0(s) + O(s^7) \tag{3.9}$$

In practice, if there exists $(x, y) \in \mathcal{D}_s$ such that $|f(x, y)| > s$, a large bias can occur. Indeed, the volume of the intersection of a ball with the interior of the surface is bounded by the volume of the ball, whereas the volume of the intersection with the cylinder can be infinite. This happens when there exists a subset of the local integration disc such that the surface has no orthogonal projection on this subset. This situation occurs when s is too large w.r.t. the local feature size. For convenience and to avoid infinite volume scenarii, we assume that s is small enough so that the intersection the local heightfield $|f| < s$. Thus, we assume that f is inside a cylinder of height $2s$ and of radius s. If not, s is too large to describe the local geometry. Such areas can be seen as outliers at a given scale. However, a good side effect of this limitation is that such quantities are asymptotically bounded by the volume of a ball of radius s, which allows us to still be able to compare those volumes to each others and to sort them.

In order to link $a_n(s)$ and $V_P^n(s)$, the same precautions regarding the volume of a cylinder and of a ball must be taken. Unfortunately, the error bound between a volume computed using a cylinder or a ball cannot be bounded using the work in [HT03]. However, a more general result comes from the work in [DM14]. It is shown that computing the volume between a ball of radius s and a local heightfield f between the tangent plane and the surface at some point P, such that $f = O(s^l)$, where $l \in \mathbb{N}$, induces an error in $O(s^{l+4})$.

Recalling that $a_n(s)$ is the radial integration of concentric Fourier transforms, and the result of equation (3.8), the following stands:

$$V_P^n(s) = 2\pi a_n(s) + O(s^{|n|+6}) \tag{3.10}$$

A computation shows that the Taylor expansion of $a_n(s)$ is:

$$a_n(s) = \sum_{k=|n|}^{\infty} \frac{\phi_{k,n}}{k+2} s^{k+2} \tag{3.11}$$

Hence, the *Volume descriptor* of order n can be written as a Taylor expansion out of the expression of functions $a_n(s)$:

$$V_P^n(s) = 2\pi \frac{\phi_{|n|,n}}{|n|+2} s^{|n|+2} + 2\pi \frac{\phi_{|n|+2,n}}{|n|+4} s^{|n|+4} + O\left(s^{|n|+6}\right) \tag{3.12}$$

The same remark can be done for $n \neq 0$ regarding the values of s for which this equation is still applicable. Let us go back to the case $n = 0$. Using the Taylor

expansion of $a_0(s)$ in (3.9), one has:

$$\begin{aligned} V_P(s) &= \frac{2\pi}{3}s^3 + 2\pi a_0(s) + O(s^7) \\ &= \frac{2\pi}{3}s^3 + \frac{\pi\mathcal{H}(P)}{4}s^4 + O(s^6) \end{aligned} \tag{3.13}$$

Remark 4. *The bound $O(s^5)$ in equation (3.6) is improved to $O(s^6)$. As a consequence, the Taylor expansion of the volume descriptor introduced in [Pot+09] has a better bound than it appeared.*

3.3 Differential properties

In this section, we discuss the generalization of the concept of mean curvature for 2D smooth surfaces embedded in 4D, using an expression involving Wirtinger derivatives. We finally show how to recover the tangent plane out of the volume descriptor of order ± 1 as well as the curvatures out of the volume descriptor of order ± 2.

3.3.1 Links with Wirtinger derivatives

The integral invariants introduced in Definition 6 have links with Wirtinger derivatives; First, we need to define the following operator $\mathcal{F}$

$$\mathcal{F}(f)(s,\theta) = \int_0^s f(r,\theta)dr \tag{3.14}$$

Property 6. *Given $f \in \mathscr{F}^K$, and $a_n(s) \in \mathbb{C}$ the series coefficients from equation (3.1). For $n \geq 0$:*

$$\begin{aligned} a_n(s) &= \frac{1}{2\pi}\mathcal{V}_s \circ \mathcal{F}^n \circ \frac{\partial^n}{\partial z^n} f \\ a_{-n}(s) &= \frac{1}{2\pi}\mathcal{V}_s \circ \mathcal{F}^n \circ \frac{\partial^n}{\partial z^{*n}} f \end{aligned} \tag{3.15}$$

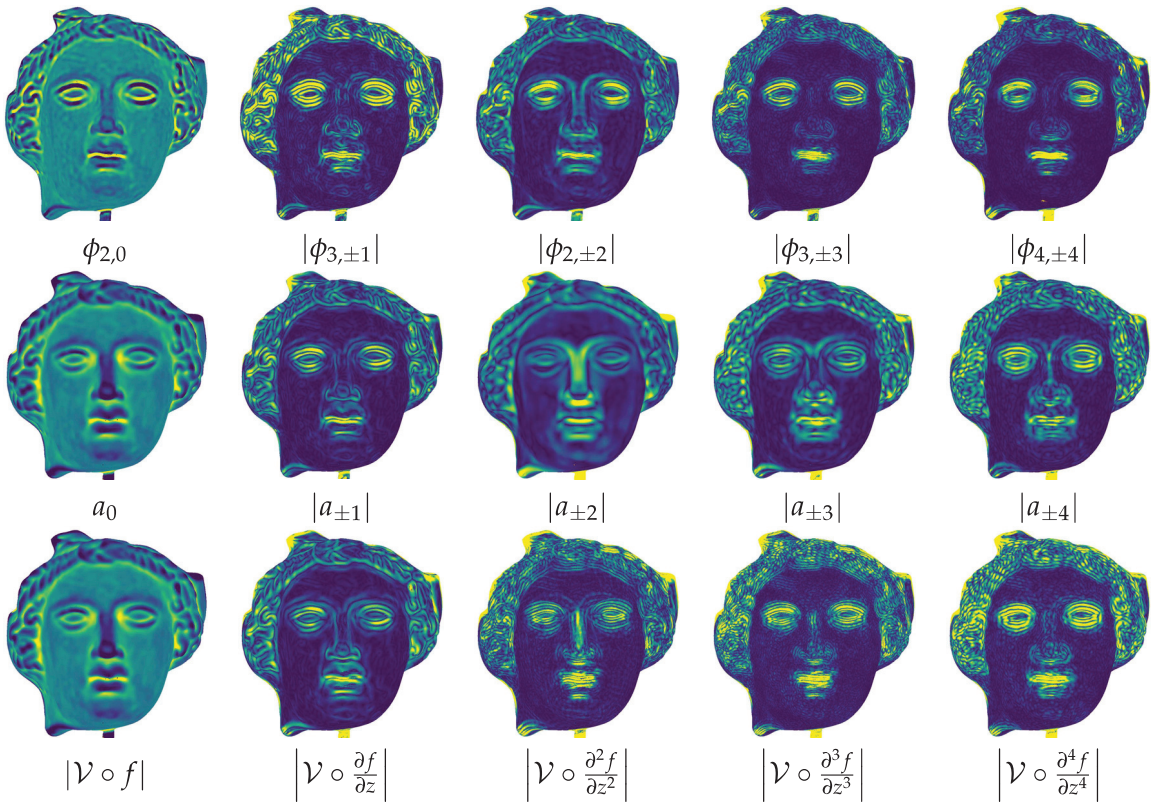

FIGURE 3.2: First row: magnitude of the lowest non-zero order wavejet coefficient field over a shape for each frequency. Second row: integral invariants defined in equation (3.1) of Wavejets of order 7 computed over a surface. Third row: magnitude of the complex volume of n^{th} order Wirtinger derivative.

Proof. From lemma 1, noticing that $r = |z|$, the following derivation can be written for $m \in \mathbb{N}^+$:

$$\begin{aligned}
\frac{1}{2\pi}\left(\mathcal{V}_s \circ \mathcal{F}^m \circ \frac{\partial^m}{\partial z^m} f\right) &= \frac{1}{2\pi}\mathcal{V}_s\left(\int \cdots \int_{[0,r]^m} \sum_{k=0}^{K-m} \sum_{n=-k}^{k} \frac{\left(m+\frac{k+n}{2}\right)!}{\frac{k+n}{2}!} \phi_{k+m,n+m} \rho^k e^{in\theta} (d\rho)^m\right) \\
&= \frac{1}{2\pi}\mathcal{V}_s\left(\sum_{k=0}^{K-m} \sum_{n=-k}^{k} \frac{k!\left(m+\frac{k+n}{2}\right)!}{(m+k)!\frac{k+n}{2}!} \phi_{k+m,n+m} r^{k+m} e^{in\theta}\right) \\
&= \frac{1}{2\pi}\int_0^{2\pi}\int_0^{s} \sum_{k=0}^{K-m} \sum_{n=-k}^{k} \frac{k!\left(m+\frac{k+n}{2}\right)!}{(m+k)!\frac{k+n}{2}!} \phi_{k+m,n+m} r^{k+m} e^{in\theta} r dr d\theta \\
&= \sum_{k=0}^{K-m} \frac{k!\left(m+\frac{k}{2}\right)!}{(m+k)!\frac{k}{2}!} \frac{\phi_{k+m,m}}{k+m+2} s^{k+m+2} \\
&= a_m(s) + O(s^{m+4})
\end{aligned} \tag{3.16}$$

The proof of the second part of equation (3.15) is straightforward since $a_n = a^*_{-n}$ and $\left(\frac{\partial}{\partial z}\right)^* = \frac{\partial}{\partial z^*}$. □

The Wirtinger derivative reduces both frequencies and orders when applied to

a function. However, recursive differentiation with Wirtinger derivatives is quite unstable for the same reasons that it is unstable with ordinary derivatives. Figure 3.2 shows scalar fields over a surface of the magnitude of the *Volume descriptor* at order n, as well as the magnitude of the volume of the Wirtinger derivative of order n. The *Volume descriptor* at order n is smoother. Let us discuss the stability of such quantities.

Property 7. *Let $(K,n) \in \mathbb{N}^2$, sB be a ball of radius s following an ℓ^2 norm, and $f \in \mathscr{C}^{K+n}(sB,\mathbb{R})$. Let $\phi_{k,m}$ be the coefficients of the Wavejet decomposition of f at order K and frequency m. For $n > 0$:*

$$\begin{aligned}(n+2)\frac{a_n(s)}{s^{n+2}} &= \phi_{n,n} + (n+2)\sum_{k=n+2}^{K}\frac{1}{k+2}\phi_{k+n,n}s^k + O\left(\frac{ns^K}{K}\right)\\ 2\frac{\mathcal{V}_s\left(\frac{\partial^n f}{\partial z^n}\right)}{\pi s^2} &= \phi_{n,n} + 2\sum_{k=2}^{K}\frac{\prod_{m=1}^{\frac{k}{2}}(n+m)}{\left(\frac{k}{2}+2\right)!}\phi_{k+n,n}s^k + O\left(\frac{\left(s\sqrt{n}\right)^K}{K}\right)\end{aligned} \tag{3.17}$$

Proof. The first part of the property is directly retrieved from equation (3.1).

The second part can be shown using Lemma 1:

$$\begin{aligned}2\frac{\mathcal{V}_s \circ \frac{\partial^p f}{\partial z^p}}{\pi s^2} &= 2\frac{1}{\pi s^2}\int_0^{2\pi}\int_0^s \sum_{n=-\infty}^{K}\sum_{k=0}^{\infty}\frac{\left(p+\frac{k+n}{2}\right)!}{\frac{k+n}{2}!}\phi_{k,n}s^k e^{in\theta} r dr d\theta\\ &= \frac{2}{p!}\sum_{k=0}^{\infty}\frac{\left(\frac{k}{2}+p\right)!}{\frac{k}{2}!\left(\frac{k}{2}+2\right)}\phi_{k+p,p}s^k\\ &= \phi_{p,p} + 2\sum_{k=2}^{\infty}\frac{\prod_{m=1}^{\frac{k}{2}}(p+m)}{\frac{k}{2}+2}\phi_{k+p,p}s^k\\ &= \phi_{p,p} + 2\sum_{k=2}^{K}\frac{\prod_{m=1}^{\frac{k}{2}}(p+m)}{\frac{k}{2}+2}\phi_{k+p,p}s^k + O\left(\frac{\left(s\sqrt{p}\right)^K}{K}\right)\end{aligned} \tag{3.18}$$

□

Thus, $|a_n(s)|$ is more stable than $\left|\mathcal{V}\circ\frac{\partial^n f}{\partial z^n}\right|(s)$. Indeed, coefficients of high order involved in $\mathcal{V}_s\left(\frac{\partial^n f}{\partial z^n}\right)$ are amplified by a polynomial in n. Let s be the largest radius for which $a_n(s)$ yields a close enough approximation of $\phi_{n,n}$. Then, $\frac{s}{\sqrt{n}}$ is the largest radius for which $\mathcal{V}\circ\frac{\partial^n f}{\partial z^n}(s)$ gives a similar approximation of $\phi_{|n|,n}$. Thus, for large n, $a_n(s)$ becomes a much better approximation of $\phi_{|n|,n}$. Operator $\mathcal{F}$ applied n times stabilizes the n^{th} Wirtinger derivative before the volume computation. This recursive radial integration recovers the lost orders in the derivation process, but does nothing about the lost frequencies, which allows the volume operator $\mathcal{V}_s$ to catch stable quantities related to the Wirtinger derivative of order n. The same remark can be made for the conjugate of the Wirtinger derivative when n is negative.

3.3.2 Real 2-manifolds of codimension 2

Study framework

In this section, we review a few local geometric properties of smooth real 2-manifolds of codimension 2. A real 2-manifold of codimension 2 is a real 2-manifold embedded

in $\mathbb{R}^4$. Let us note the set of such objects $\mathscr{M}$. When one applies the Wirtinger derivative operator to a local heightfield, the surface $\mathcal{S} \in \mathscr{S}$ outlined by this heightfield is transformed into a manifold $\mathcal{M} \in \mathscr{M}$. We aim to give a few tools to give hints on differential properties of such objects, and especially will focus on their curvature. This will be found especially useful for interpreting $a_{\pm 1}(s)$, which unravels a differential property of surfaces that is poorly used in geometry processing. An example of its use is shown in chapter 4.

Let us consider an element $\mathcal{M} \in \mathscr{M}$. The tangent space at each point of $\mathcal{M}$ is a two dimensional space, which we refer as a tangent plane $\mathcal{T}$. However, in contrast with elements of $\mathscr{S}$, the space orthogonal to the tangent plane at each point $P \in \mathcal{M}$, is two-dimensional as well. We note the plane orthogonal to the tangent plane $\mathcal{T}^\perp$.

In the general case, we note $\mathcal{P}$ any plane passing by $P \in \mathcal{M}$ such that the angle between $\mathcal{P}$ and $\mathcal{T}$ is in $O(s)$ at given radius s. Let $(\boldsymbol{x}, \boldsymbol{y})$ be an orthonormal basis of $\mathcal{P}$, where $(\boldsymbol{x}, \boldsymbol{y}) \in \mathbb{R}^4 \times \mathbb{R}^4$. We note $\mathcal{P}^\perp$ the plane orthogonal to $\mathcal{P}$ passing by P, and note $(P, \boldsymbol{n_1}, \boldsymbol{n_2})$ an orthogonal basis of such a plane, where the coordinates of P are $(0, 0)$ in both basis.

It is often convenient for 2-dimensional spaces to use the complex plane instead of $\mathbb{R}^2$. Hence, we canonically map a complex plane to $\mathcal{P}$ (resp. $\mathcal{P}^\perp$), where the complex number $z = x + \boldsymbol{i}y$ (resp. $h = h_1 + \boldsymbol{i}h_2$) maps to (x, y) (resp. (h_1, h_2)) in $\mathcal{P}$ (resp. $\mathcal{P}^\perp$). From now on, $\mathcal{P}$ (resp. $\mathcal{P}^\perp$) refers to itself or its complex plane.

Let $\mathcal{D}_s^{\mathbb{C}}$ be a disc of radius s in the complex plane. Let $\Omega \subset \mathcal{M} \in \mathscr{M}$ such that $P \in \Omega$ and that, given any point $Q = (x, y, h_1, h_2) \in \Omega$ expressed in the basis $(\boldsymbol{x}, \boldsymbol{y}, \boldsymbol{n_1}, \boldsymbol{n_2})$ formed by the concatenation of the basis of $\mathcal{P}$ and $\mathcal{P}^\perp$, there exists a function $g : \mathcal{D}_s^{\mathbb{C}} \to \mathbb{C}$, uniquely mapping each complex $z = x + \boldsymbol{i}y$ to the complex $g(z) = h_1 + \boldsymbol{i}h_2$.

$\mathcal{M}$ being a manifold, around $P \in \mathcal{M}$, there exists a small neighborhood $\Omega \subset \mathcal{M}$ that can be parameterized over $\mathcal{D}_s^{\mathbb{C}}$ a disc of radius s in $\mathcal{P}$. Let us define $g_n(z)$ for $n \geq 0$ (resp. $n < 0$) as $g_n(z) = \frac{\partial^n f}{\partial z^n}$ (resp. $g_n(z) = \frac{\partial^{|n|} f}{\partial z^{*n}}$).

Complex functions $g_n(s)$ have properties that are difficult to apprehend. For example, only positive frequency coefficients from the Wavejets decomposition of a real function f are required to infer the entire function because the negative frequency coefficients are the conjugates of the positive ones. This is not the case anymore for g_n. Noting $\psi^n_{k,m}$ the Wavejet decomposition of g_n, one would need an other approach for describing the horse saddle equivalent to those functions, held by coefficients $\psi^n_{2,\pm 2}$. The same remark can be done for the tangent plane held by coefficients $\psi^n_{1,\pm 1}$. Luckily, for $k > |n|$, coefficients $\phi_{k,n}$ of f, which are the coefficients appearing in the Taylor expansion of a_n and the quantities we as interested in, are proportional to coefficients $\psi^n_{k-|n|,0}$ of g_n, alleviating the necessity of discussing the case of frequencies $m \neq 0$ for complex functions.

Fundamental forms

Two main operators are usually used for locally analyzing a surface: the First Fundamental form, noted I, and the Second Fundamental form, noted II. The First Fundamental form is an operator transforming two vectors of the tangent plane to a scalar. It generalizes the inner product to manifold and can be expressed as a matrix w.r.t. the local parameterization basis in the tangent plane. The Second Fundamental form is an operator taking as inputs two vectors of the tangent plane $(\boldsymbol{u}, \boldsymbol{v})$ which can be used, for example, to compute the inner product between the gradient in direction $\boldsymbol{u}$ of the normals, with $\boldsymbol{v}$. Those forms exist for any N-manifold of codimension

1. They can also be generalized to any N-manifold of codimension strictly greater than 1. The Second Fundamental form is usually expressed as a the Hessian of the local heightfield w.r.t. tangent plane. It expresses the best quadric locally fitting the manifold at P.

The First and the Second Fundamental forms can be used to define instrinsic, as well as extrinsic properties of a manifold, including the mean curvature $\mathcal{H}$, which can be computed for any point P on a smooth manifold. In the case of N-manifolds of codimension 1, $\mathcal{H} = \frac{1}{N}\text{tr}(\text{II} \times \text{I}^{-1})$ is a real number. In the case of manifolds of codimension strictly greater than 1, a mean curvature can be computed for each direction in $\mathcal{T}^{\perp}$ at P, and one can write the mean curvature at P as a vector in $\mathcal{T}^{\perp}$.

When the codimension is equal to 2, one can linearly map each plane $\mathcal{T}^{\perp}$ to the complex plane, and express this mean curvature vector as a complex number. The real part of this complex number is the mean curvature in the direction $\boldsymbol{n_1}$, and the imaginary part is the mean curvature in direction $\boldsymbol{n_2}$. We call such a mean curvature a complex mean curvature. In the case of a real function $f(z)$, the mean curvature expresses wether the surface locally evolves in the normal direction (positive mean curvature) or in the opposite direction (negative mean curvature). In the case of our function $g_n(z)$, the mean curvature does not have anymore a binary orientation, but a continuous one. The argument of the complex mean curvature at $z = 0$ expresses in which direction in $\mathcal{T}^{\perp}$ the surface locally tends to. Since $g_n(z)$ is a Wirtinger derivative of order $|n|$ of f, the argument of its complex mean curvature at $z = 0$ yields the mean orientation of such a derivative.

Before expressing the Taylor expansions of functions $a_n(s)$ using the complex mean curvature, we show, in the following paragraph, how fundamental forms can be written differently using the Wirtinger derivatives instead of the conventional ones. A side consequence of this is that a complex Gaussian curvature can be expressed out of this new expression of the fundamental forms.

Fundamental forms using Wirtinger derivatives and the complex plane

In this paragraph, we show that Fundamental forms can be expressed for complex functions $f : \mathbb{C} \to \mathbb{C}$. Let us first recall how to express the First Fundamental form in the case of real surfaces. Let $(\boldsymbol{x}, \boldsymbol{y})$ be a basis on the tangent plane of $\mathcal{S} \in \mathscr{S}$ at point P. Let $\boldsymbol{u}$ and $\boldsymbol{v}$ be two tangent vectors of $\mathcal{S}$ at point P. The inner product between $\boldsymbol{u} = (u_x, u_y)^T$ and $\boldsymbol{v} = (v_x, v_y)^T$ can be expressed in basis $(\boldsymbol{x}, \boldsymbol{y})$:

$$\begin{aligned}\langle \boldsymbol{u}, \boldsymbol{v} \rangle &= u_x v_x \langle \boldsymbol{x}, \boldsymbol{x} \rangle + u_x v_y \langle \boldsymbol{x}, \boldsymbol{y} \rangle + u_y v_x \langle \boldsymbol{y}, \boldsymbol{x} \rangle + u_y v_y \langle \boldsymbol{y}, \boldsymbol{y} \rangle \\ &= u_x v_x E + u_x v_y F + u_y v_x F + u_y v_y G \\ &= \boldsymbol{v}^T \begin{pmatrix} E & F \\ F & G \end{pmatrix} \boldsymbol{u} \\ &= \boldsymbol{v}^T \text{I} \boldsymbol{u}\end{aligned} \tag{3.19}$$

I is the First Fundamental form. Let us express it using a different base on the tangent plane. Let us linearly map the tangent plane to the complex plane and consider the following tangent vectors $\frac{1}{\sqrt{2}}(\boldsymbol{x} + \boldsymbol{i}\boldsymbol{y}, \boldsymbol{x} - \boldsymbol{i}\boldsymbol{y}) = (\boldsymbol{z}, \boldsymbol{z}^*)$. Let $\boldsymbol{u}_W = \frac{1}{\sqrt{2}}(u_x + \boldsymbol{i}u_y, u_x - \boldsymbol{i}u_y)^T$ and $\boldsymbol{v}_W = \frac{1}{\sqrt{2}}(v_x + \boldsymbol{i}v_y, v_x - \boldsymbol{i}v_y)^T$ be two tangent vectors. Let

$\langle .,. \rangle$ be the canonical hermitian inner product. We note I_W the following metric:

$$\begin{aligned}\langle \boldsymbol{u}_W, \boldsymbol{v}_W \rangle_W &= \boldsymbol{u}_W^* \begin{pmatrix} \langle \boldsymbol{z}, \boldsymbol{z} \rangle & \langle \boldsymbol{z}, \boldsymbol{z}^* \rangle \\ \langle \boldsymbol{z}^*, \boldsymbol{z} \rangle & \langle \boldsymbol{z}^*, \boldsymbol{z}^* \rangle \end{pmatrix} \boldsymbol{v}_W \\ &= \boldsymbol{u}_W^* \begin{pmatrix} E_W & F_W^* \\ F_W & E_W \end{pmatrix} \boldsymbol{v}_W \\ &= \boldsymbol{u}_W^* \mathrm{I}_W \boldsymbol{v}_W \end{aligned} \tag{3.20}$$

We call I_W the First Wirtinger Fundamental form.

Property 8. *Given:*

- $(u_x, u_y, v_x, v_y) \in \mathbb{R}^4$
- $\boldsymbol{u} = (u_x, u_y)^T$ *and* $\boldsymbol{v} = (v_x, v_y)^T$
- $\boldsymbol{u}_W = \frac{1}{\sqrt{2}}(u_x + \boldsymbol{i}u_y, u_x - \boldsymbol{i}u_y)^T$ *and* $\boldsymbol{v}_W = \frac{1}{\sqrt{2}}(v_x + \boldsymbol{i}v_y, v_x - \boldsymbol{i}v_y)^T$*:*

Then:

$$\boldsymbol{v}^T \mathrm{I} \boldsymbol{u} = \boldsymbol{v}_W^* \mathrm{I}_W \boldsymbol{u}_W \tag{3.21}$$

Proof. Let us expand $\boldsymbol{u}_W^* \mathrm{I}_W \boldsymbol{v}_W$:

$$\begin{aligned}\boldsymbol{u}_W^* \mathrm{I}_W \boldsymbol{v}_W &= \frac{1}{2} \boldsymbol{u}_W^* \begin{pmatrix} \langle \boldsymbol{x} + \boldsymbol{i}\boldsymbol{y}, \boldsymbol{x} + \boldsymbol{i}\boldsymbol{y} \rangle & \langle \boldsymbol{x} + \boldsymbol{i}\boldsymbol{y}, \boldsymbol{x} - \boldsymbol{i}\boldsymbol{y} \rangle \\ \langle \boldsymbol{x} - \boldsymbol{i}\boldsymbol{y}, \boldsymbol{x} + \boldsymbol{i}\boldsymbol{y} \rangle & \langle \boldsymbol{x} - \boldsymbol{i}\boldsymbol{y}, \boldsymbol{x} - \boldsymbol{i}\boldsymbol{y} \rangle \end{pmatrix} \boldsymbol{v}_W \\ &= \frac{1}{2\sqrt{2}} \boldsymbol{u}_W^* \begin{pmatrix} \langle \boldsymbol{x}, \boldsymbol{x} \rangle + \langle \boldsymbol{y}, \boldsymbol{y} \rangle & \langle \boldsymbol{x}, \boldsymbol{x} \rangle - \langle \boldsymbol{y}, \boldsymbol{y} \rangle + 2\boldsymbol{i}\langle \boldsymbol{x}, \boldsymbol{y} \rangle \\ \langle \boldsymbol{x}, \boldsymbol{x} \rangle - \langle \boldsymbol{y}, \boldsymbol{y} \rangle - 2\boldsymbol{i}\langle \boldsymbol{x}, \boldsymbol{y} \rangle & \langle \boldsymbol{x}, \boldsymbol{x} \rangle + \langle \boldsymbol{y}, \boldsymbol{y} \rangle \end{pmatrix} \begin{pmatrix} v_x + \boldsymbol{i}v_y \\ v_x - \boldsymbol{i}v_y \end{pmatrix} \\ &= \frac{1}{2} \begin{pmatrix} u_x - \boldsymbol{i}u_y & u_x + \boldsymbol{i}u_y \end{pmatrix} \begin{pmatrix} v_x \langle \boldsymbol{x}, \boldsymbol{x} \rangle + \boldsymbol{i}v_y \langle \boldsymbol{y}, \boldsymbol{y} \rangle + \boldsymbol{i}\langle \boldsymbol{x}, \boldsymbol{y} \rangle (v_x - \boldsymbol{i}v_y) \\ v_x \langle \boldsymbol{x}, \boldsymbol{x} \rangle - \boldsymbol{i}v_y \langle \boldsymbol{y}, \boldsymbol{y} \rangle - \boldsymbol{i}\langle \boldsymbol{x}, \boldsymbol{y} \rangle (v_x + \boldsymbol{i}v_y) \end{pmatrix} \\ &= u_x v_x \langle \boldsymbol{x}, \boldsymbol{x} \rangle + u_y v_y \langle \boldsymbol{y}, \boldsymbol{y} \rangle + (u_x v_y + u_y v_x) \langle \boldsymbol{x}, \boldsymbol{y} \rangle \\ &= \boldsymbol{u}^T \mathrm{I} \boldsymbol{v} \end{aligned} \tag{3.22}$$

Which concludes the proof. □

Property 9. I_W *and* I *are similar matrices:*

$$\mathrm{I}_W = C^* \mathrm{I} C \tag{3.23}$$

Where $C = \frac{1}{\sqrt{2}} \begin{pmatrix} 1 & -\boldsymbol{i} \\ 1 & \boldsymbol{i} \end{pmatrix}$ *is a unitary matrix.*

Proof. It is straightforward to see that:

$$\mathrm{I}_W = \frac{1}{4} \begin{pmatrix} E + G & E - G - 2\boldsymbol{i}F \\ E - G + 2\boldsymbol{i}F & E + G \end{pmatrix} \tag{3.24}$$

We now need to expand $C^* \mathrm{I} C$:

$$\begin{aligned} C^* \mathrm{I} C &= \frac{1}{4} \begin{pmatrix} 1 & 1 \\ \boldsymbol{i} & -\boldsymbol{i} \end{pmatrix} \begin{pmatrix} E + G & E - G - 2\boldsymbol{i}F \\ E - G + 2\boldsymbol{i}F & E + G \end{pmatrix} \begin{pmatrix} 1 & -\boldsymbol{i} \\ 1 & \boldsymbol{i} \end{pmatrix} \\ &= \frac{1}{2} \begin{pmatrix} 1 & 1 \\ \boldsymbol{i} & -\boldsymbol{i} \end{pmatrix} \begin{pmatrix} E - \boldsymbol{i}F & -\boldsymbol{i}G + F \\ E + \boldsymbol{i}F & \boldsymbol{i}G + F \end{pmatrix} \\ &= \begin{pmatrix} E & F \\ F & G \end{pmatrix} \end{aligned} \tag{3.25}$$

□

Similarly, we define the Second Wirtinger Fundamental form, using the Wirtinger derivatives instead of the conventional ones. Given a heightfield f between the tangent plane and a smooth surface $\mathcal{S}$ at some point $P \in \mathcal{S}^2$, the Second Fundamental form has the following expression:

$$\mathrm{II} = \begin{pmatrix} \frac{\partial^2 f}{\partial x^2} & \frac{\partial^2 f}{\partial xy} \\ \frac{\partial^2 f}{\partial xy} & \frac{\partial^2 f}{\partial y^2} \end{pmatrix} = \begin{pmatrix} L & M \\ M & N \end{pmatrix} \tag{3.26}$$

We now define a Second Wirtinger Fundamental form:

$$\mathrm{II}_W = 2 \begin{pmatrix} \frac{\partial^2 f}{\partial z \partial z^*} & \frac{\partial^2 f}{\partial z^2} \\ \frac{\partial^2 f}{\partial z^{*2}} & \frac{\partial^2 f}{\partial z \partial z^*} \end{pmatrix} = \begin{pmatrix} M_W & L_W \\ N_W & M_W \end{pmatrix} \tag{3.27}$$

Property 10. II_W *and* II *are similar matrices:*

$$\mathrm{II}_W = C^* \mathrm{II} C \tag{3.28}$$

Where $C = \frac{1}{\sqrt{2}} \begin{pmatrix} 1 & -\boldsymbol{i} \\ 1 & \boldsymbol{i} \end{pmatrix}$.

Proof. Let us express II_W w.r.t. ordinary derivatives:

$$\mathrm{II}_W = \frac{1}{2} \begin{pmatrix} L+N & L-N+2\boldsymbol{i}M \\ L-N-2\boldsymbol{i}M & L+N \end{pmatrix} \tag{3.29}$$

We now need to expand $C^* \mathrm{II}_W C$:

$$\begin{aligned} C^* \mathrm{II}_W C &= \frac{1}{4} \begin{pmatrix} 1 & 1 \\ \boldsymbol{i} & -\boldsymbol{i} \end{pmatrix} \begin{pmatrix} L+N & L-N+2\boldsymbol{i}M \\ L-N-2\boldsymbol{i}M & L+N \end{pmatrix} \begin{pmatrix} 1 & -\boldsymbol{i} \\ 1 & \boldsymbol{i} \end{pmatrix} \\ &= \frac{1}{2} \begin{pmatrix} 1 & 1 \\ \boldsymbol{i} & -\boldsymbol{i} \end{pmatrix} \begin{pmatrix} L+\boldsymbol{i}M & \boldsymbol{i}(-N+\boldsymbol{i}M) \\ L-\boldsymbol{i}M & \boldsymbol{i}(N+\boldsymbol{i}M) \end{pmatrix} \\ &= \begin{pmatrix} L & M \\ M & N \end{pmatrix} \end{aligned} \tag{3.30}$$

□

Those forms were purposely named using the terminology First and Second Wirtinger Fundamental forms because one can compute the complex mean curvature as well as a complex version of the Gaussian curvature using those forms in the exact same way they are defined with the regular Fundamental forms. Of course, a complex function having complex ordinary derivatives, one could directly derive a complex version out of the Fundamental forms out of those by splitting this function into its real and imaginary parts. However, Wirtinger derivatives having been built to simplify the differential analysis of complex functions, they are more handy to work with for studying complex function between the tangent plane and a manifolds $\mathcal{M} \in \mathscr{M}$ at some point $P \in \mathcal{M}$. This way, we constructed a differential framework which is directly usable with Wirtinger derivatives. We show that this other way of writing the Fundamental forms ends up with a similar expression of the mean and

Gaussian curvatures.

$$\left\{\begin{array}{lcll}\mathcal{H} & = & \frac{1}{2}\mathrm{tr}\left(\mathrm{II}\times\mathrm{I}^{-1}\right) & = & \frac{1}{2}\mathrm{tr}\left(\mathrm{II}_W\times\mathrm{I}_W^{-1}\right)\\ \mathcal{K} & = & \frac{\det(\mathrm{II})}{\det(\mathrm{I})} & = & \frac{\det(\mathrm{II}_W)}{\det(\mathrm{I}_W)}\end{array}\right. \tag{3.31}$$

Proof. Since C^*C is obviously invertible, $C^*C(C^*C)^{-1} = \mathrm{Id}$, where Id is the identity matrix. Since square matrices of the same dimension are commutative inside the trace, $\mathrm{tr}(C^*\mathrm{II}C(C^*\mathrm{I}C)^{-1}) = \mathrm{tr}(\mathrm{II}\times\mathrm{I}^{-1})$. Similarly, $\frac{\det(C^*\mathrm{II}C)}{\det(C^*\mathrm{I}C)} = \frac{\det(\mathrm{II})}{\det(\mathrm{I})}$. □

Remark 5. *Since a function $g:\mathbb{C}\to\mathbb{C}$ is differentiable in the complex plane if and only if $\frac{\partial g}{\partial z^*}=0$, if f is differentiable in the complex plane, then it has zero mean and Gaussian curvature.*

Mean curvature of high order Wirtinger derivatives

As shown in Lemma 1, if $f\in\mathscr{C}^K$, given a natural $p\leq K$,

$$\frac{\partial^p f}{\partial z^p}(z) = \sum_{k=0}^{K-p}\sum_{n=-k}^{k}\frac{\left(p+\frac{k+n}{2}\right)!}{\frac{k+n}{2}!}\phi_{k+p,n+p}z^{\frac{k-n}{2}}z^{*\frac{k+n}{2}} + O(|z|^{K-p}) \tag{3.32}$$

A Taylor expansion of order 2 for $p\leq K-2$ yields:

$$\begin{aligned}\frac{\partial^p f}{\partial z^p}(z) =& p!\phi_{p,p} + (p+1)!\phi_{p+1,p+1}z + p!\phi_{p+1,p-1}z^*\\ &+\frac{(p+2)!}{2}\phi_{p+2,p+2}z^2 + (p+1)!\phi_{p+2,p}zz^* + p!\phi_{p+2,p-2}z^{*2} + O(|z|^3)\end{aligned} \tag{3.33}$$

Note that linear components in this Taylor expansion are not necessarily equal to zero. However, using the stability Theorem in section 2.2.5 (Theorem 2), one can show that the complex mean curvature of such functions can be estimated using only the coefficient bound to zz^*, inducing an error of its estimate negligible w.r.t. the linear coefficients. Indeed, the complex mean curvature of a complex function is the concatenation of the mean curvatures of its real and its imaginary parts. If there is no linear component, i.e. the parameterization plane is the tangent plane, the mean curvature is proportional to the coefficient of the monomial $r^2 = zz^*$. If not, Theorem 2 states that this coefficient is stable with an error in $o(r)$ (with $o(r)=o(z)=o(z^*)$), i.e. it is negligible w.r.t. the linear part of its Taylor expansion. By concatenating the real and imaginary parts, the mean curvature of a complex function at $z=0$ is proportional to the quadratic coefficient bound to zz^* with an error negligible w.r.t. the linear coefficients. Thus, one can write the following Taylor expansion for the mean curvature of the p^{th} order Wirtinger derivative of f:

$$\mathcal{H}\left(\frac{\partial^p f}{\partial z^p}\right) = \frac{1}{2}\mathrm{tr}\left(\mathrm{II}\left(\frac{\partial^p f}{\partial z^p}\right)\left(\mathrm{I}\left(\frac{\partial^p f}{\partial z^p}\right)\right)^{-1}\right) = 2(p+1)!\phi_{p+2,p} + o(\phi_{p+1,p\pm1}) \tag{3.34}$$

Combining equations (2.68) and (3.1), coefficients $a_n(s)$ have the following Taylor expansion for $n \geq 0$:

$$\begin{aligned} a_n(s) &= \frac{1}{n!(n+2)} \frac{\partial^n f}{\partial z^n}(0) s^{n+2} + \frac{1}{2(n+1)!(n+4)} \mathcal{H}\left(\frac{\partial^n f}{\partial z^n}\right) s^{n+4} + o(s^{n+4}) \\ a_{-n}(s) &= \frac{1}{n!(n+2)} \frac{\partial^n f}{\partial z^{*n}}(0) s^{n+2} + \frac{1}{2(n+1)!(n+4)} \mathcal{H}\left(\frac{\partial^n f}{\partial z^{*n}}\right) s^{n+4} + o(s^{n+4}) \end{aligned} \tag{3.35}$$

3.3.3 Approximation of the tangent plane

Let us go back to real surfaces $\mathcal{S} \in \mathscr{S}$. The volume descriptors of order ± 1 can be used to estimate the tangent plane in a way similar to the one of Jets and Wavejets.

Property 11. *Let $\mathcal{S} \in \mathscr{S}^1$ be a surface. Let $(\boldsymbol{x}, \boldsymbol{y})$ be an orthonormal basis in a plane $\mathcal{P}$ close to the tangent plane at point P, where $\mathcal{P}$ passes by P, and let $\phi_{k,n}$ be the Wavejets decomposition of $\mathcal{S}$ of the heightfield between $\mathcal{P}$ and $\mathcal{S}$ in basis $(\boldsymbol{x}, \boldsymbol{y})$:*

$$\phi_{1,\pm 1} = -\frac{3}{2\pi} \lim_{s \to 0} \frac{V_P^{\pm 1}(s)}{s^3} \tag{3.36}$$

Where $V_P^n(s)$ is as defined in Definition 6 in section 3.2.

Proof.

$$V_P^{\pm 1}(s) = -2\pi \left(\frac{\phi_{1,\pm 1}}{3} s^3 + \frac{\phi_{3,\pm 1}}{5} s^5 \right) + o(s^5) \tag{3.37}$$

This yields for $s \neq 0$:

$$-\frac{V_P^{\pm 1}(s)}{2\pi s^3} = \frac{\phi_{1,\pm 1}}{3} + \frac{\phi_{3,\pm 1}}{5} s^2 + o(s^2) \tag{3.38}$$

Equation 3.36 follows.

□

A direct consequence of Property 11 is that if we can estimate the limit of the volume descriptor of orders ± 1 divided by s^3 at zero, we can correct under the small error hypothesis, the tangent plane estimation. From now on, we will assume that the tangent plane is *correct*, i.e. $\phi_{1,\pm 1} = 0$.

3.3.4 Curvatures

Given a surface $\mathcal{S} \in \mathscr{S}^2$, the volume descriptors of order ± 2 computed at point $P \in \mathcal{S}$ w.r.t. the tangent plane give a direct estimate of the principal directions. Combining it with the volume descriptor of order 0 gives access to the Gaussian curvature $\mathcal{K}(P)$ as well as principal curvatures $\kappa_1(P)$ and $\kappa_2(P)$, where $P \in \mathcal{S}$.

Property 12. *Let $\mathcal{S} \in \mathscr{S}^2$ and let $P \in \mathcal{S}$. Given local parameterization in the tangent plane of $\mathcal{S}$ at point P parameterized by $(\boldsymbol{x}, \boldsymbol{y})$. The phase of $V_P^{\pm 2}(s) = -2\pi a_{\pm 2}(s)$ gives an estimation in $O(s^2)$ of the principal directions of order 2 of $\mathcal{S}$ at point P. In particular, the principal direction corresponding to the highest principal curvature is aligned with $Re(a_2(s))\boldsymbol{x} - Im(a_2(s))\boldsymbol{y}$.*

Proof. Assuming that the local computation of $a_{\pm 2}$ is done using the tangent plane, the phase of $\phi_{2,\pm 2}$ holds information about principal directions, as discussed in section 2.2.3. Noticing that $\frac{a_{\pm 2}(s)}{s^2} = \frac{\phi_{2,\pm 2}}{4} + O(s^2)$ concludes the proof. □

Property 13. *Let $\mathcal{S} \in \mathscr{S}^2$ and let $P \in \mathcal{S}$. Given the local parameterization $(\boldsymbol{x}, \boldsymbol{y})$ in the tangent plane at point P, the principal curvatures κ_1 and κ_2 and the Gaussian curvature $\mathcal{K}(P)$ are a linear combination of the* Volumes descriptors *of order 0, -2 and 2:*

$$\begin{aligned} \kappa_1 &= \frac{4}{s^2}\left(a_0(s) + a_2(s) + a_{-2}(s)\right) + O(s^2) \\ \kappa_2 &= \frac{4}{s^2}\left(a_0(s) - a_2(s) - a_{-2}(s)\right) + O(s^2) \\ \mathcal{K}(P) &= \frac{16}{s^4}\left(a_0^2 - 4a_{-2}a_2\right) + O(s^2) \end{aligned} \tag{3.39}$$

Proof. To prove the two first equations, we use equation (2.28) and associate coefficients $\phi_{k,n}$ with the coefficients of the Taylor expansion of $a_n(s)$ from equation (3.35). The Gaussian curvature result follows by multiplication. □

3.4 Computation of the *Volume descriptor*

3.4.1 From Wavejets

One can directly estimate functions $a_n(s)$ using the local Wavejets decomposition of a surface in the tangent plane. Wavejets coefficients appear in its Taylor expansion (see equation (3.1)). However, one should be aware that there can be instability when computing the Wavejets decomposition in some cases. If the orthonormal projection of the surface in the tangent plane is surjective, then one cannot express a heightfield, and the Wavejet decomposition cannot be safely computed. Moreover, if there lacks points near the boundaries of the neighborhood used to estimate the Wavejet decomposition, Wavejets coefficients computed by solving equation (2.89) can have high magnitudes. Indeed, in this case, the system has no constraints. This can locally induce high variations on the estimated surface so it matches better the point positions in the rest of the neighborhood, which translates into high magnitude coefficients.

To conclude, one can retrieve $a_n(s)$ from the local Wavejet decomposition of the surface almost everywhere, but a few outliers can appear in some well-defined cases.

3.4.2 Using Monte Carlo method

One can compute functions $a_n(s)$ by randomly sampling a sphere of radius s around each point of the surface. Given oriented normals, one can determine wether a point close enough to the surface is inside or outside w.r.t. the normal orientation (see [Hop+92]). Let $\mathcal{S} \in \mathscr{S}$ be a surface and let X_ℓ be a point randomly sampled in a ball of radius s centered a point $P \in \mathcal{S}$, following a uniform probability distribution over the ball. Let Q_ℓ be the closest point on $\mathcal{S}$ from X_ℓ. Noting $\boldsymbol{n}_\ell$ the normal at Q_ℓ, if $\langle Q_\ell - X_\ell, \boldsymbol{n}_\ell \rangle \geq 0$, then X_ℓ is said to be in the interior of $\mathcal{S}$. Otherwise, it is said to be in the exterior of $\mathcal{S}$. In the case of a point set surface $\mathcal{S}$, one can use a kd-tree structure to store the set of sampled points, and define Q_ℓ to be the closest point to X_ℓ in this kd-tree. Let N be the number of random samples taken in the ball and let $\mathbb{1}_{\mathcal{S}}(X_\ell)$ be the indicator function returning 1 if X_ℓ is in the interior of $\mathcal{S}$, 0 otherwise. Given a direct orthonormal basis $(\boldsymbol{x}, \boldsymbol{y})$ spanning the tangent plane at P, noting $\boldsymbol{v}_\ell$

FIGURE 3.3: $a_n(s)$ estimated using a Monte Carlo method. First row: 10k samples per point. Second row: 100k samples per points. As $|n|$ increases, one needs more samples for convergence.

the orthogonal projection of $Q_\ell - X_\ell$ in the tangent plane and θ_{v_ℓ} the oriented angle between $\boldsymbol{x}$ and $\boldsymbol{v}_\ell$:

$$V_p^n(s) = \frac{4\pi}{3} s^3 \lim_{N\to\infty} \frac{1}{N} \sum_{\ell=1}^{N} \mathbb{1}_S(X_\ell) e^{-i\theta_{v_\ell}} \tag{3.40}$$

A major benefit of this method is that the volume descriptor of order n can be computed even if s is too large so the orthogonal map between the tangent plane and the surface is not a heightfield. Of course, the Taylor expansion of $V_p^n(s)$ for too large values of s does not apply. Thus, differential quantities computed in such regions are necessarily false using this method. However, those cases are rare, and when it happens, one is still able to attach one value to each local geometric structure.

However, this method converges very slowly, and one needs a large amount of samples per ball in order to correctly estimate the volume descriptors. Figure 3.3 shows estimates of our integral invariants computed using Monte Carlo. The case $a_0(s)$ converges quite fast. However, as $|n|$ increases, the computation of $|a_n(s)|$ is noisier and needs more samples. This drawback makes this method not usable in the general case. However, if someone wants to compute *ground truth* volume descriptors, this method is the one to use given N large enough.

3.4.3 Radial integration of Fourier transforms

One can also estimate the volume descriptors by integrating the heightfield between the tangent plane and the surface, weighted by complex exponentials. Indeed, for

$n \neq 0$, one can write:

$$\begin{aligned}\int_0^{2\pi}\int_0^s f(r,\theta)re^{-in\theta}drd\theta &= \int_0^{2\pi}\int_0^s \sum_{m=-\infty}^{\infty}\sum_{k=|m|}^{\infty}\phi_{k,m}r^{k+1}e^{im\theta}e^{-in\theta}drd\theta \\ &= \int_0^{2\pi}\int_0^s \sum_{m=-\infty}^{\infty}\sum_{k=|m|}^{\infty}\phi_{k,m}r^{k+1}e^{i(m-n)\theta}drd\theta \\ &= 2\pi\sum_{k=|n|}^{\infty}\frac{\phi_{k,n}}{k+2}s^{k+2} \\ &= 2\pi a_n(s) = -V_P^n(s)\end{aligned} \tag{3.41}$$

One can compute the volume descriptors using a well-chosen grid that we introduce in this section.

Given a parameterization plane, we consider a circular grid of elements of equal areas. Such a grid can be computed by splitting the disc $\mathcal{D}_R$ of radius R into L rings, each ring being split into M evenly spaced cells. Such rings $\mathcal{R}_\ell$ are the following:

$$\mathcal{R}_\ell = \mathcal{D}_{s_\ell} \backslash \mathcal{D}_{s_{\ell-1}} \tag{3.42}$$

Where $s_\ell = s_0\sqrt{1+\ell}$ for $\ell \geq -1$ and $s_0 = \frac{R}{\sqrt{L}}$. By convention, $\mathcal{R}_{-1}$ is a ring of zero radius.

Proof. We want that for s_ℓ, $\mathcal{R}_\ell$ has constant area for all $\ell \in \mathbb{Z}$ such that $\ell \geq -1$. Setting $s_{-1} = 0$, first ring $\mathcal{R}_0$ is the disc $\mathcal{D}_{s_0}$. Thus, we want the area of each ring $\mathcal{R}_\ell$ to be πs_0^2 for all natural ℓ. Then, the constant area property can be written as follows:

$$s_{\ell+1} = \sqrt{s_\ell^2 + s_0^2} \tag{3.43}$$

Now, Let us show by recurrence that:

$$s_\ell = s_0\sqrt{\ell+1} \tag{3.44}$$

Obviously, $s_{-1} = s_0\sqrt{-1+1} = 0$. Let us assume that for a certain integer ℓ, we have $s_\ell = s_0\sqrt{\ell+1}$, then:

$$s_{\ell+1} = \sqrt{s_\ell^2 + s_0^2} = \sqrt{(\ell+1)s_0^2 + s_0^2} = s_0\sqrt{\ell+2} \tag{3.45}$$

Noticing that $s_{L-1} = R$, we have $s_{L-1} = s_0\sqrt{L} = R$, leading to $s_0 = \frac{R}{\sqrt{L}}$, which concludes the proof. □

Such a grid results in the sampling pattern of Figure 3.5 where each sample is on a vertex of the grid. Such a sampling pattern is a collection of regularly discretized circles that we index in the same manner we indexed disks $\mathcal{D}_\ell$. Note that as s_ℓ increases, the radial distance between two circles decreases, leading to an accumulation of samples near the edge of the disk of radius R. In the meanwhile, the center of the disk seems poorly sampled. This might be an unexpected behavior since this procedure is supposed to compute differential quantities which need by construction to have access to very local quantities. However, if the sampling pattern was radially regular, one would not compute the volume of the intersection between a ball and the interior of a surface. Indeed, since we add up samples, all circles have the same weight in the integration process, regardless of their radius. A regular grid made of

FIGURE 3.4: From top to bottom: integral invariants computed with $s = 2.5\%, s = 3.5\%, s = 4.5\%$ of the diagonal of the shape by integrating on the grid presented in section 3.4.3. The grid size is 21×21.

equally spaced circles would then oversample the region near the center, inducing a bias. It would be equivalent with polarly integrating while ignoring the weighting function originating from the following Jacobian:

$$dxdy = rdrd\theta \tag{3.46}$$

Let us now talk about how dense should be the grid. Let us assume that the function f we want to integrate on the disk $\mathcal{D}_R$ has vanishing derivatives of order greater than a natural K. If each circle has at least $2K+1$ points, then a Discrete Fourier Transform can be performed respecting Shannon criteria, leading to an exact estimate of f along the circle. Volumes $2\pi a_n(s_\ell)$ for each ℓ can then be computed by integrating the Fourier coefficient estimated on each circle, with the trapeze method for example. For $0 \leq m < M$ and $0 \leq \ell < L$, let $f_{m,\ell}$ be the sample of a function f at position (m, ℓ) in our sampling pattern. Let us call $\tilde{a}_n(s_\ell)$ the estimate of $a_n(s_\ell)$ at radius s_ℓ using our integration process. We have:

$$\tilde{a}_n(s_{\ell+1}) = \tilde{a}_n(s_\ell) + \frac{s_0^2}{4}(\hat{f}_{n,\ell} + \hat{f}_{n,\ell-1}) \tag{3.47}$$

Where $\tilde{a}_n(s_0) = \frac{s_0^2}{4}\hat{f}_{n,0}$ and $\hat{f}_{n,\ell}$ is the Fourier coefficient of frequency n at circle ℓ:

$$\hat{f}_{n,\ell} = \frac{1}{M}\sum_{m=0}^{M-1} f_{m,\ell}e^{-inm\Delta\theta} \tag{3.48}$$

Where $\Delta\theta = \frac{2\pi}{M}$ is the angular step of the sampling pattern.
Using the trapeze integral formula, the general expression of $\tilde{a_n}(s_\ell)$ is:

$$\tilde{a_n}(s_\ell) = \frac{s_0^2}{2M}\left(\frac{1}{2}\sum_{m=0}^{M-1}(f_{m,0} + f_{m,\ell})e^{-inm\Delta\theta} + \sum_{l=1}^{\ell-1}\sum_{m=0}^{M-1} f_{m,l}e^{-inm\Delta\theta}\right) \tag{3.49}$$

Integral invariants computed using various radii s are displayed in Figure 3.4. As one can see, when the radius gets large, larger scale geometry variations are taken into account, as smaller scale geometry get blurred.

3.4.4 Comparison of the methods

A numerical comparison of the methods is presented on Figures 3.3 and 3.4. Monte Carlo method is in theory the one getting the best results since it converges to the correct value. However, the amount of time to compute an acceptable estimate is huge when $|n| > 1$ (see Figure 3.3). The results using the Wavejet decomposition of the surface and the integration on a grid give very similar results. Differences usually appear on cases where there lacks points (outliers appear when inverting the linear system), or where the neighborhood cannot be properly expressed as a function $f(r, \theta)$, which happens when s is too large. The grid method has two main advantages. First, even on ill-defined cases (the local heightfield cannot be expressed as a function or the sampling rate is insufficient), this method produces bounded values. Thus, even if those cases are not supposed to be handled by the Wavejets framework, one can have an estimate of the integral invariants and use them. However, the reader should keep in mind that in such cases, those estimates have poor geometrical meanings. Finally, estimating the volume descriptors for any order is much faster when using a grid. Thus, it is adviced to use the integration on a grid to compute the integral invariants. Concerning processing times, using a

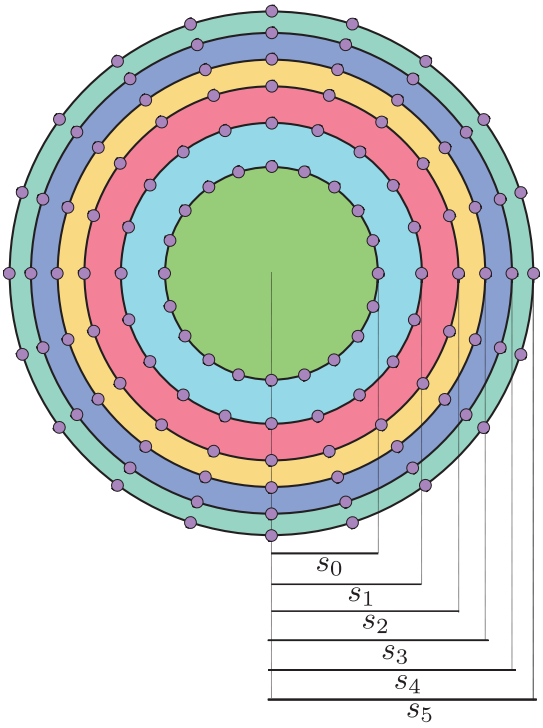

FIGURE 3.5: The circles of radius s_ℓ from equation 3.44 for a given s_0. Each colored ring has constant area πs_0^2. Purple points are an example of a sampling pattern we can generate out of the circles of radius s_ℓ. In this example, there are 22 samples per circle, which mean that Shannon criterion is respected if and only if the Wavejet decomposition of the heightfield between a parameterization plane and the surface has vanishing coefficients $\phi_{k,n}$ for $|n| \geq 10$.

multi-threaded algorithm on 16 threads on an intel Xeon, Monte Carlo takes around 2 hours to compute four integral invariants, using 10,000 samples per points on a point set of 600,000 points. The same point set requires 9 minutes if one does a Wavejet decomposition of order 8 over the shape, and 15 seconds if integrating on grid of 21 circles and 21 samples per circle as described in Figure 3.5.

3.5 Retrieving Wavejet coefficients from the *Volume descriptor*

The grid constructed in section 3.4.3 is composed of L concentric circles. It allows to compute values $\tilde{a}_n(s_\ell)$ for $0 \leq \ell < L$, which is an approximation of samples of $a_n(s_\ell)$. Since for a given integer $K \leq \frac{L}{2}$,

$$a_n(s_\ell) = \sum_{k=|n_\ell|}^{K} \frac{\phi_{k,n_\ell}}{k+2} s^{k+2} + O(s_\ell^{K+4}) \tag{3.50}$$

Let S is a matrix filled at index $\left(\left\lfloor \frac{k}{2} \right\rfloor, \ell\right)$ with s_ℓ^{k+2} for $k \geq |n|$ and k of same parity as $|n|$, and let ϕ_n is the vector of $\left\lfloor \frac{K-|n|}{2} \right\rfloor$ elements $\phi_{k,n}$ for $k \leq K$ and k of same parity of $|n|$. Let A_n be a vector of dimension L filled with $\tilde{a}_n(s_\ell)$ for $0 \leq \ell < L$. Vector ϕ_n of coefficients $\phi_{k,n}$ can be retrieved by solving the following minimization:

$$\phi_n = \underset{\phi_n}{\operatorname{argmin}} \|S\phi_n - A_n\|^2 \tag{3.51}$$

3.6 Stability of the *Volume descriptor* of order n

The stability of the volume descriptor of order 0 was already studied in [Pot+09]. Let $\mathcal{S}$ be a surface such that each point of $\mathcal{S}$ is perturbed by a centered Gaussian noise of standard deviation σ in a random orientation in $\mathbb{R}^3$ following a uniform distribution. The Taylor expansion of $a_0(s)$ at each point of $\mathcal{S}$ features a normal offset in its first term. By construction, for $\sigma = 0$, the point on which $a_0(s)$ is computed is on the surface. Thus, this offset equals zero. If $\sigma \neq 0$, this assumption does not hold any more. It was shown in [Pot+09] that the volume descriptor is resilient to noise if and only if the input maximum deviation is negligible w.r.t. radius s and if and only if the inverse of the mean curvature, $\mathcal{H}(P)^{-1}$, is in $O(s)$. This is mostly due to the fact that points perturbed by noise are not necessarily on the surface.

When $n \neq 0$, the offset from the point to the surface is not critical any more. Indeed, this offset is entirely stored in the coefficient $\phi_{0,0}$ of the local Wavejet decomposition, which does not influence $a_n(s)$ for $n \neq 0$. However, a noisy point set does not necessarily have the same normals as a finely detailed noise free version. Non noisy normals computed on noisy data have to be smoother and coarser than the theoretical ones. As a consequence, a bias is induced in both the point position and the tangents along the local heightfields, yielding a wrong estimate of $\phi_{1,\pm1}$. As shown in Theorem 2, one can retrieve each Wavejet coefficients computed using the tangent plane out of an estimate using an arbitrary parameterization plane with an error in $o(\gamma)$, where γ is the angle error between the tangent plane and the parameterization plane. Thus, the error induced by coarse normals induces a small bias in the estimated Wavejets coefficients. Coefficients $a_n(s)$ being radial polynomials whose coefficients are proportional to the Wavejets coefficients of frequency n, the

estimate of $a_n(s)$ on a noisy point set has a small bias compared to the theoretical one. Obviously, $a_{\pm 1}(s)$ are the most impacted functions since they directly feature the tangential error in their Taylor expansions. $a_{\pm 2}(s)$, on the contrary, has been found to be not that much impacted from this bias in our experiments.

In this section, we show how the standard deviation of an input noise in position on a sampled surface influences the values of $a_n(s)$ for $n \neq 0$. Since it is impossible to have a sharp estimate of normals on a sampled surface corrupted by a position noise, we replace the theoretical normals by smoother ones such that their computation by Principal Component Analysis is stable (i.e. the normal field is smooth over the surface) w.r.t. the input noise given an arbitrary radius of interest. As a consequence, because of its strong link with the tangential information, the scalar field $|a_{\pm 1}(s)|$ over the surface is strongly biased compared to its theoretical one given correct input normals. Scalar fields $a_n(s)$ for frequencies $|n| \neq 1$ are also biased, but much less. The reader can refer to Theorem 2 in section 2.2.5 to appreciate the amount of bias for each frequency n. The point of this section is not to study the accuracy of the computation of the volume descriptors of order n on noisy data, but rather to study its smoothness. Thus, for simplicity, we assume this bias to be equal to zero and do not discriminate the case $|n| = 1$. However, we do not consider the case $n = 0$ since it already was addressed in [Pot+09], and because the standard deviation of $a_0(s)$ has a non-zero asymptotic limit for any number of samples on the integration grid. Indeed, the point of coordinate $(0, 0)$ in the local coordinate system is perturbed by a centered Gaussian noise $\mathcal{N}(0, \sigma)$ of standard deviation σ, which means that $\phi_{0,0} \sim \mathcal{N}(0, \sigma)$ as well. Thus, the standard deviation of the estimate of $a_0(s)$ is at least $\frac{\sigma}{2}s^2$. Wavejets coefficients of frequency $n \neq 0$ do not suffer from this issue. Hence, we study how noisy the field of functions $a_n(s)$ is over a noisy sampled surface given an input centered Gaussian noise for $n \neq 0$.

Given estimated tangent planes over $\mathcal{S}$, we note $\varepsilon \sim \mathcal{N}(0, \sigma)$ the centered Gaussian noise of standard deviation σ perturbing the local heightfield in the normal direction. Let $f_{m,\ell}$ be a sample of a function f following the sample pattern of section 3.4.3 with L circles and M samples per circle, such that $m \in [\![0, M[\![$ and $\ell \in [\![0, L[\![$. Let us call $\epsilon_{m,\ell}$ one realization of ε. Each function $a_n(s)$ has the following form:

$$\begin{aligned}\tilde{a}_n(s_{L-1}) &= \frac{s_0^2}{2ML}\left(\frac{1}{2}\sum_{m=0}^{M-1}(f_{m,L-1}+\epsilon_{m,L-1})e^{-inm\Delta\theta} + \sum_{\ell=0}^{L-2}\sum_{m=0}^{M-1}(f_{m,\ell}+\epsilon_{m,\ell})e^{-inm\Delta\theta}\right)\\ &= \frac{1}{L}\left(\frac{1}{2}(\hat{f}_{n,L-1}+\hat{\epsilon}_{n,L-1}) + \sum_{\ell=0}^{L-2}(\hat{f}_{n,\ell}+\hat{\epsilon}_{n,\ell})\right)\end{aligned} \tag{3.52}$$

$\hat{\epsilon}_{\ell,n}$ is the Fourier coefficient of frequency n of a realization of the noise along circle ℓ, and $\hat{f}_{\ell,n}$ a the Fourier coefficient of frequency n of f along circle ℓ. Thus, $\hat{\epsilon}_{\ell,n}$ is a realization of a random variable that we note $\hat{\varepsilon}_n$. Let us determine what is the distribution of $\hat{\varepsilon}_n$. Let us note the complex random variable $Z_\alpha = \frac{1}{M}\varepsilon e^{i\alpha}$. By construction, we have:

$$\hat{\varepsilon}_n = \sum_{m=0}^{M-1} Z_{nm\Delta\theta} \tag{3.53}$$

Given a real random variable X, there exists a bijection transforming X into what is called the characteristic function $\varphi_X(t)$. Characteristic functions have useful properties for characterizing the sum of random variables. [And+95] generalized them for complex variables. The characteristic function of Z_α that we note $\varphi_{Z_\alpha}(t)$ has

the following definition:

$$\varphi_{Z_\alpha}(t) = \mathbb{E}\left(e^{i\mathrm{Re}(t^* Z_\alpha)}\right) \tag{3.54}$$

Where $\mathbb{E}(X)$ is the expected value of random variable X. A property of the characteristic function is:

$$\varphi_{\hat{\varepsilon}_n}(t) = \varphi_{\sum_{m=0}^{M-1} Z_{nm\Delta\theta}}(t) = \prod_{m=0}^{M-1} \varphi_{nm\Delta\theta}(t) \tag{3.55}$$

Given X and Y two random variables, $\varphi_X = \varphi_Y$ if and only if $f_X = f_Y$, where f_X is the probability density function of X. Therefore, if we can estimate the product of all characteristic functions of $Z_{nm\Delta\theta}$, we can deduce the distribution of $\hat{\varepsilon}_n$. Let $\omega_\alpha(t) = \mathrm{Re}(t^* e^{i\alpha})$. Since Z_α is a complex variable:

$$\begin{aligned}
\varphi_{Z_\alpha}(t) &= \mathbb{E}\left(e^{i\mathrm{Re}(t^* Z_\alpha)}\right) \\
&= \mathbb{E}\left(e^{i\frac{\varepsilon}{M}\omega_\alpha(t)}\right) \\
&= \varphi_{\frac{\varepsilon}{M}}(\omega_\alpha(t)) \\
&= e^{-\frac{\sigma^2 \omega_\alpha(t)^2}{2M^2}}
\end{aligned} \tag{3.56}$$

Because $\frac{\varepsilon}{M} \sim \mathcal{N}(0, \frac{\sigma}{M})$ and $\omega_\alpha(t) \in \mathbb{R}$. Let us now express the characteristic function of $\hat{\varepsilon}_n$:

$$\begin{aligned}
\varphi_{\hat{\varepsilon}_n}(t) &= \prod_{\substack{\alpha = nm\Delta\theta \\ m \in [\![0, M-1]\!]}} \varphi_{Z_\alpha}(t) \\
&= \exp\left(-\sum_{\substack{\alpha = nm\Delta\theta \\ m \in [\![0, M-1]\!]}} \frac{\sigma^2}{2M^2} \omega_\alpha(t)^2\right) \\
&= \exp\left(-\frac{\sigma^2}{8M^2} \sum_{\substack{\alpha = nm\Delta\theta \\ m \in [\![0, M-1]\!]}} \left(t^* e^{i\alpha} + t e^{-i\alpha}\right)^2\right) \\
&= \exp\left(-\frac{\sigma^2}{8M^2} \sum_{\substack{\alpha = nm\Delta\theta \\ m \in [\![0, M-1]\!]}} \left(2t^* t + t^2 e^{-2i\alpha} + t^{*2} e^{2i\alpha}\right)\right) \\
&= \exp\left(-\frac{|t|^2 \sigma^2}{4M}\right)
\end{aligned} \tag{3.57}$$

Note that terms in $e^{\pm 2i\alpha}$ vanish because α regularly angularly samples over a circle, and the sum of such exponentials equals zero. We now have to determine which probability density function $\hat{\varepsilon}_n$ has characteristic function $\varphi_{\hat{\varepsilon}_n}$. Given $(\mu, \gamma, c) \in \mathbb{C}^3$, and $\Sigma = \begin{pmatrix} \gamma & c \\ c^* & \gamma^* \end{pmatrix}$, the random variable Z following the complex normal distribution $\mathcal{CN}(\mu, \Sigma)$ of mean μ and covariance matrix Σ has the following probability density function:

$$f_Z(z) = \frac{1}{2\pi\sqrt{|\Sigma|}} \exp\left(-\frac{1}{2}\begin{pmatrix} z \\ z^* \end{pmatrix}^* \Sigma^{-1} \begin{pmatrix} z \\ z^* \end{pmatrix}\right) \tag{3.58}$$

FIGURE 3.6: $a_n(s)$ computed over shapes with different additive noise. First row: noise free - Second row: $\sigma = 0.45\%$ of the diagonal - Third row: $\sigma = 1.25\%$ of the diagonal. In all examples, $s = 4.5\%$ of the diagonal. When noise is added, considered normals are smooth over the shape, i.e. are computed using large neighborhood sizes. First row features fine normal estimates.

And the corresponding characteristic function is (see [And+95]):

$$\varphi_Z(t) = \exp\left(-i\mathrm{Re}(t^*\mu) - \frac{1}{4}(\gamma|t|^2 + \mathrm{Re}(c|t|^2))\right) \tag{3.59}$$

Thus, using equation (3.57), $\hat{\varepsilon}_n \sim \mathcal{CN}\left(0, \frac{\sigma^2}{M} I_2\right)$ where I_2 is the identity matrix of size 2×2. This probability density function is isotropic in the complex plane. This is something we would expect since the input noise is the same along each circle.

Let us now discuss the influence of integrating on multiple circles. Summing L Gaussian random variables results in increasing the variance by a factor L. Since we divide the sum by L in the integration process, the resulting variance is multiplied by a factor L^{-1}. Thus, summing $L-2$ times the complex random variable $\frac{s_0^2\hat{\varepsilon}_n}{2L}$ and twice the random variable $\frac{s_0^2\hat{\varepsilon}_n}{4L}$ results in that the *Volume descriptor* of order n computed on a surface with input additive Gaussian noise $\mathcal{N}(0,\sigma)$ is perturbed by an additive complex Gaussian noise of distribution $\mathcal{CN}\left(0, \frac{s_0^2(2L-2)\sigma^2}{4LM} I_2\right)$.

However, even if we reduce the noise by integrating the signal, the average magnitude of functions $a_n(s)$ decreases as $|n|$ gets larger. For example, Figure 3.6 shows the first estimated $a_n(s)$ given a noise of 1.25% of the largest diagonal of a shape. $|a_{\pm2}(s)|$ is quite unstable, while $|a_{\pm3}(s)|$ is not usable. Moreover, one can see that $a_{\pm2}(s)$ is the most resilient quantity. $a_{\pm1}(s)$, on the other hand, vanishes as normals get blurred.

Chapter 4

Shape detail amplification

In this chapter, we present a method for amplifying or modifying geometric details on surfaces represented by point clouds.

4.1 Related work

While the literature for detail exaggeration in image or video processing is large (e.g. [Liu+05; Dek+15]) it has been far less studied for surfaces. In image processing, there are two main methods performing detail amplification: *high-boost filtering* and *Unsharp masking* [PRM00; Mit+91; Ram+96]. High-boost filtering stems from signal processing. It can be performed by amplifying the high frequency coefficients of a spectral decomposition of this signal. Let f be a signal and let $\mathfrak{F}$ be a high-pass filter. $\mathfrak{F}(f)$ cuts low frequencies of f while preserving high frequencies. Considering that the details of a signal are the fast varying part of f, i.e. high frequency components of the spectral decomposition of f, $\mathfrak{F}(f)$ holds the details of f. Thus, given $\alpha \in \mathbb{R}$, $f + (\alpha - 1)\mathfrak{F}(f)$ exaggerates the details of f with a gain α while preserving the general aspect of f. This filter is called the High-boost filter.

Unsharp masking performs similarly, but instead of using the whole function f through its Fourier Transform, it locally changes the value $f(x)$ so it locally amplifies the dynamics of f. This idea dates back to Gabor [Gab65; LFB94]. The principle is the following. Let K be a blurring operator (a convolution with a Gaussian kernel for example). Applying K to a function f results in a smoother function $K(f)$. Let us note $\delta = f - K(f)$. δ are the details of f. Thus, given $\alpha \in \mathbb{R}$, $f + (1 - \alpha)(f - K(f))$ represents f with exaggerated details with a gain α. This local filter is called *unsharp masking*. The main drawback of unsharp masking is that it produces overshoots near sharp features.

Even if high-boost filtering and unsharp masking both perform detail amplification, their construction is different, and the results might differ a lot. Unsharp masking generally has two parameters: a neighborhood size or a kernel width, and a gain. Usually, the size parameter should be of the order of the size of the details to enhance, and the gain parameter tells how much of those details should be amplified. On the other hand, since high-boost filtering enhances the high frequency components of the signal, there are usually more parameters: one gain per frequency. As a consequence, high-boost filtering a signal can amplify its details in various manners. The drawback is that the design of the high-boost filter is more tedious, because one has to set one gain per frequency as well as determining a limit between low frequencies and high frequencies. The outcome of the filter is harder to determine *a priori*.

Detail amplification is usually thought as enhancing the local dynamics of a function. In the case of surfaces, there are two main types of functions over the

FIGURE 4.1: Both pictures show a rendering of the same shape. The only difference are the normals considered over the shapes. On the left: normals estimated with great precision - On the right: poorly estimated normals

surface on which one can amplify details. The most obvious one is the position of each point over the shape: one can locally move each point to amplify the local geometry. We call this *position amplification*. The second function on which one can amplify details is the normal mapped to each point on the surface. Indeed, our visual system is very sensitive to normal variations. Given the same geometry, poorly estimated normals result in a blurred shape (see Figure 4.1). Hence, one can also alter the normal definition over the shape, and amplifying the local dynamics of the normals can give the illusion that geometric features are sharper. We call this *normal amplification*. This method makes the viewer see non-existing geometry, which can cause weird optical illusions. For instance, highly amplified normals dynamics on almost flat shapes can look incoherent given certain angles of view. The false normals directions with regards to the geometry can induce highly carved areas that are supposed to be almost flat. This can induce some points of the surface to be visible while they should be occluded if that surface was coherent with the normals. surface being almost coplanar with the light rays coming from the camera. Note that in the case of position amplification, normals must be updated in order to visualize the detail amplification.

Position dynamic amplification can be trivially performed within the high-boost filtering framework by relying on the manifold harmonic decomposition of the surface [VL08]. It is also possible to adapt unsharp masking. Given an operator K blurring a surface $\mathcal{S}$, let $K(P)$ be the blurred position of a point $P \in \mathcal{S}$, position unsharp masking can be performed by moving each point P as follows:

$$P \leftarrow P + (1 - \alpha)(P - K(P)) \tag{4.1}$$

Where α is the gain of the filter. The key element is the definition of the blurring operator K, which will be discussed in next Section. Indeed, if K has a wide support, it deteriorates slow varying geometry, i.e. geometry that is of greater scale than the considered geometric details, geometric details amplification becomes less sharp.

A method for normal dynamic amplification was proposed in [CST05]. Normals are iteratively updated in a direction opposite to the arithmetic mean of the normals computed in a neighborhood. This process can be seen as an unsharp masking applied to the normals. [RBD06] proposed a rendering method that produces enhanced details that also do not modify the vertex position. However, this method does not enhance the normal dynamics, but rather proposes a rendering method inferring sharper geometric details. The principle is to apply a multi-scale toon shading. All the scales

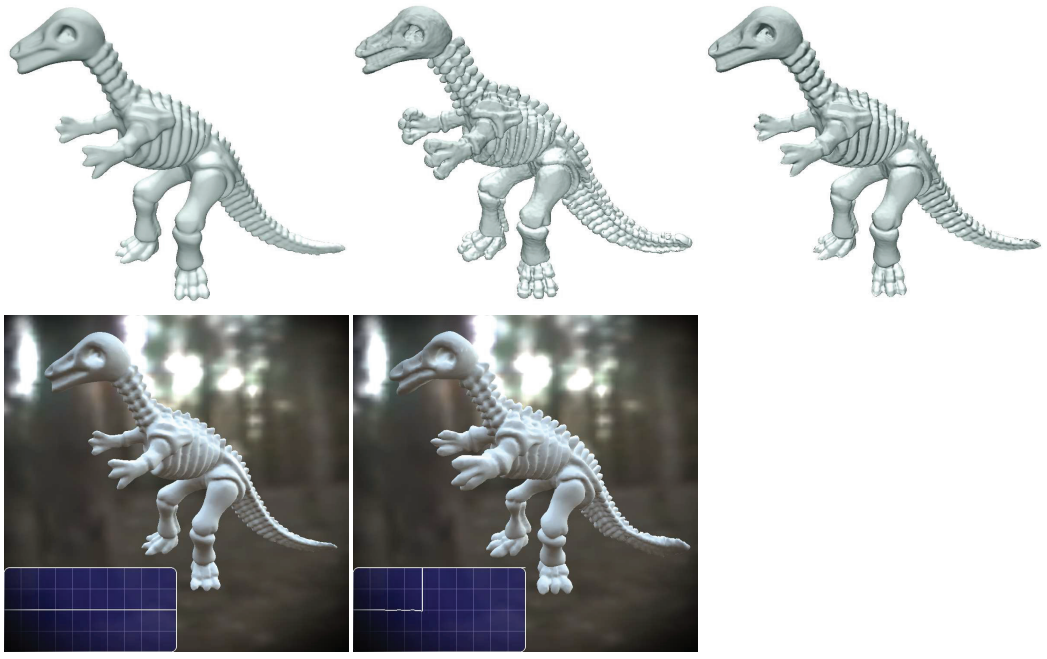

Original Positions enhanced Normals enhanced

FIGURE 4.2: On the left: input shape. On the top right: our position and normal enhancement method. On the bottom right: the result of a high-boost filter applied to manifold harmonics [VL08] of the dino (no normal enhancement is defined using this method). Our position enhancement method highlights more local details as the Manifold-Harmonics based high-boost filter. The rendering of the second row is a capture of the MHB demo provided by the authors.

are then taken into account to determine the color output. This method is thus view dependent, which is not the case for our method or the one of [CST05]. We will compare our method to [Rug+06] for the sake of completeness, but the reader should keep in mind that the process is not comparable.

4.2 Surface fairing

4.2.1 Goals

In order to define a method to do unsharp masking, we need a good surface fairing definition. The only parameter for smoothing should be a radius related to the size of the neighborhood one wants to smooth out. This way, the user only needs to know the scale of details to be enhanced. As a consequence, one only needs to specify which procedures it wants to perform.

4.2.2 Mean curvature motion

Surface fairing with mean curvature motion has been widely studied. In order to compute mean curvature motion, one needs a definition of the mean curvature as well as the normal at each point. Indeed, given a point P on a surface $\mathcal{S}$ and $\boldsymbol{n}$ the normal at P, one can write the mean curvature motion equation as follows:

$$\frac{dP}{dt} = \beta \Delta P \boldsymbol{n} \tag{4.2}$$

Where β is the velocity of the flow. Instead of taking into account the Laplacian Δ, one may refer to the mean curvature $\mathcal{H} = \frac{1}{2}\Delta$. For convenience β is usually set to two, so one has:

$$\frac{dP}{dt} = \mathcal{H}(P)\boldsymbol{n} \tag{4.3}$$

Taubin [Tau95] proposed a slightly different approach for surface fairing avoiding normal computation. The method relies on the eigenfunctions of a discretized Laplacian operator for meshes, which can be seen as an extension of the Fourier basis to manifolds. The mesh is iteratively updated by applying a linear operator to the positions such that low frequencies tend to be invariant, whereas high frequencies tend to zero. The flow for each point follows the mean curvature motion, which has the drawback of shrinking the volume. To avoid that shrinking effect, and unshrinking step which inflates the surface by an appropriate amount is added.

Meyer et al. [Mey+03] developed a wide set of tools for surface analysis, including the computation of the mean curvature on a mesh using the cotangent formula. They naturally proposed to use those to perform a mean curvature motion on surfaces. Sorkine et al. [Sor+04] proposed to encode geometric details using Laplacian coordinates for meshes. In their method, the detail at each point P of the mesh is defined as the difference between the point and the distance-weighted average of their 1-ring neighborhood. This operation results in computing the Laplacian coating of the surface, separating the geometric details from the surface. Doing so, they can perform geometric detail transfers between meshes and can handle various kinds of details, including details that cannot be described as a heightfield over a tangent plane. Belkin et al. [BSW09] proposed a method to compute the Laplacian operator on point sets, which could then be used to apply a mean curvature motion. One can perform mean curvature motion as soon as one can compute the mean curvature over a surface. In this sense, Algebraic Point Set Surfaces (APSS) [GG07], which were introduced to have a stable projection or interpolation method on a surface, can be used for mean curvature estimation. Indeed, a side consequence of APSS is that one can compute the mean curvature by taking the inverse of the radius of the algebraic spheres. Similarly, all integral invariants introduced by [Pot+09] feature an estimate of the mean curvature. Thus, those methods can be used to perform mean curvature motion over the shape. In the method we propose, unsharp masking on positions is performed, given a heuristic on the step amplitude, using the mean curvature computed from the volume descriptor in [Pot+09] discussed in chapter 3. Using the generalization of the volume descriptor at order $n = \pm 1$, we will show that normals can be amplified as well.

Mean curvature motion is usually done by an iterative algorithm. Time is discretized, and one can express the t^{th} iteration of the mean curvature motion as follows:

$$P_{t+1} = P_t + \beta\mathcal{H}(P_t)\boldsymbol{n}_t \tag{4.4}$$

Where β is the velocity of the flow. Note that β has a different definition than in equation (4.2). Mean curvature motion can also be achieved by using the heat kernel, since equation (4.2) is the heat equation. Given an initial heat distribution over the surface, the heat equation expresses how the heat diffuses over the shape after a time t. Computing the heat diffusion can be done by convolving the initial surface by the heat kernel. For the case of mean curvature motion on a surface, the initial state is the set of positions $P \in \mathcal{S}$. Convolving each position coordinate by coordinate, by the heat kernel of variance $4t$, is equivalent with performing a mean curvature motion.

Given $Q \in \mathcal{S}$, the heat kernel is defined as follows:

$$K(P,Q) = \frac{1}{4\pi t} e^{-\frac{d(P,Q)^2}{4t}} \tag{4.5}$$

Where $d(P,Q)$ is the geodesic distance between P and Q on $\mathcal{S}$, i.e. the length of the shortest path between P and Q on $\mathcal{S}$.

One can estimate such kernels using the spectral decomposition of a surface [VL08]. The heat kernel was used in [SOG09] to define a local descriptor on shapes: the Heat Kernel Signature, but one could use this formulation to convolve the surface by the heat kernel to smoothen the surface. One flaw of this method is that it requires to compute the manifold harmonics, which can be time consuming. Moreover, it is memory consuming, since one has to store around 100 eigenvectors of the size of the number of input points. A few shapes featuring very sharp parts, like the legs of an animal or the fingers of a hand for example, can require the computation of many more eigenfunctions in order to correctly describe the shape. A solution localizing the eigenfunctions of the Laplacian was proposed in [Mel+17] to correct this drawback.Using enough eigenfunctions, this smoothing solution would work for point positions, but, unfortunately, not necessarily for normals smoothing. One could argue that one could consider the signal we want to smooth to be the normal coordinates instead of the point positions. However, there is no guarantee that the norm of the smoothed normals do not vanish, or that the normals could not flip near highly curved neighborhoods. This could lead to outliers and instabilities.

Digne et al. [Dig+11] showed that mean curvature motion can be done by recursively projecting the points on the local best fitting plane. The normal of the best fitting plane is shown to be stable enough to consider it as a reliable normal estimate. It is bounded by $O(s)$. This method was used to better estimate the orientation of raw point sets and to mesh while preserving fine details. Indeed, the mean curvature motion on a point set simplifies its geometry. Thus, it is safer and easier to apply state of the arts algorithms on this simplified data, and the results can be then propagated back to the original surface.

Our method relies on a similar procedure as described in [Dig+11]: points are projected on the local best fitting plane. However, we rely on the volume descriptor to induce this projection, and only one iteration is performed. This is because we do not want to amplify parts of the shape which are not details at a certain scale. Geometric details of a certain scale can be mostly erased given a certain neighborhood size. We will show that this procedure can be done on point positions and on normals as well, yielding a unified framework for both amplification methods with similar parameters.

4.3 Position amplification

4.3.1 Method

Recall that we look for a filter K such that $K(\mathcal{S})$ corresponds to $\mathcal{S}$ without any geometric details. We define geometric details to be the residue between local regression plane given a neighborhood of radius s, and the surface. In other words, parts that do not lie on a plane estimated at radius s are considered to be details of the surface. As a consequence, non-planar parts of low mean curvature are thus considered as details, but their amplitude is so low that it is negligible compared to actual details. This definition of details is quite relative because details at radius s might not be

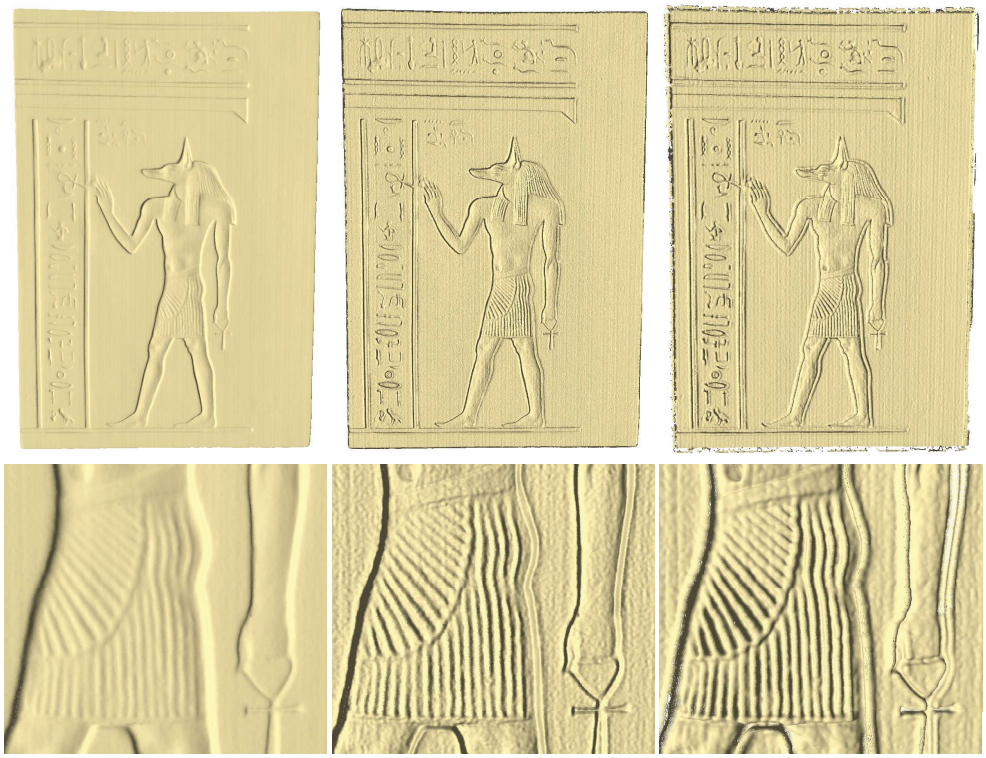

Original Normal enhanced Position enhanced

FIGURE 4.3: Applying order 9 (normal exaggeration) and order 8 filters (position filter) to the Anubis datasets with $\alpha_0 = \alpha_{\pm 1} = 2$.

considered as details for radius $s' << s$. Noting $\delta = \mathcal{S} - K(\mathcal{S})$ the details, amplifying positions can be done by computing $\mathcal{S} + (\alpha_0 - 1)\delta$, where α_0 is called the gain of the amplification. Let us now show how this can be performed from the computation of function $a_0(s)$.

Given a Wavejet decomposition over the tangent plane at point $P \in \mathcal{S}$ (hence $\phi_{1,\pm 1} = 0 =$ and $\phi_{0,0} = 0$), let us write coefficient $a_0(s)$ from equation (3.1):

$$\begin{aligned} a_0(s) &= \frac{\phi_{0,0}}{2}s^2 + \frac{\phi_{2,0}}{4}s^4 + O(s^6) \\ &= \frac{\phi_{0,0}}{2}s^2 + \frac{1}{8}\mathcal{H}s^4 + O(s^6) \end{aligned} \tag{4.6}$$

Where $\mathcal{H}$ is the mean curvature at P. Note that $\phi_{0,0} = 0$ since the parameterization plane passes by P. A non zero $\phi_{0,0}$ would mean that the parameterization plane does not necessarily contain P, and that the signed distance between the surface and the plane at $(0,0)$ is $\phi_{0,0}$. Also, recall that $2\pi a_0(s)$ quantifies the signed volume between the surface and the tangent plane. Thus, $\frac{2\pi a_0(s)}{\pi s^2} = \frac{2a_0(s)}{s^2}$ quantifies the average height of the surface in the neighborhood of P in a disc of radius s. Using the result of Theorem 1 in [Dig+11], moving P to the position $P - \frac{2a_0(s)}{s^2}\boldsymbol{n}$, where $\boldsymbol{n}$ is the normal at P, is equivalent with moving P to the centroid of the local neighborhood up to a bound in $o(s^2)$. Theorem 2 in [Dig+11] also shows that one can equivalently use a coarser normal, computed by a principal component analysis (PCA) on the covariance of the neighborhood positions, instead of the true normal when moving P: the error induced is in $o(s^2)$. Note that doing so is equivalent to orthogonally projecting P on the local best fitting plane. In our case, it is better to use a coarse normal instead of

FIGURE 4.4: Applying order 7 (normal filter) and order 6 filters (position filter) to the Pyramid datasets with $\alpha_0 = \alpha_{\pm 1} = 2$.

the true normal of the surface. Indeed, given a chosen radius s, details of magnitude negligible w.r.t. s, i.e. details we do not want to amplify, induce fast varying normals. If we use those fast varying normals, moving points in these directions might tear the surface. This does not happen if one uses normals computed using a PCA

at radius s, which better describes the surface at this given scale. This problem does not appear as much when performing a mean curvature motion for multiple operations with a small enough radius, because the normals become smoother as the positions are smoothened. We propose in the next section an other method to compute a smooth normal using the volume descriptor of order ± 1.

We can now describe the procedure. Given an estimate of coefficient $a_0(s)$ and $\widetilde{\boldsymbol{n}}$ a smooth estimated normal at P, we move each point P as:

$$P \leftarrow P + \frac{2a_0(s)}{s^2}(1 - \alpha_0)\widetilde{\boldsymbol{n}} \tag{4.7}$$

Coefficient α_0 is called the gain of amplification. In order to enhance geometric details, one needs to set $\alpha_0 > 1$. If $\alpha_0 = 0$, the surface becomes blurred and details are removed from the surface. As we will see in section 4.5, setting $\alpha_0 < 0$ results in geometric details inversion.

One should be aware that we do not take any collision aspects into account, meaning that applying our method to some surfaces might make parts of the surface self-intersect. For example, eye cavities in the dino shape in Figure 4.2 can go through each other if the amplification gain is too large.

Recall that $a_0(s)$ can be computed in various manners. If $a_0(s)$ is computed using local Wavejet decompositions, coefficients $\phi_{k,n}$ can sometimes have quite high magnitudes. This can happen if a part of the neighborhood of interest is sample free, or if the shape is not locally a heightfield because the radius is too large. This would make some points move far away when applying unsharp masking. In order to avoid those artifacts, we set a maximum threshold on the points motion. In our

FIGURE 4.5: Unsharp masking relying on mean curvature estimates using local Wavejet decompositions with same gain $\alpha_0 = 6$ and different radii s. Left row: mean curvature estimated out of Wavejet decompositions of order 8. Middle row: mean curvature estimated out of Wavejet decompositions of order 2 (note that this is equivalent to using $a_0(s)$ estimated with the same decomposition). Right row: unsharp masking using $a_0(s)$.

experiments, we set it to be the radius of the neighborhood. This threshold is used in Figure 4.5. This limitation does not hold if $a_0(s)$ is computed using Monte Carlo or the regular grid described in chapter 3 since $|a_0(s)|$ is bounded by $\frac{2}{3}s^3$.

4.3.2 Experiments

Let us now compare the results between using $a_0(s)$ and other approximations of the mean curvature for our algorithm. Estimating $a_0(s)$ out of the local Wavejets decomposition permits to control the precision with regards to the Wavejets order K. A low order K gives a coarse estimation, while a higher order gives a finer estimation. In particular, setting $K = 2$ is equivalent with locally approximating the shape with a paraboloid, yielding a coarse mean curvature estimation. Similarly, a high order Wavejet (for example $K = 8$) gives access to an estimate of the mean curvature in $O(r^6)$, which is quite high. Figure 4.5 shows what happens when our pipeline is used with an estimate of the mean curvature computed out of Wavejets decompositions for different order given different neighborhood radii, and compares it to an estimation

Scale 4 Scale 10 Scale 20 Scale 30

FIGURE 4.6: Unsharp masking using the mean curvature estimation of APSS [GGG08] for different scale parameters. Each point is moved by 3 times the estimated mean curvature. Scale 20 gives the best results for this example.

of $a_0(s)$ computed out of Wavejets of order 8. It turns out that $a_0(s)$ is less sensitive to the radius choice than a coarse estimate of the mean curvature, which is due to the influence of higher order terms that are inside the Taylor expansion of $a_0(s)$. In particular, one can see that a one-shot smoothing of the shape given a fine estimate of the mean curvature does not work, and that a simple second order estimation tends to blur out the shape too much. In this last scenario, the shape is more blurred because the detail layer used for unsharp masking catches larger scales variations as well. Figure 4.6 shows examples of unsharp masking on positions using the mean curvature estimation given by APSS [GGG08] for different parameters. Similar results can be retrieved as with our method. However, the choice of the parameter is more sensitive than ours, and the scale parameter of APSS might be harder to predetermine contrary to a gain and a neighborhood radius.

To conclude, unsharp masking on shapes can be performed with a one-shot smoothing procedure relying on some estimation of the mean curvature. However, the parameter choice is made easier with the integral invariant $a_0(s)$.

4.4 Normal amplification

The normal amplification procedure is very similar to the position amplification procedure. Let us recall the expression of coefficient $a_{\pm1}(s)$ from equation (3.1) given Wavejets coefficients:

$$a_{\pm1}(s) = \frac{\phi_{1,\pm1}}{3}s^3 + \frac{\phi_{3,\pm1}}{5}s^5 + O(s^7) \tag{4.8}$$

Another way to write that is to use the generalization of the mean curvature to complex functions thanks to the Wirtinger derivatives discussed in section 3.3.2. Let us express equation (3.35);

$$\begin{aligned} a_1(s) &= \frac{1}{3}\frac{\partial f}{\partial z}(0)s^3 + \frac{1}{10}\mathcal{H}\left(\frac{\partial f}{\partial z}\right)(0)s^5 + O(s^7) \\ a_{-1}(s) &= \frac{1}{3}\frac{\partial f}{\partial z^*}(0)s^3 + \frac{1}{10}\mathcal{H}\left(\frac{\partial f}{\partial z^*}\right)(0)s^5 + O(s^7) \end{aligned} \tag{4.9}$$

Where $\mathcal{H}\left(\frac{\partial f}{\partial z}\right)(0)$ is the complex mean curvature of the first Wirtinger derivative of f at $(0,0)$ in the local parameterization. Note that if the parameterization plane

is the tangent plane, $\phi_{1,\pm1} = 0$. Thus, $a_{\pm1}(s)$ can be used to estimate the complex mean curvature of the first derivative of Wirtinger. Remember that coefficients $\phi_{1,\pm1}$, which are proportional to the first Wirtinger derivatives, can be mapped by a bijection with a rotation of the parameterization plane. When their estimates on a surface are non zero, one can use them to retrieve a better estimate of the tangent plane at this location. Thus, a way to interpret the mean curvature of the first Wirtinger derivatives is the following: it gives information about the orientation in which the mean tangent plane of the neighborhood tends to go w.r.t. local parameterization plane orientation (thanks to its phase), and about how much it deviates (thanks to its magnitude). In other words, the mean curvature of the first Wirtinger derivatives can be bijectively mapped to the mean normal in a small neighborhood.

Let us now discuss how the position amplification procedure can be generalized to a normal amplification procedure. Given a surface $\mathcal{S}$ and function $a_0(s)$ at point $P \in \mathcal{S}$, let us note $\widetilde{\phi}_{0,0} = -\frac{2a_0(s)}{s^2}$. This value is the average height of the neighbors around P, and moving P in the normal direction by $\widetilde{\phi}_{0,0}$ is equivalent to projecting P on the local best regression plane.

Functions $a_{\pm1}(s)$ have a similar aspect as $a_0(s)$ in their Taylor expansion. As $\phi_{0,0}$ expresses an offset of the positions, $\phi_{1,\pm1}$ can be thought as an angular offset of the tangential components. Adding an angular offset $\widetilde{\phi}_{1,\pm1}$ results in rotating the tangent plane at P. $a_{\pm1}(s)$ is proportional to the mean curvature of the first Wirtinger derivative at P and holds the tangential information. Thus, $a_{\pm1}(s)$ can be used to rotate the local parameterization plane in a mean curvature motion like procedure near P. We defined the blurring position procedure to be the procedure moving each point P to the centroid of each neighborhoods. Doing so is equivalent with moving the parameterization plane to a position such that computing the volume between a ball and the interior of the surface equals zero. By analogy, we define a blurred tangent plane to be the parameterization plane for which the volume descriptor of order ±1 computed using this plane equals zero. This way, the blurred tangent plane is equal to an average of the neighborhood tangent planes. Thus, we need to add a tangential offset $\widetilde{\phi}_{1,\pm1}$ such that:

$$\frac{\widetilde{\phi}_{1,\pm1}}{3}s^3 + a_{\pm1}(s) = 0 \tag{4.10}$$

This yields:

$$\widetilde{\phi}_{1,\pm1} = -\frac{3a_{\pm1}}{s^3}(s) \tag{4.11}$$

Since $\widetilde{\phi}_{1,\pm1}$ is homogeneous to a tangential orientation, one can retrieve the corresponding smooth normal using equation (2.21). The procedure can be described as follows: Given estimated coefficients $a_{\pm1}(s)$ in the tangent plane in a neighborhood of radius s, apply the normal correction procedure by replacing $\phi_{1,\pm1}$ by:

$$\phi_{1,\pm1} \leftarrow \frac{3a_{\pm1}(s)}{s^3}(1 - \alpha_{\pm1}) \tag{4.12}$$

Note that there are two coefficients $\alpha_{\pm1}$. In the general case where someone wants to enhance geometric details, $\alpha_1 = \alpha_{-1} > 1$. The case $\alpha_{\pm1} = 0$ blurs the normals. Thus, this can be used to have a consistent way to define blurred normals used for amplifying positions instead of computing coarse normals using principal component analysis. α_1 and α_{-1} can be different coefficients in case one wants to skew geometric details coherently as explained in next section

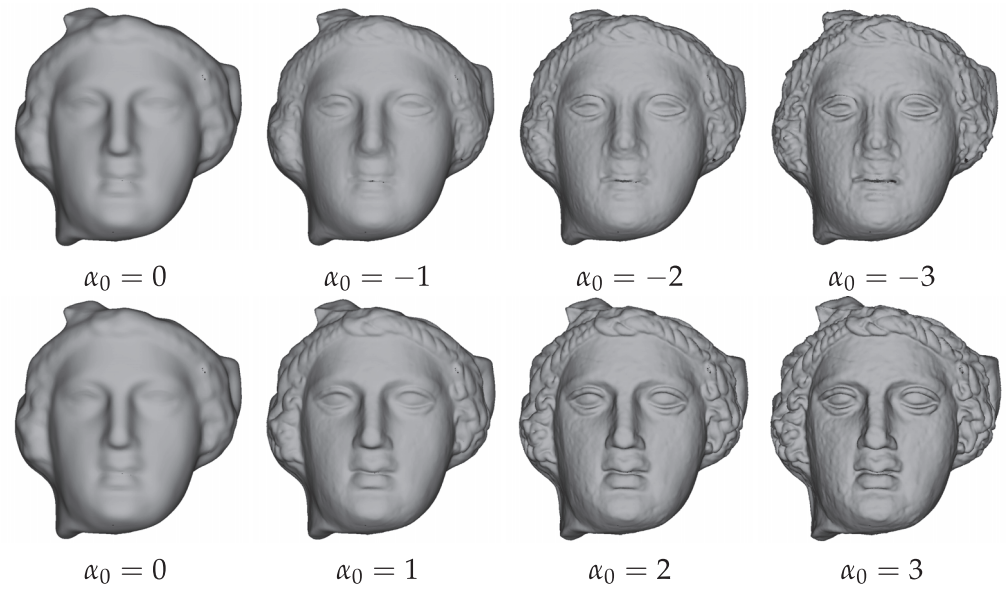

FIGURE 4.7: Influence of position amplification gain α_0. $a_0(s)$ is computed using the regular grid integration in chapter 3. When $\alpha_0 < 0$, the shape tends to be carved in the orientation opposite to the details (visually similar to normal filtering with $\alpha_{\pm 1} < 0$, Fig. 4.8).

4.5 Inverting and skewing geometric details

In sections 4.3 and 4.4 we described a method for amplifying geometric details by either moving points or changing the normals direction. Both methods are very similar and depend on a radius parameter s and a gain (α_0 for amplifying positions, and $\alpha_{\pm 1}$ for amplifying normals). In order to enhance details, gains should be positive and strictly larger than 1. However, one can design a larger variety of filters on the geometric details of a surface, such as inverting them by setting negative gains α_0 and $\alpha_{\pm 1}$, or even producing skewed-like geometric details in a coherent manner over the surface by setting $\alpha_{\pm 1} \in \mathbb{C}$.

Inverting geometric details seems straightforward regarding the way this procedure enhances them. Let us focus on the position amplification method. Given a surface $\mathcal{S}$ and the smoothing procedure discussed in section 4.3 which transforms $\mathcal{S}$ to $K(\mathcal{S})$, one can note $\delta = \mathcal{S} - K(\mathcal{S})$ the geometric details of $\mathcal{S}$. Thus, subtracting δ to $\mathcal{S}$ erases geometric details, and adding $\alpha_0\delta$ to $K(\mathcal{S})$ amplifies them if $\alpha_0 > 1$, or restores them if $\alpha_0 = 1$. It comes naturally that setting $\alpha_0 < 1$ would carve the geometric details in the surface in the wrong direction, yielding a detail inversion. Setting $\alpha_0 = -1$ leads to what could be named *anti-details*, and setting $\alpha_0 < -1$ would enhance them. Figure 4.7 shows an example of detail inversion.

The same rationale can be applied for normal amplifications. As discussed in Section 4.4, a displacement of the tangential component in the local Wavejet decomposition of a surface can be expressed as a complex number. Let $K_1(\mathcal{S})$ be the surface $\mathcal{S}$ with smoothened normals using our method. Let there be an arbitrary local coordinate system in tangent plane to $\mathcal{S}$. Noting $R(P)$ the rotation matrix rotating normal $\boldsymbol{n}$ at $P \in \mathcal{S}$ to the smooth normal of $K_1(\mathcal{S})$, let the local basis spanning each smooth tangent plane over $K_1(s)$ be the corresponding basis at P in $\mathcal{S}$ rotated by $R(P)$. Let $\frac{\partial \mathcal{S}}{\partial z}$ (resp. $\frac{\partial \mathcal{S}}{\partial z^*}$) be the set of first order Wirtinger derivative (resp. its conjugate) of the local heightfield at each point in surface $\mathcal{S}$ w.r.t. local system coordinates. In other words, it associates a set of complex numbers associated to a point P of the surace.

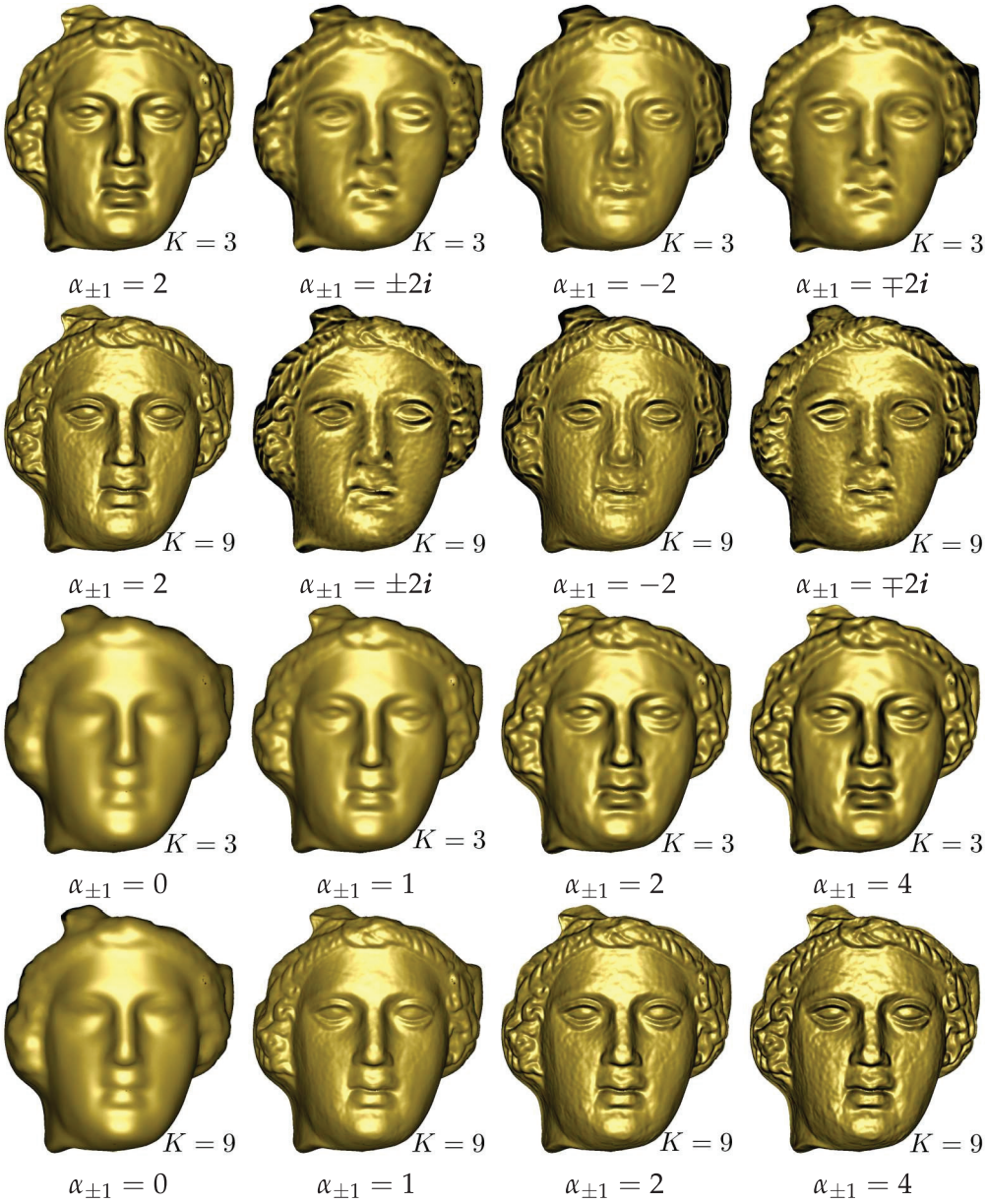

FIGURE 4.8: Normal amplification. $a_{\pm 1}(s)$ is computed using local Wavejet decompositions for Wavejets of different orders K. Influence of normal amplification gain $\alpha_{\pm 1}$ and of order K. The phase of $\alpha_{\pm 1}$ sets the orientation followed by normal amplification. When $\alpha_{\pm 1} = 0$, the normals are blurred.

The normal displacement can be written as two complex scalar fields $\delta_{\pm 1}$ over the surface that can be written as follows:

$$\begin{aligned} \delta_1 &= \frac{\partial \mathcal{S}}{\partial z} - \frac{\partial K_1(\mathcal{S})}{\partial z} \\ \delta_{-1} &= \frac{\partial \mathcal{S}}{\partial z^*} - \frac{\partial K_1(\mathcal{S})}{\partial z^*} \end{aligned} \tag{4.13}$$

$\delta_{\pm 1}$ is the expression of the displacement of the normals between their correct position to a blurred version. Thus, moving in the opposite direction from the blurred version would invert the visual aspect of geometric details as well. Doing so would make the normals evolve in the opposite direction to the geometry. However, since our visual system is more sensitive to the normal orientations than the geometry, unless the geometry varies so much that our visual system could catch the position variations as well as the normal information and debunk the incoherence, one would see inverted geometric details without being much confused. When our visual system sees inverted details, it actually infers a geometry which does not match the real geometry.

More can be done with normal amplification. Since amplifying normals is equivalent with displacing the tangent planes using complex numbers, one could imagine, instead of setting a real gain $\alpha_{\pm 1}$, to set it as a complex number. Linearly interpolating in the real number axis $\alpha_{\pm 1} = 1$ to $\alpha_{\pm 1} = -1$ would smoothly go from the input surface with regular normals, to a surface with blurred normals, to a surface with inverted geometric details inferred by the normals orientation. Instead of linear interpolation, if one performs an interpolation in the unit circle of the complex plane, what would happen? First, one should note that, necessarily, $\phi_{1,1} = \phi^*_{1,-1}$ in order to have a real tangent plane and a real normal. Thus

$$\frac{3a_1(s)}{s^3}(1-\alpha_1) = \frac{3a^*_{-1}(s)}{s^3}(1-\alpha^*_{-1}) \tag{4.14}$$

Which yields $\alpha_1 = \alpha^*_{-1}$. Thus, if α_1 evolves along the half unit circle of positive imaginary part, $\alpha_{\pm 1}$ should evolve in the half unit circle of negative imaginary part, being symmetric to α_1 w.r.t. real numbers axis. Doing so, the absolute value of the tangent plane displacement with the blurred tangent plane is constant, while the orientation varies. One can see a change of magnitude of $\alpha_{\pm 1}$ as a change in the angle of rotation transforming a normal to the other. Similarly, a change of phase changes the axis of rotation. The normal ends up rotating around the blurred normal until it reaches the position of the normal inducing inverted geometric details. Setting $\alpha_{\pm 1} \in \mathbb{C}$ makes all normals move in a coherent manner as far as all tangential parameterizations are direct frames. The reason for that is that the displacement of tangent planes does not depend on the coordinate system of the local parameterization plane. The value of $\delta_{\pm 1}$ may differ, but the geometric transformation applied to the normal is invariant when transforming these scalar fields into rotation matrices. Multiplying $\delta_{\pm 1}$ at point P by a gain $\alpha_{\pm 1}$ angularly shifts $\delta_{\pm 1}$ by the phase of $\alpha_{\pm 1}$, resulting into rotating this normals around the blurred normal. This results in infering geometric details which can look odd or unnatural while still being coherent.

It is interesting to see that inverting details using either the position or normal amplification framework results in quite similar results (compare results with a negative gain in Figures 4.7 and 4.8). One might expect this, but both procedures rely on local quantities expressing parts of the heightfield being orthogonal with each other (frequency 0 is orthogonal with frequencies ± 1). Figures 4.8 and 4.9 shows

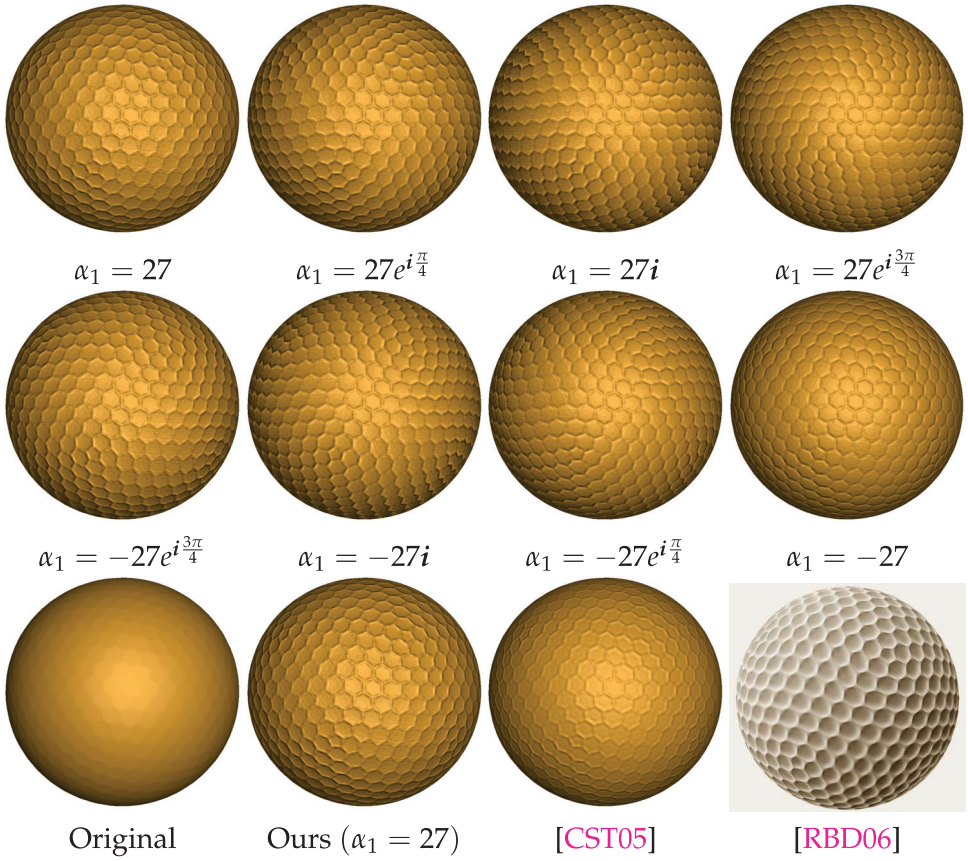

FIGURE 4.9: Normal enhancement on a golf ball. First and Second row : normal amplification for different α_1. Note that $\alpha_{-1} = \alpha_1^*$ on every examples. Last row: comparison with [CST05] normal enhancement algorithm and with [RBD06] detail exaggerating shading.

examples of skewed normals using our method. We also compare to [CST05] and [RBD06]. Even if [CST05] enhances normals by doing a mean curvature motion like algorithm on normals, we could not amplify them on the golf ball as much as we do with our method. This is due to the fact that their procedure is iterative, and that each step involves a normalization that can tend to produce a division by zero after a certain amount of iterations. This results in an upper limit for amplifying normals. On the other hand [RBD06] seems to perform better, but recall that they rely on a shader and not on changing normal directions. Thus, their algorithm is different from unsharp masking. They also take a mesh as input while we use point sets.

It might be a good idea to investigate higher orders detail changes and to see how this impacts the shape. That is far from trivial since the order 2 volume descriptor deals with curvature and principal directions, and amplifying principal directions is far less intuitive than order 0 or order 1 detail amplification.

Conclusion

Summary

The main contribution of this thesis is the introduction of a new polar function basis for local shape analysis: the *Wavejets*. Given a plane close enough to a tangent plane at some point P, given an arbitrary orthonormal basis in this plane, the shape is locally analyzed using the Wavejets by decomposing the local heightfield between the parameterization plane and the surface near P. Computating the Wavejets coefficients to locally describe a surface can be done by solving a linear system of equations. There is a linear map between the coefficients of the Taylor expansion of a heightfield and its Wavejets decomposition.

Wavejets offers a new way to locally comprehend a surface. On one hand, radial parts of same order k hold the differential properties of the surface in the sense of the canonical derivatives. On the other hand, a frequency property n is introduced by this basis, featuring linear combinations of coefficients of different orders k. An important step in the understanding of quantities expressed by the Wavejets comes by linking them to the Wirtinger derivatives [Wir27]. These complex derivative operators are not widely known. To the best of our knowledge, there has not been any work regarding properties of the Wirtinger derivatives of high order, i.e. recursively applying the Wirtinger derivatives to a function. It turns out that the Wavejets coefficients are proportional to the Wirtinger derivatives of the heightfield, deriving a frequency interpretation of such derivatives when considered at high orders. Last but not least, the Wavejets decomposition can be used to retrieve high order principal directions in that framework of symmetric supermatrices in [Qi05; Qi06; Qi07]. Symmetric supermatrices are higher dimensional arrays than matrices who appear naturally in the local surface Taylor expansion.

Another major contribution of our work comes with the generalization of the *Volume descriptor*, introduced in [Pot+09], to higher orders. Integral invariants are integral quantities that can be used as a local description of a function or a surface. The volume descriptor is defined as the volume of the intersection of a ball centered at a point on the surface, with the interior of this surface. The volume descriptor can be linked to the Wavejets by looking at the volume between the tangent plane at a point, and the surface. As a consequence, the Wavejets provide a new way to compute the volume descriptor. A side consequence of this is that the Taylor expansion bound can be improved from $O(s^5)$ to $O(s^6)$, where s is the radius of the ball, because of the expression of the Taylor expansion of the volume using the Wavejets decomposition. The Wavejets decomposition also resulted in the definition of a Fourier series $(a_n(s))_{n\in\mathbb{Z}}$. Naturally, $2\pi a_0(s)$ is the integral of the heightfield, making $a_0(s)$ is an integral invariant. Similarly, for any integer n, $|a_n(s)|$ are integral invariants. This allows the definition of a generalization of the volume descriptor. We call volume descriptor of order $n \neq 0$ at radius s the quantity $2\pi|a_n(s)|$. It can be shown that the Taylor expansion of such quantities involves the Wirtinger derivatives at high order $\frac{\partial^n}{\partial z^n}$ and $\frac{\partial^n}{\partial z^{*n}}$. A nice property of these high order derivatives is that they

are angularly orthogonal with regards to each other. Hence, coefficients $a_n(s)$ locally decomposes the surface in differential quantities being orthogonal with each other.

We finally showed an application of coefficients $a_0(s)$ and $a_{\pm 1}(s)$ can be used for an application: geometric details amplification. Geometric details amplification can be done in two major ways: one can use the spectral decomposition and apply a high-boost filter to the spectrum, or one can look at the local dynamics of the details to be amplified, and locally modify the function to amplify those dynamics. This last method, on which we rely on, is called *unsharp masking*. There are two ways someone can amplify geometric details on a shape: moving each position, or turnings the normals so they give the illusion of sharper details. $a_0(s)$ is used to amplify positions, and $a_{\pm 1}(s)$ is used to amplify the normals.

4.6 Perspectives

The introduction of the Wavejets basis as well as the integral invariants coming from this basis opened a few directions that would need further investigation.

- There might be a great potential with contructing a local shape descriptor using coefficients $a_n(s)$. These coefficients are orthogonal and quantify the differential properties of the surface. Comparison with the Heat Kernel Signature [SOG09] as well as the Wave Kernel Signature [ASC11] would need to be done, since they perform quite well and are widely used in the current litterature as the default descriptor.

- Quantities $a_n(s)$ are built out of an integration process. However, one could think of a weighted integration scheme to create an ideal local shape descriptor. The ideal weight function could be learned using a neural network on the best way to combine the Wavejets coefficients at a given frequency n, and infer the weight function so it matches the learned linear combination. One could then use this weight function when computing the newly defined integral invariants. Note that changing the weight function is equivalent with modifying the radius series s_ℓ in section 3.4.3.

- The phases in coefficients $a_n(s)$ give a smooth estimate of the principal directions relative to the differential quantities being stored in the n^{th} Wirtinger derivative of the local heightfield. In particular, second order principal directions and third principal directions can be retrieved out of $a_{\pm 1}(s), a_{\pm 2}(s)$ and $a_{\pm 3}(s)$. Third order principal directions should give the speed of the second order derivative. Thus, there might be a way to ameliorate principal direction tracking by using the speed information given by the third order derivatives.

Bibliography

[1] H. H. Andersen et al. “The Multivariate Complex Normal Distribution”. In: *Linear and Graphical Models: for the Multivariate Complex Normal Distribution*. New York, NY: Springer New York, 1995, pp. 15–37. ISBN: 978-1-4612-4240-6. DOI: 10.1007/978-1-4612-4240-6_2. URL: https://doi.org/10.1007/978-1-4612-4240-6_2.

[2] M. Aubry, U. Schlickewei, and D. Cremers. “The wave kernel signature: A quantum mechanical approach to shape analysis”. In: *2011 IEEE International Conference on Computer Vision Workshops (ICCV Workshops)*. Nov. 2011, pp. 1626–1633. DOI: 10.1109/ICCVW.2011.6130444.

[3] Yohann Béarzi and Julie Digne. “Surface derivatives computation using Fourier Transform”. In: *JFIG 2016*. Actes des journées JFIG 2016. Grenoble, France, Nov. 2016. URL: https://hal.archives-ouvertes.fr/hal-01735374.

[4] Yohann Béarzi, Julie Digne, and Raphaëlle Chaine. “Wavejets: A Local Frequency Framework for Shape Details Amplification”. In: *Computer Graphics Forum* 37 (Feb. 2018). DOI: 10.1111/cgf.13338.

[5] Mikhail Belkin, Jian Sun, and Yusu Wang. “Constructing Laplace Operator from Point Clouds in Rd”. In: *Proceedings of the Twentieth Annual ACM-SIAM Symposium on Discrete Algorithms*. SODA ’09. New York, New York: Society for Industrial and Applied Mathematics, 2009, pp. 1031–1040. URL: http://dl.acm.org/citation.cfm?id=1496770.1496882.

[6] G. Beylkin. “On the Fast Fourier Transform of Functions with Singularities”. In: *Applied and Computational Harmonic Analysis* 2.4 (1995), pp. 363–381. ISSN: 1063-5203. DOI: https://doi.org/10.1006/acha.1995.1026. URL: http://www.sciencedirect.com/science/article/pii/S1063520385710263.

[7] Norman Biggs. *Algebraic Graph Theory*. 2nd ed. Cambridge Mathematical Library. Cambridge University Press, 1974. DOI: 10.1017/CBO9780511608704.

[8] F. Cazals and M. Pouget. “Estimating differential quantities using polynomial fitting of osculating jets”. In: *Computer Aided Geometric Design* 22.2 (2005), pp. 121–146. ISSN: 0167-8396. DOI: http://dx.doi.org/10.1016/j.cagd.2004.09.004. URL: http://www.sciencedirect.com/science/article/pii/S016783960400113X.

[9] Paolo Cignoni, Roberto Scopigno, and Marco Tarini. “A simple normal enhancement technique for interactive non-photorealistic renderings”. In: *Computers & Graphics* 29.1 (2005), pp. 125–133. ISSN: 0097-8493.

[10] Tali Dekel et al. “Revealing and Modifying Non-local Variations in a Single Image”. In: *ACM Trans. Graph.* 34.6 (Oct. 2015), 227:1–227:11. ISSN: 0730-0301.

[11] Julie Digne and Jean-Michel Morel. “Numerical analysis of differential operators on raw point clouds”. In: *Numerische Mathematik* 127.2 (2014), pp. 255–289. ISSN: 0945-3245.

[12] Julie Digne et al. “Scale Space Meshing of Raw Data Point Sets”. In: *Comput. Graph. Forum* 30 (2011), pp. 1630–1642.

[13] A. Dutt and V. Rokhlin. “Fast Fourier Transforms for Nonequispaced Data, II”. In: *Applied and Computational Harmonic Analysis* 2.1 (1995), pp. 85–100. ISSN: 1063-5203. DOI: https://doi.org/10.1006/acha.1995.1007. URL: http://www.sciencedirect.com/science/article/pii/S106352038571007X.

[14] Dennis Gabor. “Information theory in electron microscopy”. In: *Laboratory Investigation* 14 (6 1965), pp. 801–807.

[15] M. Lindenbaum, M. Fischer, and A.M. Bruckstein. “On Gabor’s Contribution to Image Enhancement”. In: *Pattern Recognition* 27 (1994), pp. 1–8.

[16] P. Goupillaud, A. Grossmann, and J. Morlet. “Cycle-octave and related transforms in seismic signal analysis”. In: *Geoexploration* 23.1 (1984). Seismic Signal Analysis and Discrimination III, pp. 85–102. ISSN: 0016-7142. DOI: https://doi.org/10.1016/0016-7142(84)90025-5. URL: http://www.sciencedirect.com/science/article/pii/0016714284900255.

[17] Gaël Guennebaud, Marcel Germann, and Markus Gross. “Dynamic Sampling and Rendering of Algebraic Point Set Surfaces”. In: *Computer Graphics Forum* 27.2 (2008), pp. 653–662. ISSN: 1467-8659. DOI: 10.1111/j.1467-8659.2008.01163.x. URL: http://dx.doi.org/10.1111/j.1467-8659.2008.01163.x.

[18] Gaël Guennebaud and Markus Gross. “Algebraic point set surfaces”. In: *ACM Trans. Graph.* 26 (3 2007). Proc. SIGGRAPH 2007. ISSN: 0730-0301.

[19] Peter Henrici, ed. *Applied and Computational Complex Analysis. Vol. 3: Discrete Fourier Analysis&Mdash;Cauchy Integrals&Mdash;Construction of Conformal Maps—univalent Functions*. New York, NY, USA: John Wiley & Sons, Inc., 1986. ISBN: 0-471-08703-3.

[20] Hugues Hoppe et al. “Surface Reconstruction from Unorganized Points”. In: *SIGGRAPH Comput. Graph.* 26.2 (July 1992), pp. 71–78. ISSN: 0097-8930. DOI: 10.1145/142920.134011. URL: http://doi.acm.org/10.1145/142920.134011.

[21] Dominique Hulin and Marc Troyanov. “Mean Curvature and Asymptotic Volume of Small Balls”. In: *The American Mathematical Monthly* 110.10 (2003), pp. 947–950. DOI: 10.1080/00029890.2003.11920037. eprint: https://doi.org/10.1080/00029890.2003.11920037. URL: https://doi.org/10.1080/00029890.2003.11920037.

[22] Pushkar Joshi and Carlo Séquin. “An Intuitive Explanation of Third-order Surface Behavior”. In: *Comput. Aided Geom. Des.* 27.2 (Feb. 2010).

[23] A. Khotanzad and Y. H. Hong. “Invariant image recognition by Zernike moments”. In: *IEEE Transactions on Pattern Analysis and Machine Intelligence* 12.5 (May 1990), pp. 489–497. ISSN: 0162-8828. DOI: 10.1109/34.55109.

[24] Simon Xinmeng Liao. “Image Analysis by Moments”. PhD thesis. University of Winnipeg, 1993.

[25] Ce Liu et al. “Motion Magnification”. In: *ACM Trans. Graph.* 24.3 (July 2005), pp. 519–526. ISSN: 0730-0301.

[26] Stéphane Mallat. *A Wavelet Tour of Signal Processing*. Jan. 1999. ISBN: 0-12-466606-X.

[27] Siddharth Manay et al. “Integral Invariant Signatures”. In: *ECCV*. 2004.

[28] A. Maximo et al. "A Robust and Rotationally Invariant Local Surface Descriptor with Applications to Non-local Mesh Processing". In: *Graph. Models* 73.5 (Sept. 2011), pp. 231–242. ISSN: 1524-0703. DOI: 10.1016/j.gmod.2011.05.002. URL: http://dx.doi.org/10.1016/j.gmod.2011.05.002.

[29] Even Mehlum and Christian Tarrou. "Invariant smoothness measures for surfaces". In: *Advances in Computational Mathematics* 8.1 (1998), pp. 49–63. ISSN: 1572-9044. DOI: 10.1023/A:1018931910836. URL: http://dx.doi.org/10.1023/A:1018931910836.

[30] Simone Melzi et al. "Localized Manifold Harmonics for Spectral Shape Analysis". In: *CoRR* abs/1707.02596 (2017). arXiv: 1707.02596. URL: http://arxiv.org/abs/1707.02596.

[31] Mark Meyer et al. "Discrete Differential-Geometry Operators for Triangulated 2-Manifolds". In: Springer-Verlag, 2002, pp. 35–57.

[32] Mark Meyer et al. "Discrete Differential-Geometry Operators for Triangulated 2-Manifolds". In: *Visualization and Mathematics III*. Ed. by Hans-Christian Hege and Konrad Polthier. Berlin, Heidelberg: Springer Berlin Heidelberg, 2003, pp. 35–57. ISBN: 978-3-662-05105-4.

[33] Gatarić Milana. "Nonuniform generalized sampling". PhD thesis. University of Cambridge, 2015.

[34] S. K. Mitra et al. "A new class of nonlinear filters for image enhancement". In: *Proc. ICASSP*. 1991, 2525–2528 vol.4.

[35] Marcin Novotni and Reinhard Klein. "3D Zernike Descriptors for Content Based Shape Retrieval". In: *Proceedings of the Eighth ACM Symposium on Solid Modeling and Applications*. SM '03. Seattle, Washington, USA: ACM, 2003, pp. 216–225. ISBN: 1-58113-706-0. DOI: 10.1145/781606.781639. URL: http://doi.acm.org/10.1145/781606.781639.

[36] Gabriel Peyré and Stéphane Mallat. "Surface Compression With Geometric Bandelets". In: *ACM Transactions on Graphics* 24 (July 2005). DOI: 10.1145/1073204.1073236.

[37] H. Poincaré. "Sur les propriétés du potentiel et sur les fonctions Abéliennes". In: *Acta Math.* 22 (1899), pp. 89–178. DOI: 10.1007/BF02417872. URL: https://doi.org/10.1007/BF02417872.

[38] A. Polesel, G. Ramponi, and V. J. Mathews. "Image enhancement via adaptive unsharp masking". In: *IEEE Transactions on Image Processing* 9.3 (Mar. 2000), pp. 505–510. ISSN: 1057-7149. DOI: 10.1109/83.826787.

[39] M. D. Pompeiu. "Sur une classe de fonctions ďune variable complexe et sur certaines équations intégrales". In: *Rendiconti del Circolo Matematico di Palermo (1884-1940)* 35.1 (Dec. 1913), pp. 277–281. ISSN: 0009-725X. DOI: 10.1007/BF03015607. URL: https://doi.org/10.1007/BF03015607.

[40] Helmut Pottmann et al. "Integral Invariants for Robust Geometry Processing". In: *Comput. Aided Geom. Des.* 26.1 (Jan. 2009), pp. 37–60. ISSN: 0167-8396. DOI: 10.1016/j.cagd.2008.01.002. URL: http://dx.doi.org/10.1016/j.cagd.2008.01.002.

[41] Helmut Pottmann et al. "Principal curvatures from the integral invariant viewpoint". In: *CAGD* 24.8-9 (2007), pp. 428–442.

[42] Liqun Qi. "Eigenvalues and invariants of tensors". In: *Journal of Mathematical Analysis and Applications* 325.2 (2007), pp. 1363–1377. ISSN: 0022-247X. DOI: https://doi.org/10.1016/j.jmaa.2006.02.071. URL: http://www.sciencedirect.com/science/article/pii/S0022247X06001764.

[43] Liqun Qi. "Eigenvalues of a real supersymmetric tensor". In: *Journal of Symbolic Computation* 40.6 (2005), pp. 1302–1324. ISSN: 0747-7171. DOI: https://doi.org/10.1016/j.jsc.2005.05.007. URL: http://www.sciencedirect.com/science/article/pii/S0747717105000817.

[44] Liqun Qi. "Rank and eigenvalues of a supersymmetric tensor, the multivariate homogeneous polynomial and the algebraic hypersurface it defines". In: *Journal of Symbolic Computation* 41.12 (2006), pp. 1309–1327. ISSN: 0747-7171. DOI: https://doi.org/10.1016/j.jsc.2006.02.011. URL: http://www.sciencedirect.com/science/article/pii/S0747717106000861.

[45] Gianni Ramponi Giovanni et al. "Nonlinear unsharp masking methods for image contrast enhancement". In: *J. Electronic Imaging* 5 (July 1996), pp. 353–366.

[46] M. R. Ruggeri et al. "Approximating Geodesics on Point Set Surfaces". In: *Proceedings of the 3rd Eurographics / IEEE VGTC Conference on Point-Based Graphics*. SPBG'06. Boston, Massachusetts: Eurographics Association, 2006, pp. 85–94. ISBN: 3-905673-32-0. DOI: 10.2312/SPBG/SPBG06/085-093. URL: http://dx.doi.org/10.2312/SPBG/SPBG06/085-093.

[47] Szymon Rusinkiewicz, Michael Burns, and Doug DeCarlo. "Exaggerated Shading for Depicting Shape and Detail". In: *ACM Trans. Graph.* 25.3 (July 2006), pp. 1199–1205. ISSN: 0730-0301.

[48] Peter Schröder and Wim Sweldens. "Spherical Wavelets: Efficiently Representing Functions on the Sphere". In: *Proceedings of the 22Nd Annual Conference on Computer Graphics and Interactive Techniques*. SIGGRAPH '95. New York, NY, USA: ACM, 1995, pp. 161–172. ISBN: 0-89791-701-4. DOI: 10.1145/218380.218439. URL: http://doi.acm.org/10.1145/218380.218439.

[49] O. Sorkine et al. "Laplacian Surface Editing". In: *Proceedings of the 2004 Eurographics/ACM SIGGRAPH Symposium on Geometry Processing*. SGP '04. Nice, France: ACM, 2004, pp. 175–184. ISBN: 3-905673-13-4. DOI: 10.1145/1057432.1057456. URL: http://doi.acm.org/10.1145/1057432.1057456.

[50] Jian Sun, Maks Ovsjanikov, and Leonidas Guibas. "A Concise and Provably Informative Multi-scale Signature Based on Heat Diffusion". In: *Proceedings of the Symposium on Geometry Processing*. SGP '09. Berlin, Germany: Eurographics Association, 2009, pp. 1383–1392. URL: http://dl.acm.org/citation.cfm?id=1735603.1735621.

[51] Gabriel Taubin. "A Signal Processing Approach to Fair Surface Design". In: *Proceedings of the 22Nd Annual Conference on Computer Graphics and Interactive Techniques*. SIGGRAPH '95. New York, NY, USA: ACM, 1995, pp. 351–358. ISBN: 0-89791-701-4. DOI: 10.1145/218380.218473. URL: http://doi.acm.org/10.1145/218380.218473.

[52] Bruno Vallet and Bruno Lévy. "Spectral geometry processing with manifold harmonics". In: *Computer Graphics Forum* (2008), pp. 251–260.

[53] Max Wardetzky et al. "Discrete Laplace operators: No free lunch". In: 07 (Jan. 2007), pp. 33–37.

[54] W. Wirtinger. "Zur formalen Theorie der Funktionen von mehr komplexen Veränderlichen". In: *Mathematische Annalen* 97 (1927), pp. 357–376. URL: http://eudml.org/doc/182642.

[55] von F. Zernike. "Beugungstheorie des schneidenverfahrens und seiner verbesserten form, der phasenkontrastmethode". In: *Physica* 1 (May 1934), pp. 689–704.

[56] Hao Zhang. "Discrete combinatorial Laplacian operators for digital geometry processing". In: 2004 (Jan. 2004).